

NUCLEAR MAGNETISM AND FLOW IN NORMAL
AND SUPERFLUID ^3He AT LOW PRESSURES IN
CONFINED GEOMETRIES

By

GREGORY FIELDER SPENCER

A DISSERTATION PRESENTED TO THE GRADUATE SCHOOL
OF THE UNIVERSITY OF FLORIDA IN
PARTIAL FULFILLMENT OF THE REQUIREMENTS
FOR THE DEGREE OF DOCTOR OF PHILOSOPHY

UNIVERSITY OF FLORIDA

1986

ACKNOWLEDGMENTS

There are many people without whom the effort required to produce this dissertation would have been much greater. First I must remember Dr. Winston Gottschalk who introduced physics to me during my senior year in high school. My fellow students have been a source of learning and friendship. I owe Dr. Robert (Bobby) Berg, Brad Engel, Greg Haas, Yi-hua Tang, and Dr. John Polley much in this respect. For the same reasons I must thank Drs. Ephraim Flint, Peter Alexander, Yukio Morii, Don Bakalyar, Kurt Uhlig, and Don Bittner. A great deal of appreciation must be expressed to the machinists of the department including, Harvey Nachtrieb, Ron Spencer, and Bill Malphurs, all for putting up with my intricate designs. Of the faculty I must first thank my committee members who flinched only a little when I presented them their copies and who remained patient with me during the final days. The physicists around whom I have been privileged to work include Professors Dwight Adams, Neal Sullivan, and David Tanner. Finally there are three groups of people to whom I owe a special debt. The first is of course my chairman, Professor Gary Ihas. He has taken the time and effort to impart a substantial education to me, not all of which was limited to physics. Beyond that he has proven to be a special friend willing to stand by me. Secondly, my family, including my parents, Ruth and Al Spencer, my sister, Susan, and niece, Bess, and grandmother, Hazel, have been a source of unending love, understanding, and support. Finally, my beautiful wife of 10 days, Sheila, has given me the love and also the hard work needed to see such a project to completion.

TABLE OF CONTENTS

ACKNOWLEDGMENTS	ii
ABSTRACT	v
CHAPTERS	
I INTRODUCTION	1
II THEORETICAL AND EXPERIMENTAL REVIEW	9
Introduction	9
Normal Liquid ^3He and Landau's Fermi Liquid Theory	10
Theory of Superfluid $^3\text{He-B}$	14
Liquid ^3He in an Extremely Confined Geometry	44
III EXPERIMENTAL APPARATUS	53
Refrigeration	53
Experimental Cell Heat Exchanger	54
Sample Magnetic Field Coils	58
Thermometry	61
NMR Techniques	68
Bellows Flow Pump	72
Experimental Cells	78
IV SUPERFLUID $^3\text{He-B}$ EXPERIMENTAL RESULTS AND DISCUSSION	97
Introduction	97
Superfluid $^3\text{He-B}$ in a Slab Geometry	98
Superfluid $^3\text{He-B}$ in a Cylindrical Geometry	127
Concluding Remarks and Future Work	159
V NMR AND FLOW OF ^3He INSIDE VYCOR GLASS	162
Introduction	162
Magnetism of ^3He inside Vycor	162
Flow of ^3He through Vycor Glass	172
Concluding Remarks and Future Work	204

VI CONCLUDING REMARKS207
APPENDICES	
A TABULATION OF DATA OF THE B PHASE SLAB EXPERIMENT209
B DATA-GATHERING AND ANALYSIS PROGRAMS211
C MANUFACTURER'S LIST247
REFERENCES249
BIOGRAPHICAL SKETCH255

Abstract of Dissertation Presented to the Graduate School
of the University of Florida in Partial Fulfillment of the
Requirements for the Degree of Doctor of Philosophy

NUCLEAR MAGNETISM AND FLOW IN NORMAL
AND SUPERFLUID ^3He AT LOW PRESSURES IN
CONFINED GEOMETRIES

By

GREGORY FIELDER SPENCER

AUGUST 1986

Chairman: G.G. Ihas
Major Department: Physics

In order to study the interactions of the order parameter of superfluid $^3\text{He-B}$ as well as the nuclear magnetic and flow properties of normal liquid ^3He , measurements were performed on liquid ^3He in confined geometries. Nuclear magnetic resonance (NMR), both pulsed and continuous-wave (CW), was used in all the experiments while in addition a sensitive differential pressure gauge was used in the final experiment. Flow was created by use of an isochoric double-bellows flow pump.

Two different experiments were performed in the B phase of superfluid ^3He . In the first, liquid was confined inside two stacks of plates of separation 135 μm . With their surface normals oriented perpendicularly and using a rotatable magnetic field, a number of relative configurations of field, flow, and surface were possible. The frequency shift in this geometry at 21.5 bar and 0 bar (saturated vapor pressure = s.v.p.) was measured, extending the previous knowledge of the longitudinal

resonance of the B phase with the result $\Omega_B^2(T,P) = (2.46 + 0.54P \text{ (bar)}) \times (1 - T/T_C) \times 10^{10} \text{ Hz}^2$. Additionally, no effect of flow was seen on the NMR properties, allowing an experimental limit on the flow interaction to be at least three times smaller than anticipated. In the second B phase experiment, $^3\text{He-B}$ was confined inside a 2 mm diameter cylinder. The resulting B phase n texture dramatically altered the NMR lineshape for $T < T_C$ at 0.82 and 2.89 bars. A deconvolution technique was developed in order to map the texture inside the cylinder. The 3-dimensional map thus obtained was used to compute the parameters of the Ginzburg-Landau textural free-energy and find $R_C H_B = (37.4 \pm 5)(1 - T/T_C)^{1/2} \text{ cm G}$.

In the final experiment liquid ^3He was confined in the 20 to 60 Å pores of vycor glass. The enhanced susceptibility reported by others in various porous media was measured at 1.10, 3.93, and 5.45 bars for $1 \text{ mK} \leq T \leq 200 \text{ mK}$. At the lowest temperatures, the Curie-Weiss temperature of each pressure was approximately 0.5 mK. The behavior of flowing ^3He inside the vycor was found to be quite unusual, exhibiting an apparent viscoelasticity.

CHAPTER I

INTRODUCTION

A long time ago, in the days when men were Men and Giants walked the Earth, the study of low temperature physics was begun. From those early, pioneering efforts to liquefy "atmospheric vapours" by such men as Cailletet and Pictet to its full development as a distinct field of study, low temperature physics has been an important driving force in science and technology (Mendelssohn, 1966). In the realm of experiment an almost continuous stream of important and exciting findings has punctuated the logbooks of each new generation of searchers. Among the most important and earliest of these were the discoveries of superconductivity and superfluidity. The length of time these two subjects have been studied and the wealth of knowledge they have provided are each due to the fundamental nature of their origins.

So it is with ^3He . Since its greater availability in the Atomic Age (^3He is a "waste" product from nuclear materials storage sites, due to the decay of tritium), it has become the object of considerable study for a variety of reasons. Being one of the two stable isotopes of the only element in the periodic table which remains liquid under its own vapor pressure at absolute zero makes ^3He susceptible to a variety of quantum effects which otherwise might be visible only in the cores of neutron stars or other such exotic and as yet unattainable systems. Thus, ^3He is

a quantum liquid. Similarly, due to its light mass and weak binding energy, it is a quantum solid. Having a nuclear spin of $\frac{1}{2} \hbar$ allows the quantum effects to be visible in the magnetic properties of ^3He , a richer situation than for spin-0 ^4He .

Starting when superconductivity was first understood by the Bardeen-Cooper-Schrieffer (BCS) theory (Bardeen et al., 1957), people speculated on the possibility (or rather the inevitability) of liquid ^3He 's becoming a superfluid (Brueckner et al., 1960; Emery and Sessler, 1960). From BCS, theorists could make assumptions about the strength of the interaction and thereby estimate a transition temperature, T_c , at which the superfluidity should occur. As is usually the case in such matters, the predicted T_c values were just below the minimum attainable temperatures of the contemporary experimentalists.

However, in 1972 superfluid ^3He was discovered, at a temperature of about 2.6 mK (0.0026 K) at a pressure of 34.36 bars (1 bar = 14.5 psi), by the group at Cornell University (Osheroff et al., 1972a,b). Since that time, superfluid ^3He has provided a rich variety of behaviors to be studied both experimentally and theoretically.

In its original form, the BCS theory explained the electronic superconductivity in metals as a momentum space pairing of electrons near the Fermi surface (Cooper, 1956) into spin-0 correlated pairs. The spin singlet pairing meant, due to the Pauli principle, that the correlation was of relative orbital angular momentum zero (s wave) as well. Thus for the case of metallic superconductivity, the superconducting state was isotropic and non-magnetic. The situation for ^3He was quite different. Due to the large hard core repulsion between ^3He atoms such s-wave pairing

was not possible. It was found that ^3He forms a superfluid by p-wave pairing ($\ell=1$) primarily (although under certain extreme conditions admixtures of higher order pairing may become favorable), yielding the spin triplet ($s=1$). This provided a quite different superfluid, one that was magnetic and anisotropic.

Perhaps the most striking property of ^3He as a superfluid is the fact that it forms at least three different superfluid phases in open geometries. The pressure-temperature-magnetic field phase diagram near the superfluid transition is shown in Fig.(1-1). In zero magnetic field only two superfluid phases exist, the A and B phases. At melting pressure, a second order transition occurs during cooling when the normal liquid changes to the A phase. At lower temperature a first order transition happens at the A-B boundary, with the B phase extending to zero temperature. As the pressure is reduced, the width of the A phase decreases until at approximately 21 bars, the so-called polycritical point (PCP), the A phase disappears. The line of second order transitions continues to zero pressure monotonically decreasing to 1.15 mK at $P=0$. As the magnetic field is increased from zero, the third bulk superfluid phase appears, the A_1 phase, wedging itself between the normal liquid and the A phase. As the field increases, both the A and A_1 phases widen while the B phase is suppressed disappearing entirely at about 0.6 Tesla. While the NMR resonance of bulk liquid ^3He appears at the usual Larmor frequency ν_0 given by

$$\nu_0 = \gamma H_0, \quad (1)$$

where H_0 is the external magnetic field and γ is the gyromagnetic ratio for ^3He ($\gamma = 3.2435 \text{ kHz/G}$), the formation of the superfluid state can drastically alter this. In particular, in certain conditions the frequency

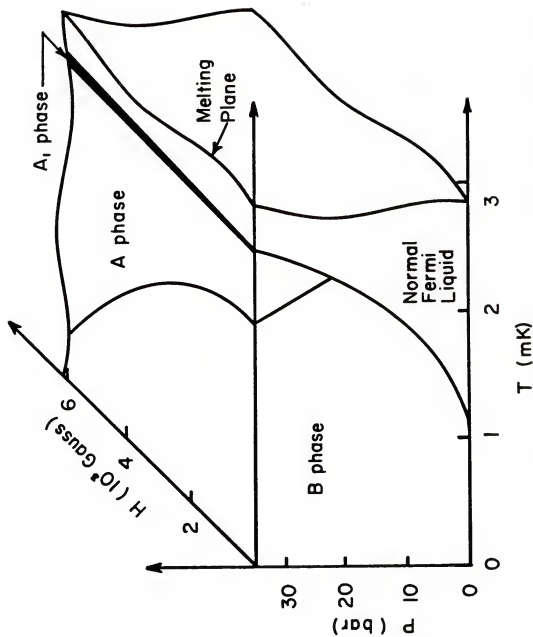


Fig.(1-1). P-T-H phase diagram of superfluid ^3He , in perspective. (Adapted from a plot by D. D. Osheroff (Lee and Richardson, 1978).)

of the ^3He resonance may shift from the Larmor value to higher frequencies, and the shift may be quite large (several kHz at one MHz). Due to the spatial anisotropy and the coupling of the spatial component of the wavefunction to the spin component (dipole-locking) the observed resonance line may be affected by the sample geometry as well as the field orientation. Additionally, the presence of superflow or normal liquid-superfluid counterflow may affect the NMR properties.

This thesis is a study of liquid ^3He in confined geometries at low temperatures and low pressures in and near the bulk B phase of superfluid ^3He . In these experiments the liquid was subjected to varying degrees of restricted container size and shape, magnetic field, and flow in order to probe the anisotropies of its properties. Nuclear magnetic resonance measurements were performed throughout the experiments although in the last experiment flow measurements using an extremely sensitive differential pressure gauge proved equally important.

The first two experiments were performed on bulk superfluid ^3He -B in two distinct cell geometries. The term bulk is used in the sense that all important container dimensions, d , are large compared to the coherence length, ξ , of the B phase which is on the order several hundred Ångströms.

In the first experiment liquid ^3He was confined inside a slab-shaped geometry formed between stacked glass plates with a plate separation of 135 μm . Two stacks of plates oriented perpendicularly to each other allowed for simultaneous measurement of the NMR properties in different anisotropic conditions. Both the magnetic susceptibility and the shift of the resonance frequency from the Larmor value were measured at pressures of 0 bar (s.v.p.) and 21.5 bars, in a field of 28.6 mT both with and without flowing liquid. This allowed comparison with similar works

at higher pressures (Brinkman et al., 1974; Osheroff et al., 1975; Ahonen et al., 1976). Our results agreed with the higher pressure experiments and extended them to saturated vapor pressure (Spencer et al., 1981). In addition, no effects of impressed flow were observed in the NMR.

In the second bulk liquid experiment it was desired to find a combination of confining geometry and magnetic field which would on the one hand produce dramatic effects on the NMR resonance while also being susceptible to detailed analysis of the exact form of the spatial anisotropy. For this case, the chosen geometry was an open cylinder of 2 mm diameter and 1.50 cm length. In this experiment, to preserve the cylindrical symmetry the 28.6 mT magnetic field was directed along the cylinder axis. The pressures were 0.82 bar and 2.89 bar. In this configuration it was possible to observe, for the first time, the flare-out texture of the B phase which had been theoretically predicted (Smith et al., 1977). By development of an NMR resonance deconvolution technique, a detailed experimental map of this spatial anisotropy field was obtained which further allowed calculation of the coefficients of the Landau-Ginzburg free-energy expansion. Finally, a varying azimuthal twist was discovered that had not been theoretically anticipated (Spencer and Ihas, 1982).

The final experiment was performed as a result of attempting to create flow in the cylindrical geometry experiment. In that attempt, liquid ^3He below the bulk transition temperature appeared to flow through a filter with very small pores (vycor glass, characteristic pore size $\sim 20\text{-}60$ Å) in a short time period and caused a disequilibrium final state in our flow pump (Ihas and Spencer, 1983). As this result was disputed by others a cell was built specifically to test the flow properties of liquid ^3He in this extremely restricted geometry. As a primary part of

this experiment, a very sensitive differential pressure gauge (manometer) was developed. The ultimate pressure sensitivity of this device was found to be $\Delta P = 59$ picobars. In addition to the direct flow measurements the NMR properties were also observed. The work was performed at low pressures (0.14, 1.10, 3.93, and 5.45 bar; low pressures were required because the manometer could only withstand an internal overpressure of ~ 10 bars) in the usual 28.6 mT field. At each pressure both susceptibility (by pulsed NMR) and flow measurements were made on the liquid inside the vycor matrix. Susceptibilities were measured between $T \sim 1$ mK and $T \sim 200$ mK at 1.10, 3.93, and 5.45 bars. By fitting the lowest temperature data to the Curie-Weiss law, Curie-Weiss temperatures of 0.573 mK, 0.546 mK, and 0.646 mK were found from 1.10, 3.93, and 5.45 bars respectively. Although the data could be made to fit the Curie-Weiss form of $(T - \theta)^{-1}$, θ being the Curie-Weiss temperature, the 1.10 bar and 5.45 bar data were each found to fit a power law in temperature over the entire range from 1 mK to 200 mK with the power law being $T^{-1.35}$. The 3.93 bar did not fit as well a single power law over the entire range, and its exponent was different, being $T^{-1.71}$. The flow of the liquid through the vycor was quite unusual. Differential pressure steps, typically of 300 to 600 μ bars, were applied to the liquid and the subsequent relaxation of this pressure head was observed. Rather than exhibiting ordinary viscous flow (not expected due to the restricted geometry) or even Knudsen flow as might have been anticipated, the flowing liquid seemed to display a complex viscoelastic behavior. As no consistent value of a minimum differential pressure to generate flow could be discerned, the system appeared to be quite history-dependent, making the system behave as if it was thixotropic. This flow behavior seemed to be both pressure and

temperature dependent complicating its explanation. Finally, an interaction between the flow and the susceptibility was observed, the maximum effect coming at the lowest temperatures (where the susceptibility was the highest). At first attributed to flow-induced heating of the confined liquid, an alternate speculation was made that the flow was depressing the susceptibility by direct action on the atoms participating in the surface magnetism.

CHAPTER II

THEORETICAL AND EXPERIMENTAL REVIEW

Introduction

This chapter presents the pertinent parts of the theory of ^3He which are necessary to understand and analyze the data which make up this work. The chapter is divided into three parts hereafter, the first dealing with the theory of normal liquid, the second concerning superfluid ^3He , the third containing the theory of ^3He magnetism and flow in an extremely confined geometry.

Excellent experimental and theoretical reviews exist for many of these topics. To study normal liquid ^3He and Landau's theory of Fermi liquids one can rely upon the text by Pines and Nozières (1966) or the review by Baym and Petick (1978). Similarly, the theory of superfluid ^3He is detailed by many authors at various levels of sophistication including Lounasmaa (1974), Leggett (1975) and Wheatley (1975), Wölfle (1979), Lee and Richardson (1978), Anderson (1978), and Brinkman and Cross (1978). The theoretical and experimental coverage of ^3He in an extremely restricted geometry, occasionally falling under the purview of the physics of thin films, is somewhat less well-documented. However, there are some reviews and monographs available including that by Daunt and Lerner (1973) and reviews by Dash and Schick (1978) and Brewer (1978).

Except for the presentation of some of the figures in this chapter, no original theoretical work appears, it truly being only a review. The

person already acquainted with these theories may omit this chapter in reading.

Normal Liquid ^3He and Landau's Fermi Liquid Theory

Below temperatures of about 100 mK (0.1 K) and above the superfluid transition temperature T_c (ranging from 1.15 mK to 2.7 mK), liquid ^3He acts like a degenerate gas of interacting spin $\frac{1}{2}$ particles. As such it is well-described by the theory of Fermi liquids developed by Landau (1956).

The Landau theory starts with a system of N free particles of spin $\frac{1}{2}$ in a unit volume. The eigenstates of such a system are the properly antisymmetrized combinations of single-particle plane-wave states characterized by momentum \vec{p} , spin $\sigma = \pm\frac{1}{2}$, and energy

$$\epsilon_p = p^2/2m = (\hbar k)^2/2m \quad (1)$$

where k is the wavevector corresponding to p . The groundstate of this system at $T = 0$ is found by filling up the N single-particle states of lowest energy to produce in momentum space the Fermi sphere bounded by the Fermi surface S_F . All states above the Fermi surface are empty, all below it filled, with the surface defined by the Fermi momentum

$$p_F = \hbar k_F = \hbar(3\pi^2 N)^{1/3}. \quad (2)$$

The low energy excitations of this system at low (but finite) temperature are created by exciting single particles near the Fermi surface (within $k_B T$ of the Fermi energy ϵ_F) into low-lying states just above S_F . The

excitations are then the various configurations of particles above S_F and holes below it. For this reason, the low temperature static properties all depend upon the density of states at S_F

$$(dn/d\varepsilon) = 3Nm/p_F. \quad (3)$$

To obtain the interacting system, the theory imagines that the interparticle potential is adiabatically turned-on, each particle finally feeling the full potential of its neighbors. Now, rather than a system of free particles, each particle moves through the system interacting with all the others within range of the interaction; each particle has become dressed by a screening cloud of its interacting neighbors. This structure is called a quasiparticle, there being a quasiparticle for each real particle in the system. As before, the low energy excitations are configurations of quasiparticles above S_F and quasiholes below S_F . The system is said to be normal if the real physical ground state is obtained by this switching-on procedure (some ground states, such as the superfluid, can not be reached by this perturbative technique). The quasiparticle energy is

$$\epsilon_k = (\hbar k)^2/2m^* \quad (4)$$

where m^* is the effective mass due to the screening. Interactions between quasiparticles may be treated by considering variations of their distribution from the ground state value, $\delta n_{k\sigma}$. Sufficiently close to the ground state, the energy is written by Taylor expansion

$$E[n_{k\sigma}] = E_0 + \sum_{k\sigma} \epsilon_k \delta n_{k\sigma} + \frac{1}{2} \sum_{k\sigma k'\sigma'} f_{k\sigma k'\sigma'} \delta n_{k\sigma} \delta n_{k'\sigma'}, \quad (5)$$

where E_0 is the ground state energy and f is the two-quasiparticle interaction. Under conditions of time reversal and reflection invariance the spin portion of f depends only on the relative spin orientation while the space portion of f depends only on the angle θ between \vec{k} and \vec{k}' since all the participants lie near S_F . Separating f into spin symmetric and anti-symmetric terms as

$$f_{kk'}(++) = f_{kk'}^s + f_{kk'}^a, \quad \text{and} \quad f_{kk'}(+-) = f_{kk'}^s - f_{kk'}^a, \quad (6)$$

allows the interaction to be decomposed by expansion in Legendre polynomials

$$\left(\frac{dn}{d\epsilon}\right) f_{kk'}^s = \sum_{l=0}^{\infty} F_l^s P_l(\cos \theta), \quad (7)$$

and

$$\left(\frac{dn}{d\epsilon}\right) f_{kk'}^a = \sum_{l=0}^{\infty} F_l^a P_l(\cos \theta) \quad (8)$$

where F_l^s and F_l^a are the dimensionless Landau parameters. All the free-particle properties are renormalized by appearance of the Landau parameters to whatever order desired. For example, the free-particle magnetic susceptibility, from $M = \chi H$, is independent of T (Pauli paramagnetism) as

$$\chi_0 = (1/4)\gamma^2 N^2 (dn/d\epsilon) \quad (9)$$

which becomes in the real liquid

$$\chi = \chi_0 / (1 + F_0^a). \quad (10)$$

This has been verified by Fairbank and Walters (1958), Anderson et al. (1962), and Thomson et al. (1962).

Other properties of the normal Fermi liquid ^3He which are of interest are the viscosity η and quasiparticle mean free path $\lambda = v_F \tau$ with τ being the quasiparticle lifetime. The viscosity was calculated by Abrikosov and Khalatnikov (1959) from kinetic theory yielding

$$\eta(T) = \frac{64}{45} \frac{\hbar^3 p_F^5}{m^* k_B} \left(\frac{1}{k_B T} \right)^2 \langle G(\theta, \phi; \omega(\theta, \phi)) \rangle \sim T^{-2} \quad (11)$$

where $\langle G \rangle$ depends upon quantities averaged over the incident and scattered quasiparticle directions θ and ϕ and the transition probability ω . Measurements of η by Abel et al. (1961) and Betts et al. (1965) found the best fit below 100 mK to be

$$\eta(T) = (3.3 \pm 0.5) T^{-2} \text{ \mu poise}. \quad (12)$$

Finally, the quasiparticle lifetime is found to be

$$\tau = \frac{8\pi^4 \hbar^6}{m^{*3} \langle \omega \rangle (k_B T)^2}$$

from which the mean free path is

$$\lambda(P, T) \sim v_F(P) \frac{(10^{-12} \text{ sec})}{T(K)^2} \text{ meters} \quad (13)$$

where the Fermi velocity is in meters per second.

Theory of Superfluid ^3He B

Although ^3He forms at least three bulk superfluid phases (A, A_1 , and B), only the B phase was studied in this work. There follows the theory of the B phase of superfluid ^3He .

The Cooper Instability and BCS Theory

Since, in general, superfluidity is believed to be the result of Bose-Einstein condensation of a system of bosons into the macroscopic occupation of a single quantum state (London, 1954), there is no direct path by which a Fermi liquid such as ^3He can so condense.

Landau's Fermi-liquid theory dealt with two-quasiparticle interactions with quasiparticle collisions being handled in the determination of the transport coefficients. However, Cooper (1956) found that a special class of quasiparticle collisions could dramatically affect the system.

The collisions of concern are those between quasiparticles of equal and opposite momenta, \vec{k} and $-\vec{k}$, in the presence of the Fermi sea. Cooper's results showed that given the Legendre components $V_{\vec{k}}$ of the Fourier transformed two particle interaction $V_{\vec{k}\vec{k}'}$, thus

$$V_{\vec{k}\vec{k}'} = \int d\vec{r} \exp[-i(\vec{k} - \vec{k}') \cdot \vec{r}] V(r); \quad (14)$$

$$V_{\vec{k}}(k, k') = \frac{1}{4\pi} \int d\Omega V_{\vec{k}k}, P_{\vec{k}}(\cos \theta) \quad (15)$$

where $\cos \theta = \vec{k} \cdot \vec{k}'$, if any one of the components $V_{\vec{k}} < 0$, then there is a bound state of the two particles, the Fermi sea being unstable against the formation of this Cooper paired state.

In their work Bardeen, Cooper, and Schrieffer (1957) dealt with the full many-body problem. They considered the state of occupation of pairs of single-particle states of equal and opposite momenta and opposite spins, thus the states $\vec{k}\uparrow$ and $-\vec{k}\downarrow$. Constructing the system wave function from the products of the occupations of these pair states and through normalization and spin considerations, writing the energy of a momentum state $E_{\vec{k}}$ as

$$E_{\vec{k}} = +(\epsilon_{\vec{k}}^2 + |\Delta_{\vec{k}}|^2)^{\frac{1}{2}}, \quad (16)$$

where $\epsilon_{\vec{k}}$ is the usual particle energy measured relative to the Fermi energy and $\Delta_{\vec{k}}$ is a complex parameter, one may find the ground state by minimization of the total energy, $\langle E \rangle = \langle K \rangle + \langle V \rangle - \mu \langle N \rangle$. In this expression $\langle K \rangle$ is the expectation value of the kinetic energy, $\langle V \rangle$ is that for the two-particle interaction, and the term $\mu \langle N \rangle$ sets the energy scale relative to the chemical potential. To include the effect of finite (i.e., nonzero) temperature, all three states of occupation of the pair states must be included: (a) the state with both single-particle states occupied; (b) that with both single-particle states empty; and (c) that with one single-particle state filled and the other empty. Assuming that the probability of a particular state of occupation of the pair states is given by the Boltzmann distribution, the free energy which

is finally minimized with respect to the parameter Δ_k ,

$$F = \langle E \rangle - TS, \quad (17)$$

gives an integral equation of the form

$$\Delta_k(T) = - \sum_{k'} V(\vec{k}, \vec{k}') \frac{\Delta_{k'}(T)}{2E_{k'}(T)} \tanh\left(\frac{E_{k'}(T)}{2k_B T}\right), \quad (18)$$

which is the finite temperature BCS gap equation. The solution of the BCS problem is then reached by finding the complex parameter $\Delta_k(T)$ which solves the gap equation for a given $V(\vec{k}, \vec{k}')$. If the interaction energy of the Cooper pairing is dominated by a single Legendre component ℓ_0 then the transition temperature may be estimated from

$$k_B T_c = 1.14 \epsilon_c \exp\{-1/[1/2(dn/d\epsilon)V_{\ell_0}]\}, \quad (19)$$

where $V_{\ell_0} < 0$, and ϵ_c is a parameter which cuts off the interaction everywhere except near the Fermi surface. The parameter $\Delta_k(T)$ is known as the energy gap or the order parameter. The latter name is used because at $T > T_c$ only the trivial solution for the gap equation exists, while non-trivial solutions appear below T_c . In this manner $\Delta_k(T)$ fits the classic prescription for an order parameter of a system. Furthermore, since the interaction $V(\vec{k}, \vec{k}')$ is in effect only near the Fermi surface where $k = k' \approx k_F$, both $V(\vec{k}, \vec{k}')$ and $\Delta_k(T)$ are independent of the magnitudes of \vec{k} and \vec{k}' giving

$$\Delta_k(T) = \Delta(\hat{k}, T) \quad (20)$$

where \hat{k} is a quasiparticle unit vector on the Fermi surface.

In this manner, through the formation of pairs of spin- $\frac{1}{2}$ fermions into spin-0 Cooper pairs in the lowest relative angular momentum state ($\ell = 0$), the BCS theory successfully describes electronic superconductivity.

Attempts were made to make ^3He fit this isotropic (i.e., $\ell = 0$, $s = 0$) BCS theory (Cooper, Mills, and Sessler, 1959), but they failed due to the large hard core repulsive interaction between the atoms which prevents the $\ell = 0$ state from being obtained. Instead, ^3He forms the paired state in a relative orbital angular momentum $\ell = 1$ which, being antisymmetric on exchange of particles, requires the spin state to be symmetric, therefore the symmetric spin triplet state occurs giving $s = 1$. The first calculations involving this state with an eye toward ^3He were by Anderson and Morel (1960a, 1960b, 1961) and Balian and Werthamer (1963).

When two spin- $\frac{1}{2}$ particles combine into the $s = 1$ triplet there are three spin substates given by

$$\begin{aligned} m_s = +1 &\rightarrow |++\rangle, \\ m_s = 0 &\rightarrow \frac{1}{\sqrt{2}} (|++\rangle + |--\rangle), \\ m_s = -1 &\rightarrow |--\rangle. \end{aligned}$$

The order parameter may be written in terms of these components

$$\Delta(\hat{k}) = \Delta_{++}(\hat{k})|++\rangle + \Delta_{+-}(\hat{k})|+-\rangle + \frac{1}{\sqrt{2}}\Delta_{-+}(\hat{k})(|+-\rangle + |-+\rangle). \quad (21)$$

This may be expressed more conveniently (after Leggett, 1975) through the use of the Pauli spin matrices, σ_i , as

$$\Delta_{\alpha\beta}(\hat{k}) = i\Delta \sum_{i=1}^3 (\sigma_i \sigma_y)_{\alpha\beta} d_i(\hat{k}) \quad (22)$$

where the components d_i define a vector in spin space. The utility of this notation comes in identifying the order parameter, now contained in \hat{d} , for a particular system (B phase ^3He in this case). But first, to aid the interpretation of d_i it is useful to note that

$$\text{Tr}(\Delta\Delta^\dagger) = 2(d_1^2 + d_2^2 + d_3^2) = 2|\vec{d}(\hat{k})|^2 \quad (23)$$

so that the vector order parameter $\vec{d}(\hat{k})$ is seen to be the amplitude of the condensate wave function at a point \hat{k} on the Fermi surface. This rewriting may be carried a step further by expanding \vec{d} in terms of the complete orthonormal basis $k_{1\rho}$ in momentum space, thus

$$d_i(\hat{k}) = \sum_{\rho=1}^3 A_{i\rho} k_{\rho} \quad (24)$$

leaving the order parameter as a 3×3 matrix $A_{i\rho}$.

The Balian-Werthamer State

The work of Balian and Werthamer (1963) was the first calculation involving the spin triplet paired state in which all three of the $s = 1$ components were properly included. The order parameter which they found is believed to be the order parameter which describes the B phase of superfluid ^3He . Their result was

$$\Delta_{\mathbf{k}} = \Delta(\hat{\mathbf{k}}) \left(\frac{4\pi}{3} \right)^{1/2} \begin{pmatrix} \sqrt{2} Y_{11}(\hat{\mathbf{k}}) & Y_{10}(\hat{\mathbf{k}}) \\ Y_{10}(\hat{\mathbf{k}}) & \sqrt{2} Y_{1-1}(\hat{\mathbf{k}}) \end{pmatrix}$$

$$\Delta_k = \Delta(\hat{k}) \begin{pmatrix} -k_1 + ik_2 & k_3 \\ k_3 & k_1 + ik_2 \end{pmatrix}, \quad (25)$$

where the Y_{lm} 's are the spherical harmonics. In the matrix formulation the order parameter is

$$A_{i\rho} = \Delta e^{i\phi} R_{i\rho} \quad (26)$$

where $R_{i\rho}$ is a 3-dimensional rotation matrix which rotates the spin coordinates with respect to the momentum space coordinates. This rotation between coordinate systems is given by the axis of rotation \hat{n} and the amount of the rotation θ , $R_{i\rho} \rightarrow R(\hat{n}, \theta)$. This relative rotation may be expressed as

$$R(\hat{n}, \theta)_{i\rho} = (1 - \cos \theta) n_i n_\rho + \delta_{i\rho} \cos \theta + \epsilon_{ij\rho} n_j \sin \theta. \quad (27)$$

At this point there are no constraints on either \hat{n} or θ , giving a degenerate class of possible states.

The BW state is also known as the isotropic state since the magnitude of the energy gap is a constant over the Fermi surface. This name is misleading, however, as it will be seen that the BW state can exhibit macroscopic anisotropies.

A property of the BW state which affects any NMR measurement is the decrease in spin susceptibility which it suffers with respect to the normal Fermi liquid. This was first discussed by Balian and Werthamer (1963) where they found that

$$\chi_{BW}^{(T=0)} = \frac{2}{3} \chi_{NFL}; \quad (28)$$

however, Leggett (1965) later made the necessary Fermi liquid corrections giving the full temperature dependence as

$$\frac{\chi_{BW}}{\chi_{NFL}} = \frac{(1 + F_o^a)[(2/3) + (1/3)Y(T)]}{(1 + F_o^a[(2/3) + (1/3)Y(T)])} \quad (29)$$

where the Yosida function (Yosida, 1958) is

$$Y(T) = \frac{1}{4\pi} \int d\Omega \int_0^\infty d\varepsilon_k \frac{1}{2} \left(\frac{1}{k_B T} \right) \text{sech}^2 \left(\frac{E_k}{2k_B T} \right). \quad (30)$$

This dependence χ_{BW}/χ_{NFL} is shown in Fig. (2-1).

Nuclear Magnetic Resonance in Normal Systems

For a spin- $\frac{1}{2}$ system in zero magnetic field the spin substates $m = \pm\frac{1}{2}$ are degenerate. However, turning on a magnetic field H_o removes this degeneracy and allows for the possibility of resonant absorption of energy between the two levels at the Larmor frequency ν_o given by

$$\nu_o = \gamma H_o \quad (31)$$

where γ is the gyromagnetic ratio for the system which relates the magnetic moment $\vec{\mu}$ to the total angular momentum \vec{J} of the nucleus by $\vec{\mu} = \gamma \vec{J}$. For ^3He , $\gamma = 3.2435 \text{ kHz/G} = 2.0380 \times 10^8 \text{ sec}^{-1} \text{ T}^{-1}$.

The macroscopic static susceptibility, χ_o , is defined from the magnetization \vec{M} of the sample in a steady field \vec{H}_o by

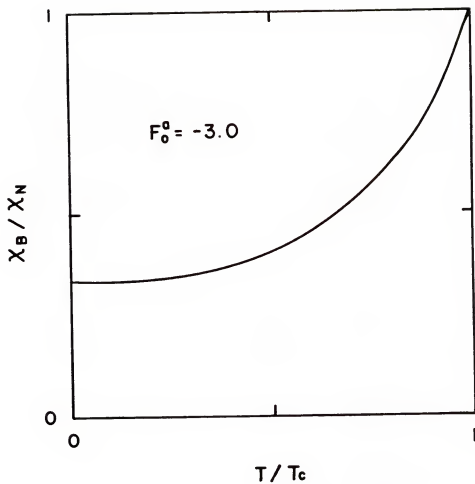


Fig. (2-1). X_B/X_N versus T/T_c from $T = 0$ to T_c .

$$\vec{M}_0 = \chi_0 \vec{H}_0. \quad (32)$$

The experimentally accessible quantity is the complex (or dynamic) susceptibility

$$\chi(\nu) = \chi'(\nu) - i\chi''(\nu), \quad (33)$$

where χ' is the dispersion and χ'' is the absorption. Use of the Kramers-Kronig equations (Andrew, 1958; Abragam, 1961) results in

$$\chi'(0) = \frac{2}{\pi\nu_0} \int_0^\infty d\nu' \chi''(\nu') = \chi_0. \quad (34)$$

Integration of the NMR absorption thereby measures the susceptibility. As has been mentioned, the susceptibility of bulk normal liquid ^3He is independent of temperature and occurs at the Larmor frequency.

Nuclear Magnetic Resonance in Superfluid ^3He

Superfluid ^3He differs from the normal Fermi liquid in that it can exhibit substantial shifts of the transverse NMR absorption from the Larmor frequency under certain conditions. In the first experiments on the B phase in bulk liquid samples, there was no shift observed (Osheroff et al., 1972a). However, subsequent measurements in restricted geometries did find a frequency shift (Osheroff et al., 1975; Webb et al., 1975; Ahonen et al., 1976). In addition, a longitudinal resonance mode (i.e., a mode of resonance with the radio-frequency excitation field H_{rf} parallel to the static field) was found which was field independent but did depend on temperature and pressure. This last was quite surpris-

ing as the usual concepts of NMR require H_{rf} to be perpendicular to H_0 in order to exert a torque on the spins and cause their precession at ν_0 , under the spin equation of motion

$$\frac{d}{dt} \vec{S} = \gamma \vec{S} \times \vec{H}(t) \quad (35)$$

where $\vec{H}(t) = \vec{H}_0 + \vec{H}_{rf}(t)$. All interactions which conserve the total spin S and its components S_i produce resonance only at ν_0 .

Once the liquid has condensed into the superfluid state, the largest interaction is expected to be the nuclear dipole-dipole interaction, all others including orientational energies being several orders of magnitude smaller (Leggett, 1975). In addition, as seen in its usual form

$$H_D = \frac{1}{2} \gamma \hbar^2 \sum_{ij} \left[\frac{\vec{\mu}_i \cdot \vec{\mu}_j}{|\vec{r}_i - \vec{r}_j|^3} - \frac{3\vec{\mu}_i \cdot (\vec{r}_i - \vec{r}_j) \vec{\mu}_j \cdot (\vec{r}_i - \vec{r}_j)}{|\vec{r}_i - \vec{r}_j|^5} \right], \quad (36)$$

the dipole interaction also breaks the spin-orbit symmetry and can produce a frequency shift. This expression can be cast into its triplet superfluid form (Leggett, 1972, 1973, 1974) by use of the vector order parameter \vec{d} of (22) to give

$$H_D = g_D \Delta^2 \int \frac{d\Omega}{4\pi} \frac{d\Omega'}{4\pi} \{ \vec{d}^*(\hat{k}) \cdot \vec{d}(\hat{k}') - 3\hat{q} \cdot \vec{d}^*(\hat{k}) \hat{q} \cdot \vec{d}(\hat{k}') \} \quad (37)$$

where $\hat{q} = (\hat{k} - \hat{k}')/|\hat{k} - \hat{k}'|$ and the strength of the interaction is $g_D(T) = 2\pi\gamma^2\hbar^2\Delta(T)/3$ which has been estimated by Leggett (1975) to be of order $10^{-3}(1 - T/T_c)$ erg/cm³, once a quasiparticle renormalization is considered. This is the contribution of the Cooper pairs to the dipole energy. The new spin equations of motion, from the system can

be written in terms of these quantities by calculation of the relevant commutation relations between \vec{d} and \vec{S} :

$$\frac{d}{dt} \vec{S} = \vec{S} \times \gamma \vec{H}(t) + \vec{K}_D \quad (38)$$

$$\frac{d}{dt} \vec{d}(\hat{k}) = \gamma \vec{d}(\hat{k}) \times \left(\vec{H}(t) - \gamma \frac{\vec{S}}{\chi} \right) \quad (39)$$

The additional dipolar torque is

$$\vec{K}_D = -\int \frac{d\Omega}{4\pi} \left(\left(\vec{d}(\hat{k}) \times \frac{\delta H_D}{\delta \vec{d}} \right) + \left(\vec{d}(\hat{k}) \times \frac{\delta H_D}{\delta \vec{d}} \right)^* \right). \quad (40)$$

It is this field-independent torque which results in the frequency shift in triplet superfluids. Combining (38) through (40) and considering small oscillations around equilibrium (as in unsaturated CW NMR) an eigenvalue equation in matrix form for the spin can be written

$$\ddot{S}_i = -\hat{\Omega}_{ij}^2 S_j, \quad (41)$$

with

$$\hat{\Omega}_{ij}^2 = \gamma^2 \chi^{-1} \hbar^{-2} [[S_i, H_D], S_j]$$

providing the restoring force for the spin. Rotation of coordinates to the principal axes of $\hat{\Omega}_{ij}^2$ diagonalizes the 3x3 matrix giving the three eigenvalues, in simplified form,

$$\Omega_i^2 = \frac{9}{2} \gamma^2 \chi^{-1} \left(\frac{g_D}{\hbar^2} \right) \text{Re} \int \frac{d\Omega}{4\pi} \left(|\hat{k} \cdot \vec{d}|_1^2 + \hat{k} \cdot \vec{d}^* k_{i1} d_1 - |\hat{k} \cdot \vec{d}|^2 \right). \quad (42)$$

If the static field H_0 is along the z-axis, these eigenvalues correspond to two transverse modes at frequencies

$$\nu^2 = \frac{1}{2} (\nu_0^2 + \Omega_x^2 + \Omega_y^2) \pm [(\nu_0^2 + \Omega_x^2 + \Omega_y^2)^2 - 4\Omega_x^2\Omega_y^2]^{\frac{1}{2}} \quad (43)$$

and a resonance along the field called the longitudinal resonance.

The system will respond in such a way as to minimize the dipolar energy. For the BW state this means that the spin and space coordinates will rotate until the rotation $R(\hat{n}, \theta)$ from (26) reaches

$$\theta_L = \cos^{-1}(-1/4) \approx 104^\circ,$$

the Leggett angle. This removes some of the degeneracy from the order parameter of (26), but the axis of rotation \hat{n} is still free. The vector \hat{n} may be influenced by the presence of other perturbations (to be discussed). Putting this result back into the BW state of (24) and (26) gives the order parameter optimized by the dipolar interaction. To determine the effect of H_D on the NMR properties this $\vec{d}(\hat{k})$ is substituted into the eigenvalue expression (42) with the result that there is no shift of the transverse resonance and there is a longitudinal resonance:

$$\Omega_x = \Omega_y = 0 \rightarrow \nu = \nu_0$$

and

$$\Omega_z = \Omega_B(T, P).$$

Since this calculation includes no other external forces (walls, fields, etc.) it is applicable to the bulk B phase and is in agreement with the observations.

To explain the existence of a transverse resonance shift in restricted or special geometries, it is noted that the \hat{n} vector, so far unconstrained, is forced to align with the direction of any external magnetic field. In this manner, if the field is along the z-axis, any rotations around the x or y axes require no dipolar energy and produce no transverse frequency shift. But rotations around the z-axis are constrained to the Leggett value with any attempted variation subject to large dipolar restoring forces to produce the longitudinal resonance. If other forces are present that cause the \hat{n} vector to deviate from the field direction, the longitudinal and transverse modes mix and a transverse frequency shift (Osheroff et al., 1975) appears as

$$\nu^2 = \frac{1}{2} (\nu_o^2 + \Omega_B^2) + \frac{1}{2} [(\nu_o^2 + \Omega_B^2)^2 - 4\nu_o^2\Omega_B^2\cos^2\beta]^{\frac{1}{2}} \quad (44)$$

where $\cos \beta = \hat{n} \cdot \hat{H}_o$. In the high field limit where $\nu_o = \gamma H_o \gg \Omega_B$ this simplifies to

$$\nu^2 = \nu_o^2 + \Omega_B^2 \sin^2 \beta. \quad (45)$$

Orientational Effects and Textures in the B Phase

To understand the NMR experiments on $^3\text{He-B}$ performed in this work it is necessary to include any orientational forces which can affect the \hat{n} vector of the B phase order parameter. These forces are orientational in nature in that they selectively depopulate the ordered system leaving

unchanged those Cooper pairs which are favorably aligned with respect to the forces.

To describe these forces, the method of choice has been to write down the effect as a free-energy expressing the orientational character of the force and perform a Ginzburg-Landau expansion of the free-energy near T_c . Engelsberg, Brinkman, and Anderson (1974) estimated the magnitude of the magnetic anisotropy energy due to the dipole interaction. Brinkman et al. (1974) calculated the forms of several of the interactions which concern us; the bending energy, surface energies and magnetic field energies. Fetter (1976) also derived similar forms for the same interactions and included the possibility of flow effects. Smith, Brinkman, and Engelsberg (1977) considered the individual effects and also performed calculations in which several of the forces were simultaneously present in specific geometries; their results will be applied directly to this work. Other works, including Leggett (1975), Brinkman and Cross (1978), Anderson (1978), and Lee and Richardson (1978), present both the forms of various interactions and estimates of their magnitudes.

The effects can be divided into two classes: those present in the bulk liquid and those which are due to the presence of surfaces.

In the bulk liquid B phase superfluid, the interactions of particular concern are; (1) the bulk-field energy, (2) the bulk-bending energy, (3) the bulk-flow energy, and (4) the field-flow energy. These first three are depicted in Fig. (2-2).

(1) The bulk-field energy attempts to align the \hat{n} vector of the order parameter along the field direction. In a system in which there is a susceptibility anisotropy, this kind of interaction would arise

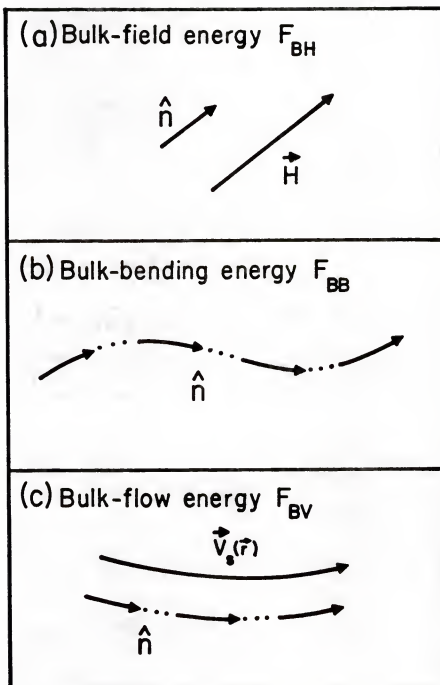


Fig. (2-2). Bulk liquid orientational energies: (a) the bulk-field energy, F_{BH} which attempts to align \hat{n} and \vec{H}_0 ; (b) the bulk-bending energy F_{BB} which smooths out spatial variations of \hat{n} ; (c) the bulk-flow energy which aligns \hat{n} and \vec{v}_s .

from the rotation of spin quantization axes in such a direction as to maximize the susceptibility along the field direction. In the B phase, with isotropic susceptibility, the force arises from the suppression of the Cooper pairs with $S_z = 0$ relative to those with $S_z = \pm 1$. The form of the free energy is

$$F_{BH} = -a \int d^3r (\hat{n} \cdot \vec{H}_0)^2, \quad (46)$$

where

$$a = \frac{35\xi(3)}{192\pi^2} \frac{1}{(1 + F_0^a)^2} \left(\frac{\bar{n}\omega_0}{k_B T_c} \right)^2 \chi_N.$$

In this expression for a , F_0^a is the zeroth antisymmetric Landau parameter, χ_N is the normal liquid susceptibility and ω_0 is given by $\Omega_B^2 = \omega_0^2(1-T/T_c)$. This aligning effect of the field is shown in Fig. (2-2a). The strength of the interaction is estimated to be $|a| \sim 4 \times 10^{-12}$ erg/cm³G². At the field of these experiments ($H_0 = 286$ G) $aH_0^2 \sim 3.3 \times 10^{-7}$ erg/cm³. A characteristic field can be defined as $(\chi_N - \chi_{BW})H_c^2 = 0.4g_D$ giving $H_c \sim 21$ G at $P = 21$ bar (PCP).

(2) The bulk-bending energy is due to the fact that the order parameter responds to local conditions which orient it but its response can not happen discontinuously. Any spatial variation occurs over finite distances. Since the energies are so small in comparison with the dipole energy, once again only the \hat{n} vector is affected. This interaction is expressed by invariant gradients of the order parameter (de Gennes, 1973) as

$$F_{BB} = c \int d^3r \{ 16(\hat{n} \times (\vec{\nabla} \times \hat{n}))^2 + 13(\vec{\nabla} \cdot \hat{n})^2 + 11(\hat{n} \cdot \vec{\nabla} \times \hat{n})^2 - 2\sqrt{15}(\vec{\nabla} \cdot \hat{n})(\hat{n} \cdot \vec{\nabla} \times \hat{n}) + 16\vec{\nabla} \cdot [(\hat{n} \cdot \vec{\nabla})\hat{n} - \hat{n}(\vec{\nabla} \cdot \hat{n})] \}, \quad (47)$$

where $c = (\hbar^2 \rho / 32m^*) (1 - T/T_c)$ with $m^* = m(1 + (1/3)F_1^S)$. F_{BB} tends to smooth out any spatial variation of the \hat{n} vector field, as shown in Fig. (2-2b).

(3) The bulk-flow energy arises by analogy with the bulk-field energy. In this case, an impressed superflow (flow of the superfluid) aligns the \hat{n} vector field along the flow direction, expressed as

$$F_{BV} = -e \int d^3r (\hat{n} \cdot \vec{v}_s)^2 \quad (48)$$

with $e \sim g_D(T)(p_F/\Delta(T))^2/v_c^2$ where the characteristic velocity is on the order of $v_c \sim 0.8$ mm/sec at the PCP (Fetter, 1976). This is shown in Fig. (2-2c).

(4) The field-flow energy arises as a cross-term in dealing with a situation in which both a magnetic field and a superflow are present. It expresses the competition, in part, between these two forces. Its form is

$$F_{HV} = -f \int d^3r (\vec{v}_s \cdot \vec{\hat{R}})^2 \quad (49)$$

where $\vec{\hat{R}} = \hat{R}(\hat{n}, \cos^{-1}(-1/4))$. The effect of this term will be discussed in detail in connection with the surface energies.

There are two surface energies which are important in these experiments: (1) the surface-dipole energy, and (2) the surface-field energy. Their effects are shown in Fig. (2-3).

(1) The surface-dipole energy comes about by the suppression by a wall of the $m_L = 0$ component of the orbital angular momentum of the Cooper pairs with respect to the surface normal vector \hat{s} . It is expressed as

$$F_{SD} = -b \int d^2r (\hat{n} \cdot \hat{s})^2 \quad (50)$$

with $b = \xi \Omega_{BW}^2 / 5\gamma^2$, ξ being the coherence length of the order parameter (the shortest distance over which it can vary) and equalling

$$\begin{aligned} \xi(T) &= (7\zeta(3)/48)^{1/2} (\hbar v_F / \pi k_B T_C) / (1 - T/T_C)^{1/2} \\ &= (7\zeta(3)/48)^{1/2} \xi_0 / (1 - T/T_C)^{1/2}, \end{aligned} \quad (51)$$

where $\zeta(3)$ is the Riemann Zeta function, $\zeta(3) \approx 1.20205$. The quantity ξ_0 is the correlation length of the quasiparticles forming the Cooper pairs and ranges from 1160 Å at $P = 0$ bar to 280 Å at the melting curve. This energy tries to align the \hat{n} vector with the surface normal \hat{s} , as shown in Fig. (2-3a). This energy is by far the smallest of all in the usual experimental magnetic fields.

(2) The surface-field energy expresses the interplay between the surface-aligning and field-aligning forces when both are present at a surface. It is written as

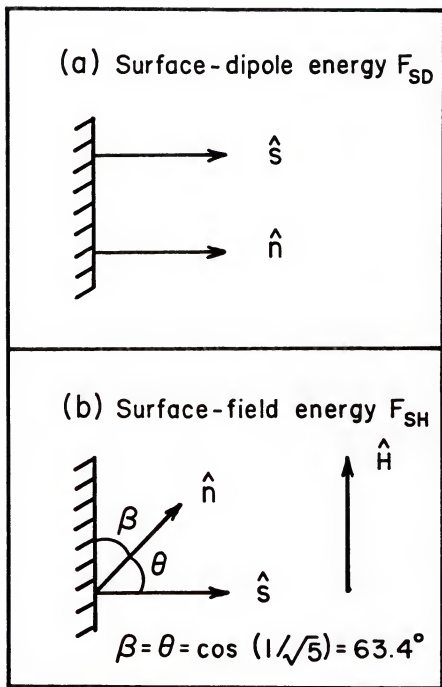


Fig. (2-3). Surface orientational energies: (a) the surface-dipole energy F_{SD} which aligns \hat{n} to the surface normal \hat{s} ; (b) the surface-field energy F_{SH} in a configuration with $\hat{n} \perp \hat{s}$. The resulting \hat{n} vector is at an angle $\cos^{-1}(1/\sqrt{5})$ with respect to \hat{H} and \hat{s} .

$$F_{SH} = -d \int d^2r (\hat{s} \cdot \vec{R} \cdot \vec{H})^2.$$

Insertion of the expression for $R(\hat{n}, \theta)_{1\rho}$ in (27) with the Leggett value of $\cos^{-1}(-1/4)$ changes this easily to

$$F_{SH} = -\frac{25}{16} d \int d^2r [(\hat{n} \cdot \hat{s})(\hat{n} \cdot \vec{H}) + \sqrt{3/5} \hat{n} \cdot (\hat{s} \times \vec{H}) - \frac{1}{5} \hat{s} \cdot \vec{H}] \quad (52)$$

where $d \sim \xi(T)(\chi_N - \chi_B)$. The field-flow energy of (49) would take the same form by replacing \hat{s} with \vec{v}_s . The surface-field energy F_{SH} (and F_{HV}) depend upon the experimental configuration of walls and fields (and superflows). In the simplest case with \hat{s} and \vec{H} parallel (\vec{H} and \vec{v}_s parallel for F_{HV}), F_{SH} (or F_{HV}) is minimized for the \hat{n} vector also parallel to these two vectors. Another important configuration is when \hat{s} and \vec{H} are perpendicular (\vec{H} and \vec{v}_s perpendicular). For definiteness, take \vec{H} to be the x-axis, $\hat{s} \times \vec{H}$ on the y-axis, and \hat{s} on the z-axis (see Fig. (2-3b)). Taking $\hat{n} \cdot \hat{s} = \cos\theta$ and $\hat{n} \cdot \vec{H} = \cos\phi$ and writing $\hat{n} = (\sin\theta\cos\phi, \sin\theta\sin\phi, \cos\theta)$, the energy per unit area at the surface is

$$f_{SH} = -\frac{25}{16} dH^2 (\cos\theta\sin\theta\cos\phi + \sqrt{3/5} \sin\theta\sin\phi)^2. \quad (53)$$

Minimization of this with respect to ϕ yields the solution

$$\tan \phi = \frac{\sqrt{3/5}}{\cos \theta}.$$

Upon substitution of this result back into (53) a second minimization with respect to θ gives

$$\cos^2 \theta = 1/5 \rightarrow \theta = 63.4^\circ.$$

This then is the angle between \hat{n} and \hat{s} . Simple geometry finally gives the result important for NMR, the angle between \hat{n} and \hat{H} , as

$$\cos^2 \beta = \sin^2 \theta \cos^2 \phi = 1/5, \quad (54)$$

the same angle. The interpretation of this result, with the unusual angles between the \hat{n} vector and \hat{s} and \hat{H} , is straightforward. Referring to Fig. (2-4) in which the three vectors are illustrated, it can be rather easily shown that with \hat{n} residing at the given angle $\cos^{-1}(1/\sqrt{5})$, a rotation about the \hat{n} axis of the Leggett angle $\theta_L = \cos^{-1}(-1/4)$ rotates the surface normal vector \hat{s} into the magnetic field direction. Thus, these two perturbations which separately would align \hat{n} to minimize either the $m_s = 0$ (\vec{H}) or $m_L = 0$ (\hat{s}) component with respect to their directions, when acting together at a surface rotate \hat{n} to simultaneously minimize both components while maintaining the Leggett angle forced by the dipole interaction.

The presence of several of these orientational energies at the same time, as is unavoidable in an experiment, produces a competition amongst them for the alignment of the \hat{n} vector field of the ^3He sample. Being a physical system, the $^3\text{He-B}$ seeks to minimize its total free energy and will find the configuration of \hat{n} which achieves this. The resulting construct, a continuous variation of \hat{n} across the sample, is called an \hat{n} texture (de Gennes, 1973). For this B phase work, two specific textures are of interest: the texture in a narrow slab of $^3\text{He-B}$; and the texture in a cylinder of $^3\text{He-B}$. Both of these have been calculated

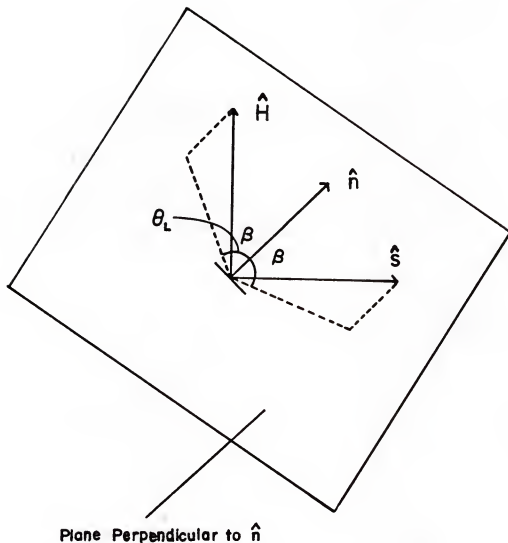


Fig. (2-4). The effect of F_{SH} on \hat{n} when \hat{s} is perpendicular to \hat{h} . The plane is perpendicular to the \hat{n} vector and shows that rotation about \hat{n} by $\theta_L = \cos^{-1}(-1/4)$ takes one from the \hat{s} direction to the \hat{h} direction.

by Smith, Brinkman, and Engelsberg (1977). By taking ratios of the various strength coefficients in the free-energy expressions, they introduce several constants characteristic of the interactions. One combination of these will be of particular relevance to this work. A characteristic length and magnetic field can be defined respectively as

$$R_c = c/b \quad \text{and} \quad H_B = (b^2/ac)^{1/2},$$

using the coefficients from the bulk-bending (c), surface-dipole (b), and bulk-field (a) free-energies. The product of these plays a part in the transverse resonance lineshape (Brinkman et al., 1974; Osheroff, 1975). It is given by

$$\begin{aligned} R_c H_B &= (c/a)^{1/2} \\ &= 1.32[(1 + F_O^a) \chi_N / \chi_B]^{1/2} (\Delta g/g)^{-1/2} (E_F / \hbar \gamma k_F) (1 - T/T_c)^{1/2}. \end{aligned} \quad (55)$$

Their results for the two \hat{n} textures were the following:

Texture in a slab geometry

The geometry in question is a rectangular slab of $^3\text{He-B}$ formed by two walls separated by a distance $l = 0.5 R_c H_B / H$. The walls are both parallel to the xy -plane, the surface normal being in the z direction.

As already stated, in the presence of parallel field and surface normal, F_{SH} is minimized for parallel \hat{n} as well. This simultaneously minimizes all the other non-flow free-energies (F_{BH} and F_{SD} are trivially minimized, $F_{BB} = 0$). This slab texture is shown in Fig. (2-5a).

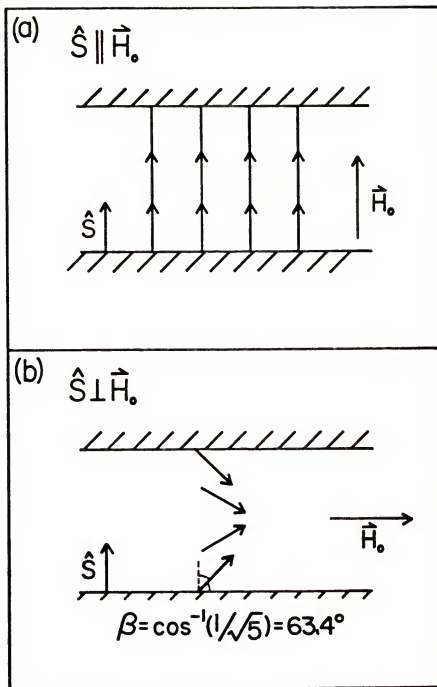


Fig. (2-5). \hat{n} textures in a slab: (a) for parallel \hat{S} and \vec{H} ; (b) for perpendicular \hat{S} and \vec{H} .

For the situation of perpendicular \vec{H} and \hat{s} (taking the same orientations as in Fig. (2-3b)) it is necessary to minimize $F_{BB} + F_{BH} + 2F_{SH}$. The \hat{n} vector is once again written in its spherical coordinates (θ, ϕ) and a variational solution is sought. The important point for NMR is $\beta = \beta(z) = \cos^{-1}(\hat{n} \cdot \hat{H})$ and the result is

$$\cos^2(\beta(z)) = \frac{1}{5} \left\{ 1 + \frac{13}{64} \left(\frac{\ell H}{R_c H_B} \right)^2 \left(1 - \frac{4z^2}{\ell^2} \right) \right\} \quad (56)$$

which gives the proper boundary conditions for β at the walls. This is shown in Fig. (2-6).

Texture in a cylindrical geometry

There are presumably many conceivably stable \hat{n} textures in a cylinder. Smith et al. (1977) considered two of the simplest and only one of these is stable in a magnetic field along the cylinder axis, the flare-out texture. To make their calculation tractable, they worked in the limit of low fields ($H \ll R_c H_B / R$, R = cylinder radius) where the only important free-energies were the bulk-bending F_{BB} and the surface-dipole F_{SD} . The \hat{n} vector was parametrized in cylindrical coordinates as

$$\hat{n} = (n_x, n_y, n_z) = (\cos \alpha \sin(\beta r/R), \sin \alpha \sin(\beta r/R), \cos(\beta r/R))$$

with α being the azimuthal angle and $\beta = \cos^{-1}(\hat{n} \cdot \hat{z})$ and $\vec{H} = H\hat{z}$. The small magnetic field is along the z-axis. The result, shown in Fig. (2-7), is a texture in which there is varying amounts of alignment of \hat{n} with \vec{H} . In Fig. (2-7a) the flare-out texture is seen in a cross-section along the cylinder axis, in Fig. (2-7b) the cylinder is seen

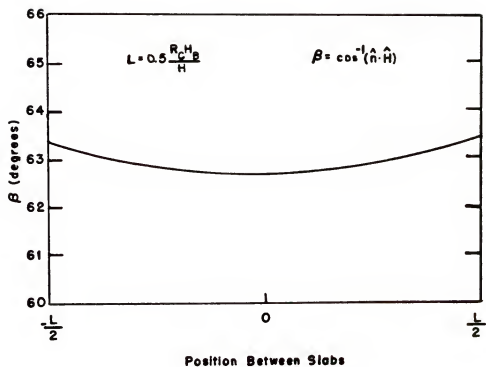


Fig. (2-6). Angle β between \hat{n} and \hat{H} across a slab of thickness $l = 0.5R_C H_P/H$ for δ perpendicular to \hat{H} . (After Smith et al., 1977.)

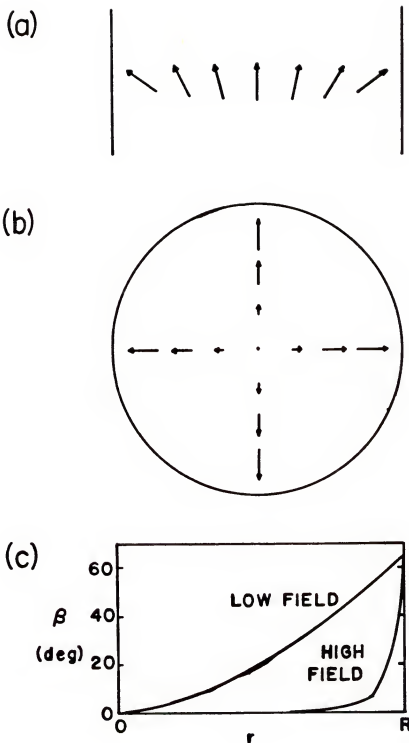


Fig. (2-7). Flare-out texture in a cylinder: (a) cross-section along the cylinder axis showing the \hat{n} vector field; (b) endview of cylinder; (c) low and high magnetic field behaviour of $\beta = \cos^{-1}(\hat{n} \cdot \hat{H})$ treating F_{BH} and F_{SH} as perturbations on $F_{BB} + F_{SD}$. (From Smith et al., 1977.)

end-on. Although the \hat{n} vector as parametrized had an azimuthal component due to α , this calculation could make no statement about it due to the symmetry of F_{SD} (which would allow no azimuthal component at the wall). Finally, by treating F_{BH} and F_{SH} as perturbations on the first two free-energies ($F_{BB} + F_{SD}$), an estimate of the behavior in low and high magnetic fields of β was given, shown in Fig. (2-7c).

Other Experimental Results

The effects of \hat{n} textures on the magnetic properties of ^3He have been seen in several other experiments, principally through use of NMR.

The lack of a frequency shift in the B phase in the very first NMR experiment (Osheroff et al., 1972a) was itself a texture effect caused by the bulk liquid geometry and F_{BH} . Over most of the sample \hat{n} was parallel to \vec{H} and thereby the shift from the Larmor frequency was zero. Osheroff and Brinkman (1974) observed a texture effect in a transverse NMR experiment in a large cylinder (1.6 cm diameter) by the presence of a high-frequency tail on the resonance line, caused by the presence of bending of \hat{n} away from the field. More quantitative results were measured in a slab geometry by Osheroff et al. (1975) and Ahonen et al. (1975). In the former experiment, the geometry was formed by flat Mylar sheets separated by 127 μm spacers with the magnetic field parallel to the sheet planes (perpendicular to the sheet surface normal vector). In this case, the surface-field energy F_{SH} should dominate and with these orientations, the \hat{n} vector would make an angle of $\cos^{-1}(1/\sqrt{5})$ to the field. Two of the bulk energies, F_{BB} and F_{BH} , caused some very slight bending of \hat{n} away from this angle in the middle of the slabs. Being at high pressure (near the melting curve) the B phase only existed below

$T/T_c \leq 0.75$. By variation of the temperature and field (298 G to 1545 G) it was possible to get an estimate of the magnetic length, finding as best fit $R_c H_B = 36(1 - T/T_c)$ cm G. This temperature dependence differed from that expected from the theory (see (55)). The latter experiment was similar, with spacers of 370 μm and the possibility of varying the magnetic field direction. The RF coils were situated to see both confined liquid and bulk liquid, giving rise to two peaks in the absorption. This experiment was subsequently repeated using spacers of both 4 μm and the original 370 μm (Ahonen et al., 1976). The thinner slabs, being much more confined, showed less bending and thus more signal at the surface-field confined angle of 63.4° . In addition, these authors measured the longitudinal resonance frequency as a function of temperature and pressure. Their results are shown in Fig. (2-8). Webb, Sager, and Wheatley (1977) measured the magnetic response of the B phase by turning a small magnetic field off and using SQUID techniques to follow the magnetization thereafter. The fields turned off were $\Delta H \leq 12$ G. In such small fields, as calculated by Smith, Brinkman, and Engelsberg (1977), F_{SD} will dominate with F_{SH} and F_{BH} providing perturbations. Calling the surface-dipole texture the "wall-pinned mode" (WPM) the authors found that this texture was extinguished (i.e., the magnetization ringing characteristic of this texture disappeared) at constant temperature for increasing initial field ΔH . Using their results they crudely estimated the bending length temperature dependence as $(1 - T/T_c)$ although stating that their results were "somewhat scattered and irreproducible." (See Webb et al., 1977, page 458.)

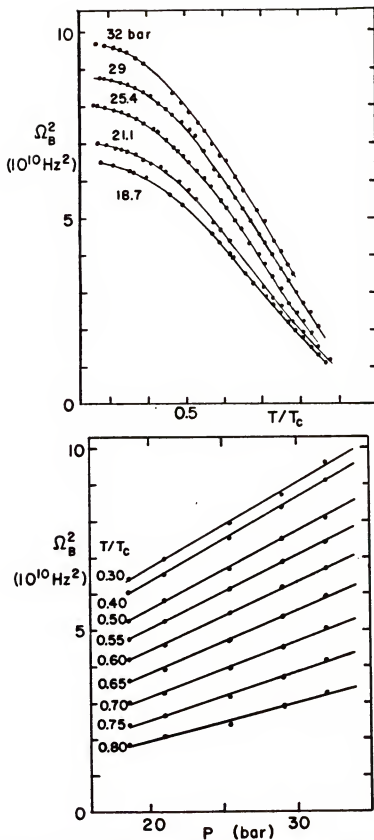


Fig. (2-8). The B phase longitudinal resonance frequencies as a function of T/T_c for several pressures. (Adapted from Ahonen et al., 1976.)

Liquid ^3He in an Extremely Confined Geometry

There are several reasons to study ^3He in an extremely restricted geometry. By placing the liquid (or thin film) in such a system one effectively magnifies the ^3He -substrate interaction above that in a bulk liquid system by the surface-to-volume ratio. This allows the experimental investigation of the fundamental physics involved in the liquid-substrate interaction. This kind of experiment is also important for ultra-low temperature technology. The surface and near-surface interactions are responsible for thermal contact between the ^3He and the substrate. A better understanding of this process can lead eventually to the resolution of the long-standing Kapitza thermal boundary resistance problem (Lounasmaa, 1974b). One could also hope to observe a new state of the liquid or possibly some exotic behavior not seen elsewhere. For example, several theoretical calculations have indicated that a thin-film superfluid phase could exist even when the film thickness is smaller than the coherence length ξ_0 (Barton and Moore, 1975; Tesanovic and Valls, 1984, 1986; Buchholtz, 1984, 1986).

Nuclear Magnetism of Confined ^3He

The magnetic properties of liquid ^3He near a substrate have been studied for some time. The generally accepted model of the density profile of ^3He in vycor has the first layer compressed to the density of bulk solid at 400 bars, the second layer being comparable to bulk liquid near the melting curve and the remaining atoms at the density of liquid at saturated vapor pressure. Theoretical calculations are performed with ^3He atoms at and near a surface. Experimentally, to be able to observe such effects requires the confinement of the ^3He in a porous medium.

Those media which have been used include sintered metal powders (e.g., copper and silver), exfoliated graphite, and insulating substrates (e.g., fluorocarbon spheres and vycor glass). The properties measured are generally the magnetic susceptibility (in some form or other) and the spin relaxation times (the spin-lattice relaxation time T_1 and the spin-spin relaxation time T_2). Concentration will be placed here on the susceptibility.

In susceptibility measurements an enhanced susceptibility of confined liquid over that of bulk liquid is observed. At the lowest temperatures this enhancement is believed due to the approach of the atoms near the surface to a ferromagnetic ordering with a Curie-Weiss temperature $\theta \lesssim 1$ mK. Several models have been suggested to explain these results. A paramagnon effect between the first solid layer of ^3He at the surface and the paramagnetic liquid was suggested by Béal-Monod and Doniach (1977). Guyer (1977) performed calculations on a model that used vacancies to induce the surface ferromagnetism. Delrieu et al. (1980) used cyclic three-particle exchange in the solid layer on the surface to produce the effect. A model popular because of its ability to arrive at exchange constants with the correct order of magnitude when compared with the observed θ is that due to Jichu and Kuroda (1982). In their second-order perturbation theory calculation, a modified Ruderman-Kittel-Kasuya-Yosida (RKKY) indirect spin exchange (Ruderman and Kittel, 1954; Kasuya, 1956; Yosida, 1957) between the adsorbed atoms mediated by the liquid atoms is responsible for the ferromagnetism. The Hamiltonian for spin-dependent interactions in the solid layer is written as

$$H_{\text{ex}} = - \sum_{i < j} J_{ij}^{(d)} \vec{s}_i \cdot \vec{s}_j \quad (57)$$

where $J_{ij}^{(d)}$ is the exchange constant. By performing a simplified calculation on a semi-infinite system of ^3He atoms bounded by a plane, the value for nearest neighbor atoms is

$$J_{ij}^{(1)} \approx 0.15 \text{ mK.} \quad (58)$$

Since J is positive, the interaction is ferromagnetic and the transition temperature can be found from mean field theory, where z is the number of nearest neighbors, to be

$$T_c = zJ_{ij}^{(1)}/2 \approx 0.45 \text{ mK.} \quad (59)$$

In addition to these calculations, two experiments should be mentioned. In the first Bozler et al. (1983) measured the susceptibility of ^3He in exfoliated graphite. In this system, the graphite is believed to be oriented into parallel planes with individual planar crystallites being a few hundred Angstroms on a side. The authors reported a deviation from the Curie-Weiss law, $\chi \propto (T - \theta)^{-1}$, below about 1.5 mK, with a Curie-Weiss temperature of 0.8 mK. Also, they measured a shift in frequency of the resonance which changed sign depending on the orientation of the magnetic field with respect to the basal planes of the graphite. For a field perpendicular to the surface normal vector, the shift was negative ($\Delta\nu = \nu - \nu_0 < 0$) while for a field parallel to the surface normal it was positive. They found rough agreement between this result and a calculation of a polarized two-dimensional sheet of spins made by Richards and Salamon (1974). In the second experiment, Okuda et al. (1985) studied a multilayer film of ^3He adsorbed on sintered 1000 Å

silver powder. They found that for films with less than six atomic layers, the susceptibility of the ^3He was Curie-like, $\chi \propto 1/T$, with the Curie constant increasing with film thickness. For films with six or more layers, the susceptibility obeyed the Curie-Weiss law with $\theta \approx 0.4$ mK. This value of θ was roughly constant from eight layers through to completely filled pores at s.v.p. This result seems to indicate that the ferromagnetism occurs only when there are six or more layers present on the substrate, in general agreement with the calculation of Jichu and Kuroda (1982).

Flow of Confined Liquids

There are many types of fluid flow some of which might be expected to occur in confined liquid ^3He . First, a very short review of the major classes of fluid flow is presented. In this only low flow rates are considered so that no effects of turbulence are discussed.

The simplest class of fluids is called Newtonian. These are fluids in which the viscosity depends only on temperature. The most common example is water. Fluids in which the viscosity depends upon flow rate or shear stress are called non-Newtonian. The simplest kind of flow in a real Newtonian fluid is viscous flow. In this flow the mass current is directly proportional to the differential pressure during the flow as

$$J(t) = \Delta P(t)/Z \quad (60)$$

with the proportionality constant being the inverse of the flow impedance Z . The impedance in turn depends upon both geometrical factors of the flow apparatus as well as the density ρ and viscosity η . For

flow through a straight pipe, commonly referred to as Poiseuille flow, this expression becomes

$$J(t) = \frac{\pi r^4 \rho}{8\eta \ell} \Delta P(t) \quad (61)$$

where r is the pipe radius and ℓ is the length (Landau and Lifshitz, 1978). The flow of a superfluid in which there is no normal fluid flow is called pure superflow and may be regarded in the simplest terms as the motion of a liquid with zero viscosity. If the velocity is increased, a critical value may be approached at which the pure superflow begins to either saturate or break down in various ways (e.g., formation of vortices).

Another type of flow is encountered when the mean free path of the particles in the fluid is comparable in size to the container dimensions. This is called Knudsen flow (Knudsen, 1909,1950; Hirschfelder et al., 1954). The mass current for Knudsen flow is

$$J \propto \frac{\lambda}{\eta} \frac{r^3}{\ell} P_m \frac{\Delta P}{P}, \quad (62)$$

where λ is the mean free path, P_m is the mean pressure across the capillary, and J is measured at pressure P . It should be noted that the quasiparticle mean free path in ^3He (equation 13) is smaller than (or at best comparable to) the pores in vycor glass at all temperatures and pressures. For example, at 3 bars, the quasiparticle mean free paths at 1 mK, 10 mK, and 100 mK are 50 μm , 5000 \AA , and 50 \AA , respectively. For this reason, Knudsen flow is the expected result of ^3He flow experiments in confined geometries. Calculations have been performed (Jaffe, 1979;

Jensen et al., 1980) to determine the behavior of Fermi liquids, specifically ^3He , in such conditions. Jaffe (1979) derived an integral equation for the velocity profile and through numerical solution found the current through the confined geometry as a function of the ratio of cell dimension d to mean free path. In his calculation a certain fraction of quasiparticles was assumed to be specularly reflected at the walls. Jensen et al. (1980) calculated the effect of slip motion at the walls of the container on the measured viscosity of ^3He above and below T_c . They included interactions in the Fermi liquid and an explicit time dependence in order to use their results to take account of frequency-dependent effects seen in torsion oscillator and vibrating wire experiments (Reppy, 1978; Alvesalo et al., 1975). They noted that their calculation would break down at $d/\lambda \rightarrow 1$, with deviations appearing at $d/\lambda \lesssim 5$.

The flow of many fluids through porous media is found to obey Darcy's law (Darcy, 1856; Scheidegger, 1960) which takes the form

$$\mathbf{J} = - \frac{k}{\eta} \Delta \vec{P}, \quad (63)$$

where k is the specific permeability of the porous medium.

Finally, anticipating the results of the ^3He -vycor flow experiment, the concept of a viscoelastic fluid is introduced. These are fluids which exhibit the characteristics of both viscous fluids and elastic solids although this is not the limit of their behavior. Viscoelastic fluids are non-Newtonian so that $\eta = \eta(T, \tau)$, where τ is the shearing stress felt by the fluid (Brodkey, 1967; Pipkin, 1972; Harris, 1977). There are many subclasses of viscoelastic behavior, two major ones being the shear-thinning and shear-thickening fluids. In these two subclasses

the behavior is quite simply separated by the variation of the viscosity with shear stress:

$$\text{shear-thinning fluids} \quad \partial\eta/\partial\tau < 0; \quad (64)$$

$$\text{shear-thickening fluids} \quad \partial\eta/\partial\tau > 0. \quad (65)$$

In Fig. (2-9a) is shown the shear rate κ as a function of shear stress τ for these two fluids. In the case of shear-thinning materials, sometimes a non-zero shear stress τ_{yield} is required to generate flow, this being called the minimum yield stress. In many materials after the application of the shear stress, the material relaxes in such a way as to completely relieve the shear. This is called a fluid response. However, some cases exist in which the limiting value of the stress appears to be non-zero. Such a system is usually designated as a solid although it may be that the relaxation time is very long compared to the experimental time. Shown in Fig. (2-9b) are these two types of responses. Common examples of viscoelastic fluids abound in everyday life: the ink in a ball-point pen is a shear-thinning fluid (it must have a low viscosity as the ball is run along the paper) while quicksand (or the wet sand strip at the seashore) is a shear-thickening fluid due to the property called dilatancy. Other examples include cornstarch solutions, some kinds of paints, clay, talc, mayonnaise, and tooth paste. Viscoelastic behavior can become much more complicated. In some fluids under shear stress the internal structure making up the fluid is broken down as time passes. This causes the viscosity to be a function of time as well. In the shear-thinning case these fluids, such as polymers, are called thixotropic while the shear-thickening case is called antithixotropic.

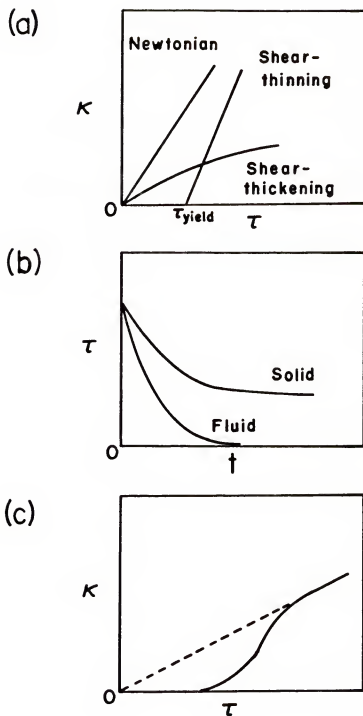


Fig. (2-9). Some properties of viscoelastic fluids. (a) Shear rate κ as a function of shear stress τ for both a shear-thinning and a shear-thickening fluid. (b) The shear stress as a function of time in two systems; one a fluid-like response, the other solid-like. (c) Shear rate versus shear stress for a shear-thinning fluid with a high-shear stress Newtonian region.

In most cases the breakdown is reversible upon cessation of the shear. Beyond this behavior, many fluids exhibit hysteresis making the understanding of them quite difficult. And finally, by going to high shear stress some fluids apparently enter a Newtonian regime in which $\kappa \propto \tau$ as in ordinary viscous fluids. This is shown in Fig. (2-9c).

CHAPTER III

EXPERIMENTAL APPARATUS

Refrigeration

The cryostat on which these experiments were performed consisted of a homemade dilution refrigerator and a copper nuclear demagnetization stage.

The dilution refrigerator was designed, assembled and made operational by Dr. E. B. Flint with the help of Dr. E. D. Adams. At maximum power the fridge circulates approximately 40 micromoles per second of ^3He . The minimum temperature without a load is 10 mK. With an experiment including a demagnetization stage mounted, a temperature of 25 mK can be reached in three days at which the demagnetization can be started.

The demagnetization stage, where the experiments are mounted, has some 7000 insulated copper wires (Allex insulation, diameter = 0.51 mm from Essex Corp.) in a close-packed cylindrical form giving some 60 moles of copper residing in the main magnetizing field. This field is produced by a commercially-built compensated superconducting solenoid (designed by Dr. Ihas, built by Americal Magnetics) with an inductance of 20.8 H and a central field of 80 T at 73.5 A.

This refrigeration system is capable of producing the temperatures required to perform milli-Kelvin experiments over the course of days and even weeks. A typical temperature cycle would start with the mag-

netization of the bundle, warming the nuclear stage and experiment to about 80 mK. The dilution fridge then cools the system back down to $T = 25$ mK in about three days. At $T \leq 25$ mK, the nuclear stage is isolated from the fridge and a demagnetization is performed, reducing the main field from 8.5 T to about 3.5 T in 30 minutes to one hour. This reduction is followed by a much slower reduction of field to final fields less than 0.2 T in a period of 10 hours. If $T_i = 30$ mK, then this demag would reach $T_f = 0.7$ mK, if ideal. The heat capacity after demagnetization, coupled with a low heat leak (heat leaks of 1 nanowatt or less are desired), permits the experiment to remain at these low temperatures for several days at least, up to a few weeks if one is very gentle during the experimentation.

Helium usage by the cryostat averages 14 liquid liters per day, transfers (refills) occurring every 3 to 3.5 days and using 41 liquid liters per transfer. (These numbers were compiled over the course of the last experiment (^3He in vycor) which at the time of writing had run for 155 days and had used 2158 liquid liters of helium in 51 transfers.) Virtually all of this helium was recovered during boil-off to be later reliquefied. The other consumable cryogen used in the operation of the cryostat was liquid nitrogen used for trapping various forms of impurities in the fridge and gas-handling systems (e.g., air, water vapor, pump oil) at the rate of about 6 liquid liters per day.

Experimental Cell Heat Exchanger

To provide good thermal contact between the experimental cell and the refrigeration stages of the cryostat is one of the most difficult problems in the field of low temperature physics. Special effort is

required to first cool the experiment to low temperature and maintain reasonable thermal contact while there. The device used to provide this service is the cell heat exchanger, so-called because the experimental cell is mounted to it and the heat exchanger in turn mounts on the demagnetization stage. The typical heat exchanger uses a pressed or sintered metal powder to achieve a large surface area per unit volume allowing better heat conduction from the sample to the exchanger. To optimize the exchanger's physical design, by which is meant to minimize the temperature difference ΔT between the ^3He and the copper demagnetization bundle, the quantities of interest include the thermal conductivity of the liquid inside the sinter and that of the sinter itself as well as the boundary resistance at the interface between the sintered powder and the liquid. In a detailed analysis, Muething (1979) calculated the maximum thickness of sinter material which could be interposed between the liquid and the copper cell in order to minimize ΔT . This thickness was found to be 0.5 cm for $T \leq 10$ mK using $2\text{ }\mu\text{m}$ Pd powder.

The heat exchanger used in these experiments is shown in cross-section in Fig. (3-1). The body material is OFHC copper. Three sets of concentric wells were milled out of the body. The body started as a 10.5 cm diameter rod stock of copper, cut to a length of 3.5 cm. The wells, to be used to pack the metal particles, were 1.59 cm deep, the outer diameter of the largest to the smallest being 2.54, 1.75, and 0.95 cm, respectively, with walls of 0.08 cm separating each well and a 0.318 cm central rod in each. The center set of wells has only the two smallest diameters. The line of 0.318 cm diameter thru-holes at the bottom of the wells allows liquid ^3He to enter the bottom of the heat exchanger for filling and flow purposes, to be discussed shortly.

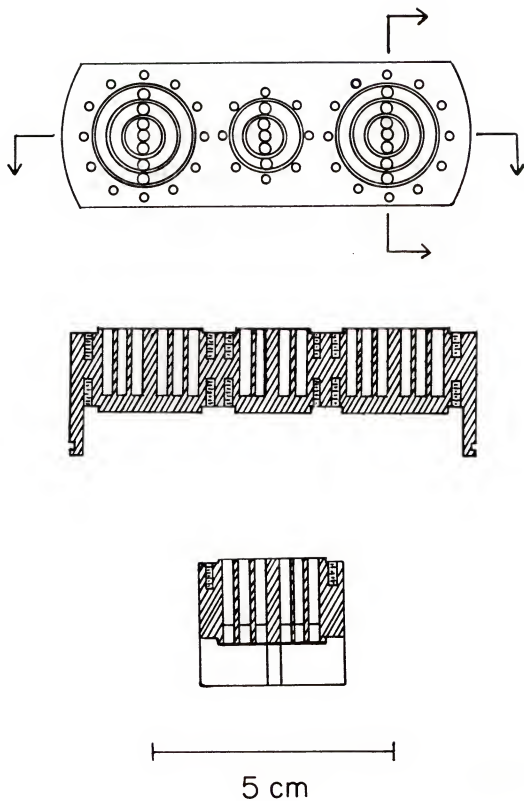


Fig. (3-1). Cross-section of the Pd heat exchanger used to thermally connect the experimental cell to the demagnetization stage.

Around each set of wells, circles of tapped bolt holes were cut to allow flanges to be secured to the body, both top and bottom.

The metal powder chosen to be used in this exchanger was 1 micron palladium powder (Leico Industries). Palladium was chosen for several reasons, chief among them being: no superconducting transition in the milli-Kelvin region (although some experiments indicate that sufficient H_2 saturation of the Pd powder at sintering temperatures may form a compound which does superconduct, rendering it useless for thermal contact); a high paramagnetism which is hoped to enhance the thermal contact with liquid 3He through magnetic boundary coupling; and finally no formation of surface oxides which might increase the thermal boundary resistance, making for no special handling problems of the powder at room temperature.

The recipe used to form the sinter was developed at Ohio State University (by Gary Ihas and Judau Landau). Complete detail is provided in the thesis of K. A. Muething (Muething, 1979). Briefly, the Pd powder was pressed using close fitting stainless steel packing rams into each well to achieve a 40% packing fraction. The packing was done in small amounts (0.5 to 2 gm per layer), the multiple layering used to insure that all of the Pd undergoes a reasonably uniform force during packing. The total mass of Pd used in the exchanger was 74.68 gm. The Pd powder was next sintered by placing the exchanger in a furnace (Lindberg) and heating to 800°C in a CO atmosphere for two hours, followed by flushing the oven retort and heating to 600°C for an additional two hours in a mixed atmosphere of 92% He and 8% H_2 . Finally, before being cooled to room temperature the oven and exchanger were flushed with 4He gas to clean out the H_2 . Test pieces of Pd sinter were found to have a residual

resistance ratio ($R(300\text{ K})/R(4\text{ K})$) of about 50. Additionally, N_2 adsorption isotherms at 77 K were measured by the standard BET method (Brunauer, Emmett, and Teller, 1938) revealing the surface area per unit mass of the Pd sinter to be $0.12\text{ m}^2/\text{gm}$, giving a total surface area of the heat exchanger of 8.96 m^2 . Finally, a series of 0.5 mm through-holes were drilled around the circumference of each sinter annulus at regular intervals to both assist in heat conduction and permit bulk fluid motion during the flow experiments.

In contrast to the usual method of attaching the heat exchanger directly to the final cooling stage (either by welds or bolts), this exchanger was placed on legs which raised it away from the bundle flange. This design followed from the intended primary purpose of this exchanger, which was to perform flow experiments on superfluid ^3He at milli-Kelvin temperatures. Once a design for the flow-creating mechanism was settled, it was realized that the act of pushing the liquid ^3He might cause heating either of mechanical or viscous origin in the pump mechanism. This could in turn disrupt the flow measurements. To avoid this problem, legs were added as an integral part of the flow system design. By mounting the flow pump underneath the exchanger and the experimental cell on top of it, the exchanger was interposed between them, to act as a heat sink for any heat produced by pushing liquid.

Sample Magnetic Field Coils

In order to have a magnetic field with a variable direction and fulfill the requirement that the field be homogeneous over the largest possible sample volume, it was decided to use two separate nested pairs of superconducting coils mounted in a nearly Helmholtz configuration. The

Table (3-1)
Physical Parameters for the Nested Helmholtz Magnetic Field Coils

Coil	I.D. (cm)	Width (cm)	Separation (cm)	Turns and Layers	H_0/I (G/A)	Homogeneous Region (cm) ($\Delta H/H < 1 \times 10^{-4}$)
Vertical H_0	12.07	2.22	4.84	669/4	97.7	1.5
Vertical gradient	---	---	---	168/1	0.862	---
Horizontal H_0	10.26	0.556	4.27	812/14	130.3	1.5
Horizontal gradient	---	---	---	58/1	0.689	---

nested configuration is shown in Fig. (3-2). The physical description of each set of coils is contained in Table (3-1). The wire used for both was NbTi monofilament superconducting wire (core diameter = 0.076 mm, copper cladding diameter = 0.114 mm, Formvar insulation, from Supercon, Inc.). The last entry in the table is the distance from the coil center along the coil axis for which the field homogeneity $\Delta H/H$ is better than 1 part in 10,000. In addition, field gradient coils were wound on top of each of the static field coils. The eight coils of wire were connected to their corresponding partners by spot-welding the leads to each other, without removal of the copper cladding. The current feed leads were brought out of the vacuum jacket and connected to persistent current switches to allow the static coils to run in a persistent mode. To drive the modulation coils, three leads were brought out for each configuration, the two end leads and the center tap lead. Having access to these allows for series use to produce a field gradient. The coils were mounted to the mixing chamber of the fridge. With this nested pair

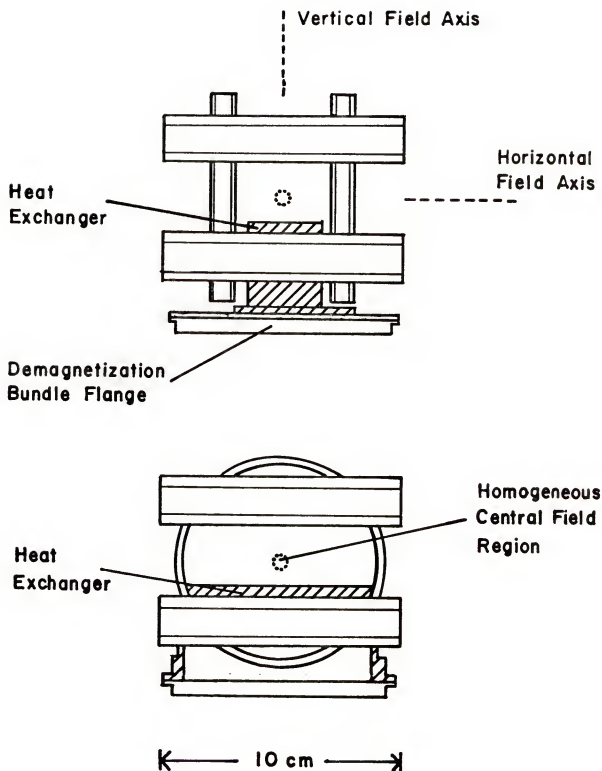


Fig. (3-2). Schematic of the nested Helmholtz magnetic field coils showing their relationship to the heat exchanger and cell.

configuration it was possible to produce magnetic fields in any direction in the plane of the two coil axes, the maximum field of any one pair being approximately 500 G.

Thermometry

In the different experiments performed for this work, the methods for measuring temperature differed from one cell to the next in some respects, others being the same. First the thermometers common to all the experiments are presented. Then the thermometers specific to a given cell are discussed.

Common Thermometry

At higher temperatures, from approximately 20 mK and up, the only thermometer which had sufficient sensitivity was the usual cut-carbon resistance thermometer (Rose-Innes, 1964). Prior to use, the resistor was calibrated against a low-temperature standard Ge resistor (Lake Shore Cryotronics) in this temperature regime. Measurement of the resistor was by standard 3-terminal techniques using a commercial AC resistance bridge (Linear Research model LR 130).

Below about 15 mK, pulsed NMR on a sample of platinum powder was used (Aalto et al., 1973). The powder sample (Leico Industries) in each case consisted of about 0.8 gm of 1-micron Pt particles (99.95% purity), packed to a 50% packing fraction. The powder was packed into an epoxy coil-former which was then wrapped with a short solenoid of 0.051 mm diameter Cu wire, diameter = 0.318 cm and length = 0.376 cm with an inductance of 450 microhenries. The NMR coil was attached to a flange to allow this thermometer to be mounted in any of the cells

with a matching female flange. A commercially manufactured instrument (PLM-3 by Instruments for Technology) performed the measurement process, firing the RF pulse and integrating the received ring-down. Because this device functions only at the fixed frequencies of 62.5, 125, 250, and 500 kHz our experimental fields were limited to those values corresponding to the Pt NMR resonance. Poor signal-to-noise prohibited using the lower frequencies and thus we were limited to fields of 28.6 and 57.2 mT, corresponding to 250 and 500 kHz resonances. To determine the absolute temperature, the instrument constant has to be found, requiring that the susceptibility be measured at a known temperature. The obvious choice for a fixed temperature point in these experiments was the superfluid transition temperature which has been measured as a function of pressure and magnetic field. To improve resolution a curve was fitted to the warming or cooling data and the temperature interpolated.

B Phase Experiment Thermometry

In the B phase cylindrical geometry experiment, measurement of the frequency shift of the superfluid provided an in-situ thermometer. Recall from Chapter II that the frequency shift is given as

$$\Delta\nu^2 = \nu^2 - \nu_0^2 = \Omega_B^2 \sin^2 \beta (\vec{r}, \vec{T}), \quad (1)$$

in the limit of large fields ($\nu_0 \gg \Omega_B$) and where ν_0 is the Larmor frequency, Ω_B is the longitudinal resonance frequency and $\beta = \cos^{-1}(\hat{n} \cdot \hat{H}_0)$. In this geometry with the surface normal perpendicular to the field, the maximum frequency shift occurs at the walls where the boundary condition is

$$\beta(\text{wall}) = \cos^{-1}(1/\sqrt{5}) = 63.4^\circ. \quad (2)$$

Measurement of the temperature is accomplished by measuring the maximum shift in the NMR absorption and then determining Ω_B^2 . From this the temperature can be found using the existing measurements of $\Omega_B^2(T,P)$ (Ahonen et al., 1976). The technique was outlined in Spencer et al. (1981). It has the obvious advantage of directly measuring the sample temperature rather than using a separate thermometer in contact with the sample.

^3He -Vycor Experiment Fixed Point Thermometer

In the ^3He in vycor glass experiment, the final cell used to collect data had no bulk ^3He under NMR observation, thus the method of thermometry outlined in the previous section could not be performed. It was decided to use the Pt pulsed NMR susceptibility as the primary thermometer and to use the attenuation of ultrasound in liquid ^3He as a fixed point. Below the bulk T_c the attenuation of ultrasound goes through a maximum, having been constant just above T_c . In cooling then, the bulk transition temperature was marked by a sudden change in the sound signal, providing a fixed point for the primary thermometer.

The sound cell is shown in Fig. (3-3). It was designed to be a self-contained unit to allow it to be moved from one experiment to another as desired. Based on the experience of the sound experiment of Berg (1983), this cell had a smaller ^3He path and used a silver delay line to move the transmitting crystal away from the receiving crystal. The former change was to decrease the effect of the attenuation maximum and allow the sound signal to be followed through the maximum. The

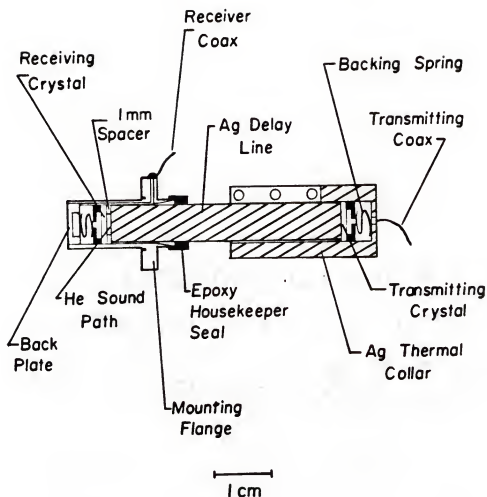


Fig. (3-3). Cross-section of the ^3He sound cell.

latter change was to decrease the electromagnetic feed-through from the transmitter to the receiver by physically moving the transmitter farther away. Also, the delay line was inserted so that the first sound pulse would not reach the receiver until well after the transmitter pulse and its feed-through had died out.

The main body was of brass, diameter = 0.991 cm and length = 1.83 cm with a bolt circle flange to allow for leaktight seals to be made. The transducers were x-cut quartz crystals with a resonance frequency of 5 MHz. They were 0.635 cm in diameter and 0.079 mm thick with thin gold films on both sides for electrical contacts. The delay line was made of 99.999% pure silver (Materials Research Corp.) 0.635 cm in diameter and 4.00 cm long, epoxied into the end of the brass body with about 2.6 cm extending out of the body. The epoxy joint was a standard housekeeper seal using Stycast 1266 epoxy (Emerson and Cuming). The spacer was 1.9 mm thick with crenelations on both sides out of phase with each other to prevent a direct sound pulse from propagating through it. It was made of copper with an inner diameter of 0.476 cm, polished on the crenelated faces and gold-plated to prevent oxidation. The receiving electrode was also of copper, diameter = 0.476 cm, encapsulated in Stycast 2850 epoxy (which is matched to the thermal contraction of Cu) except for a small pin on its backside for electrical connection. The face of the electrode facing the crystal was polished to a mirror finish (Micromesh polishing cloths, Micro-Surface Finishing Products, Inc.) and gold-plated. A non-magnetic spring behind the electrode held it firmly against the crystal. The end cap was of brass, threaded to hold it in the body. It completed the electrical shielding of the receiving crystal. The receiving lead passed along the inside diameter

of the body and out through the bolt circle flange. At the transmitting end of the delay line, the crystal was attached to the line using Apiezon N grease for physical contact. An electrode identical to the receiver was held against the crystal by another spring. To shield this end of the system, a collar of silver bar stock was constructed to slide over the end of the delay line. The bar had an inside diameter which was a close fit on the delay line and was slotted on one face along about two-thirds of its length. Small screws spanning this slot allowed the collar to be squeezed around the delay line for a rigid connection. On a second face, a blind slot ran the entire length of the collar. Into this slot an OFHC Cu plate (cross-section = 0.79 mm \times 1.91 cm) was brazed, the plate being long enough to reach from the position of the sound cell to the bundle flange. In this manner, the collar not only shielded the transmitter but also provided a thermal link for the sound cell to help cool it down.

The circuit for the ^3He sound is shown in Fig. (3-4). The I⁻V peak-peak output of the synthesizer (PTS 200) was attenuated to 0.5 V before entering the RF switch. A General Radio pulser (GR 1340) provided the gate for the switch and the pulse was further attenuated before entering the cryostat. The received pulse was amplified by the Matec amplifier chain (#310 preamp, #625 broadband receiver) and the signal passed to a boxcar integrator. The result then went to a strip-chart recorder and to a data logger (HP 3421A) and finally to a microcomputer (HP9845A). The pulse was 0.5 V attenuated by 0 to 4 dB typically, 58 microseconds in length.

The sound cell did not perform as well as hoped. Rather than reducing the recovery time of the receiver, some component of the cell was

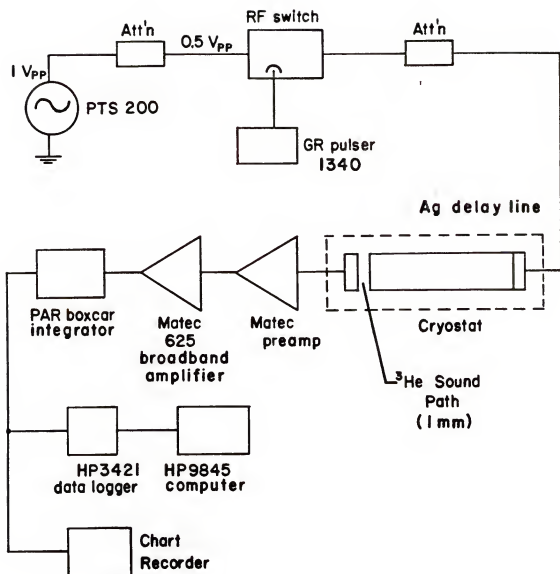


Fig. (3-4). Electrical circuit for the generation and detection of 5 MHz sound in ^3He .

found to ring for quite a long time, about 150 microseconds. This precluded observation of the first received sound pulse, which due to the delay line and ^3He travel time should have come at about 16 microseconds after the pulse. Thus, the echo which was observed (at 270 μsec , gate width = 12 μsec) had an unknown number of reflections before reaching the receiver. Nevertheless, the attenuation maximum just below T_c was clearly observed and used as a fixed point for the PLM calibration. The wiggles of the sound signal below bulk T_c were due to the interference between the feed-through and the received signal which changed due to the temperature variation of the sound velocity in the ^3He (Engel et al., 1985). The source of the feed-through problem seems to be that the delay line is not well-grounded (at low temperatures) to the cryostat ground. Improvement over the simple squeeze connection of the thermal-link collar is required. In its other desired characteristics, the sound cell clearly works excellently. For example, the sound pulse is not observed to go to zero and is easily tracked through the attenuation maximum even though the pulse being observed is a much-delayed multiply-reflected echo.

NMR Techniques

B Phase Experiments

In these experiments continuous wave (CW) NMR was performed while sweeping the persisted magnetic field through the resonance. The field sweep was performed by feeding a triangular-wave signal into a transformer coupled to the persisted circuit, a standard technique. This particular apparatus and technique was presented in Spencer et al. (1982).

The CW NMR circuit is shown in Fig. (3-5). It was a standard marginal oscillator run in a constant current mode. The signal source was an HP 3325A synthesizer. The signal was observed by a wide band pre-amplifier (Princeton Applied Research 115) with phase sensitive detection provided by a PAR 5202 lockin amplifier. The field-swept scan was sent to both a chart recorder and a signal averager (Nicolet 1170) and finally to the HP9845 computer for recording.

³He-Vycor Experiment

Pulsed NMR was used in this experiment. The circuit for this technique is shown in Fig. (3-6). Once again the HP 3325A synthesizer provided the signal source. A 1-V sine wave of the Larmor frequency was input to a gated RF amplifier (model 310HP, Matec Instrument Systems). To trigger the gate, a relay on the HP3421A data acquisition unit was closed by the microcomputer, providing a filtered 3 V pulse from two 1.5 V batteries. The attenuated pulse was fed into a RF transformer (T4-1, Mini-Circuits). The center-tapped secondary of this transformer divided the pulse into two components 180° out of phase with each other. One was sent into the tank circuit of the cryostat to excite the sample while the other component went into a dummy load constructed to mimic the sample tank circuit. The two signals were recombined via coupling capacitors and sent on to the amplifier chain. The purpose of this bridge arrangement was to block the RF pulse, of order volts, from the amplifiers. The components of the dummy load were varied until the minimum passed signal at the recombination point was within the range of the continuously tunable resistor (25 K Ω) and capacitor (100 pF). The outputs of the circuit under various levels of tuning are

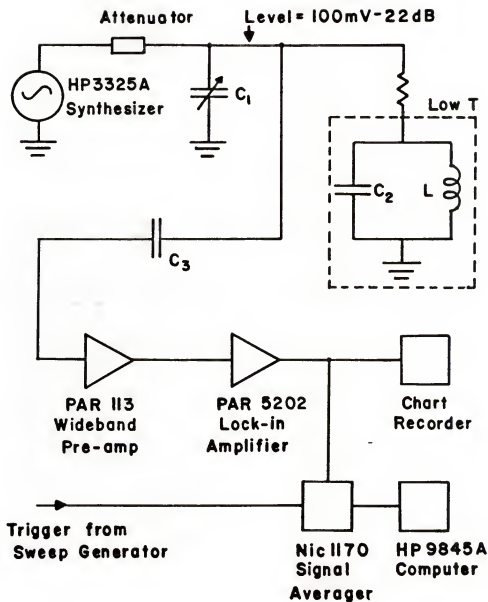


Fig. (3-5). Circuit for continuous-wave NMR.

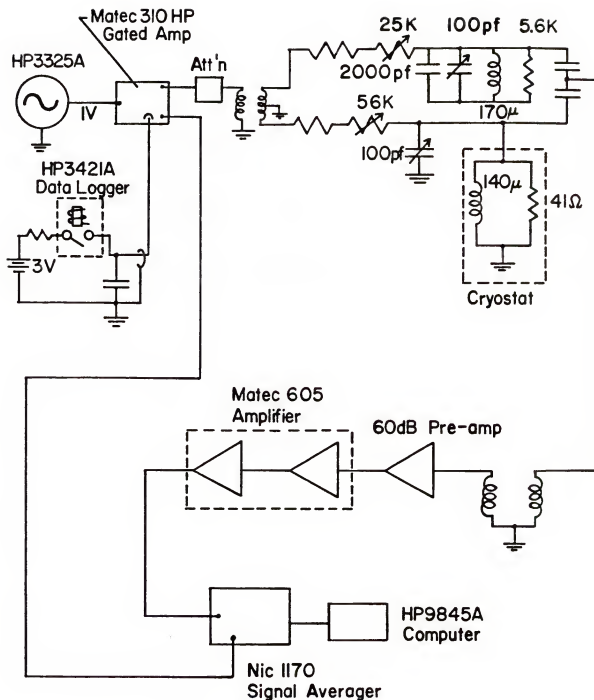


Fig. (3-6). Circuit for pulsed NMR.

shown in Fig. (3-7). In Fig. (3-7a) is shown the uncanceled pulse. In Fig. (3-7b), the cancellation bridge is poorly-tuned with a resultant long dead-time for the amplifiers before recovery permits a free-induction decay to be seen. In Fig. (3-7c), partial cancellation demonstrates the quicker recovery of the amplifiers. Finally, in Fig. (3-7d) the circuit is well-tuned.

The receiver signal traveled next to an impedance matching transformer (T16-1, Mini-Circuits) and into a 60 dB preamplifier (Analog Modules). Without this transformer, the mismatch created uncontrollable oscillations in the preamp. The amplified signal was next passed to the broadband amplifier (Matec model 605). The 1st stage amplifier was bypassed and only the 2nd stage used due to signal-to-noise degradation in the 1st stage. The detected FID was then sent to the signal averager and recorded in the computer.

Bellows Flow Pump

The device used to create flow at very low temperature was the bellows flow pump. It was designed by Gary Ihas and Ephraim Flint and built by Flint. This author claims no credit for its splendid performance. However, since no published description of it exists it will be described here. The pump is shown in cross-section in Fig. (3-8), mounted underneath the Pd heat exchanger.

Description

A number of properties were required of a flow device which must perform at milli-Kelvin temperatures. In terms of flow capabilities, the stroke of the device must be sufficient to create flows which are

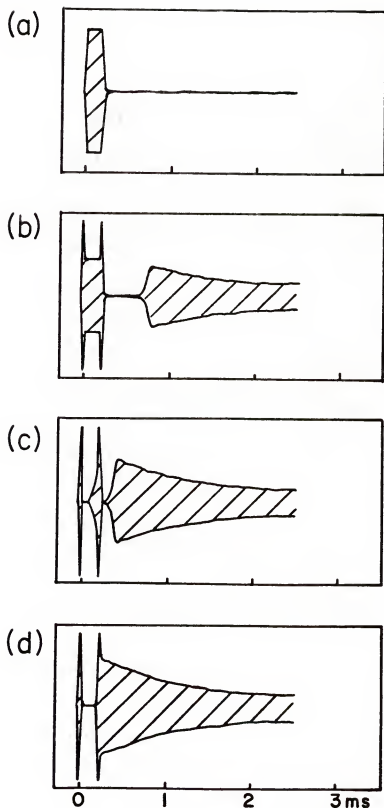


Fig. (3-7). Outputs from the pulsed NMR amplifier chain under various conditions of bridge tuning: (a) uncancelled pulse; (b) mistuned cancellation circuit; (c) partially cancelled pulse with a decrease in dead-time; (d) well-cancelled pulse with zero dead-time.

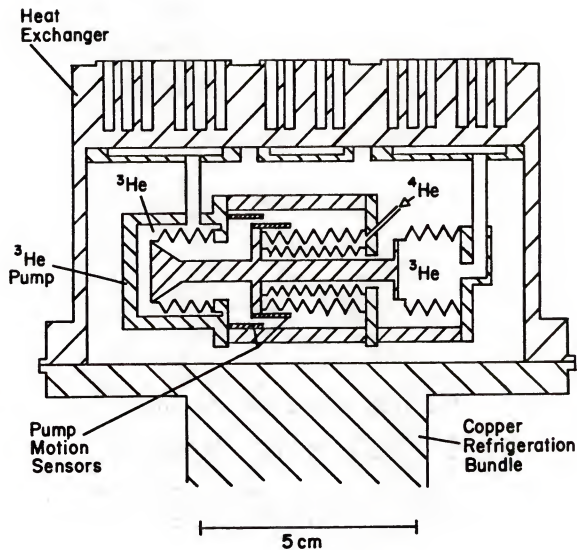


Fig. (3-8). Double bellows flow pump shown in cross-section in its operational position beneath the Pd heat exchanger.

either (a) high flow rates for convenient short-term measurements (i.e., not too short) or (b) low flow rates for long term measurements. The mechanism must maintain the volume of the cell constant to avoid heating. Also, since many interesting experiments involve motion of only the superfluid component of the liquid, the flow mechanism must be isolated from the experimental cell. In this manner any dissipative effects due to normal-superfluid conversion will not affect the measurements. Our bellows pump meets these requirements.

The flow pump consists of three separate volumes; two of them being ^3He spaces and part of the cell geometry, the third being filled with liquid ^4He and used to drive the pump. The ^3He spaces are formed by two Be-Cu bellows, diameter = 1.91 cm; on the right side the bellows forms the outer wall to contain the ^3He while on the left side the bellows is the inside wall of the container with a 2.10 cm I.D. Be-Cu can forming the outer container wall. In each case, the open end of the bellows are rigidly fixed by epoxy to the mounting flanges of the pump, while the closed ends of the bellows are free to move. The ^4He space is formed by two concentric bellows, the outer being 1.89 cm in diameter, the inner being 1.09 cm. The region between the two bellows is where the ^4He resides. The right ends of these bellows are epoxied to a fixed Be-Cu flange, the left ends are epoxied to a second Be-Cu flange which is free to move. Running along the pump axis is a push rod which is rigidly fixed by screw connections to both the free ends of the ^3He bellows and the free ends of the ^4He bellows. Movement of this rod forces all three free bellows ends to move with it. Since the two ^3He bellows are identical and mounted in complementary fashion, expansion of one of them is matched by an equal compression of the other, main-

taining a constant sample volume. The pump is epoxied using Stycast 2850 (Emerson and Cuming) to ease any necessary repair.

To drive the pump a capillary fill-line leaves the ^4He space and goes to a ^4He bomb mounted on the 4 K flange inside the vacuum jacket. Heat applied to the bomb increases the liquid pressure by evaporation, forcing liquid down the fill-line and moving the push rod. Mounted on the push rod is the inner electrode of a concentric coaxial capacitor, the outer electrode being fixed.

The pump movement is capacitively sensed in a bridge circuit, shown in Fig. (3-9). The lock-in output of this bridge may be used as feedback to either drive the pump in a specific manner or regulate its position. To do this a heater controller is used (Linear Research model LR 130). Differential pressure steps may be applied merely by changing the value of the bridge ratio transformer.

Pump Tests

To determine the change in pump volume during a stroke, δV , the pump was mounted on the heat exchanger in its operational configuration. To close the geometry, two flanges, with a tube connection between them, were mounted on top of the exchanger. Also a sensitive differential pressure gauge was mounted, one side looking at the internal pressure of this closed geometry, the other side open to atmosphere. The pump was then stroked by pressurizing the ^4He space and any change in the cell volume was sensed by a change in the internal pressure. If P_0 and V_0 are the initial internal pressure and volume and δP and δV the changes due to stroking, then to 1st order

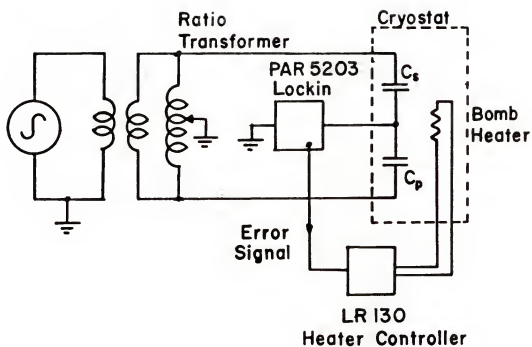


Fig. (3-9). Bridge circuit used to measure the pump motion, with feedback to regulate the pump position.

$$\delta V/V_0 = \delta P/P_0 \quad (3)$$

For substantial strokes, with ^4He pressures up to 50 psi (maximum allowed $P = 100$ psi to avoid buckling), the measured $\delta P < 1.9 \times 10^{-4}$ Torr at $P_0 = 760$ Torr, yielding the fractional volume change

$$\delta V/V_0 \leq 2 \times 10^{-7} \quad (4)$$

The stroke displacement calibration was performed by blocking one of the two top flanges on the exchanger, stroking the pump, and measuring the pressure change in just that half of the pump and exchanger. Using the same notation as above, the displaced volume will be

$$\delta V = V_0 \delta P / (P_0 - \delta P). \quad (5)$$

The initial volume was measured by expansion of ^4He gas from known volumes, using a commercial pressure gauge (MKS Baratron 10 Torr pressure head). The total volume of the heat exchanger and pump was found to be $2V_0 = 14.98 \text{ cm}^3$. The stroke displacement was found to be $1.272 \text{ cm}^3/\text{cm}$, allowing calibration of the flow measurements.

Experimental Cells

All of the cells used in these experiments were of the same basic design. For this reason the general characteristics common to all the cells are described in the first section. Following that the specifics of each particular cell are presented.

General Cell Design

The general cell schematic is shown in perspective and two cross-sections in Fig. (3-10). The central body was made of Stycast 1266 epoxy. A non-metallic material was required to allow NMR to be performed without incurring large eddy-current heating. This body had dimensions of 1.91 cm \times 3.05 cm and 1.27 cm vertical thickness. To attach the body to the heat exchanger, fill it with ^3He and allow the flow of ^3He from one side of the pump to the other, connecting tubes of 0.318 cm inside diameter were sealed to the epoxy body using house-keeper seals, having previously been brazed into elbow flanges at the ends away from the body. The elbow flanges were mounted to the heat exchanger. The reason the connecting tubes were offset rather than straight was due to the differential contraction of the cell. The epoxy having a greater thermal contraction than the metal parts, the cell was able to distribute the stresses of the contractions over a larger area by using the offset design.

To avoid the stresses of machining cured epoxy, the body is cast in a single pouring. The connecting tubes, already soldered to the flange elbows, were placed in a Teflon mold along with inserts to prevent epoxy from blocking them internally. Another insert ran along the body axis of the longest dimension to leave a 0.635 cm diameter hole in its place after the epoxy set. The epoxy was then poured into the mold and allowed to cure overnight at room temperatures. Upon removal of all the molding inserts, the basic body block was left with intersecting cylindrical cavities allowing access for the placement of the internal parts, particularly the central sample insert, specific to the desired experiment. Once all the internal additions had been made, the

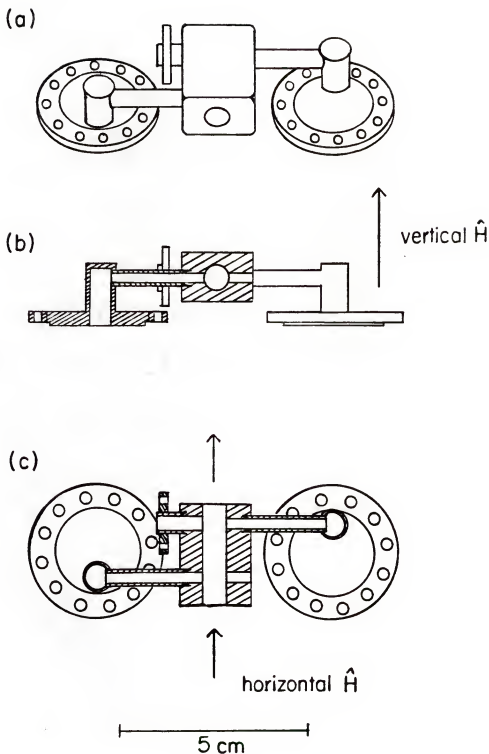


Fig. (3-10). General experimental cell schematic: (a) in perspective; (b) in a side cross-section; and (c) in a top view cross-section. Also shown are the directions of the horizontal and vertical magnetic fields.

body was sealed at each of these access holes. These seals were, in general, the final step of the cell construction.

The orientation of the cells with respect to the horizontal and vertical Helmholtz magnetic fields is illustrated in Fig. (3-10).

Slab Geometry Cell

This cell was built by Robert Mueller and was used in the first stages of the ^3He -B phase work (Spencer et al., 1981).

The sample insert consisted of two separate sets of stacked glass plates. The plates were 76 μm thick and spacers of 135 μm separated each plate from its neighbors. The two sets consisted of 11 plates each, forming 10 slab-shaped channels per stack. Shown in Fig. (3-11a), the two stacks were placed adjacent to one another with the surface normals of the two sets of plates being rotated 90° relative to each other. The stacks, each with its own RF coil for NMR, were epoxied inside the central region of the cell body in such a way that the surface normal of one stack was parallel to the vertical Helmholtz field while the normal of the other stack was perpendicular to both the vertical and horizontal Helmholtz fields. The RF coils were mounted in such a manner as to be able to perform transverse NMR in any field configuration. To ease discussion of results in the two stacks, they were given names. The stack with normal vector perpendicular to both fields was called "planar" or P stack because the plates were in the plane formed by the two fields. The stack with a vertical normal vector was called "variable" or V since its normal was capable of being at any angle from 0 to 90° with the net field of the nested Helmholtz coils. The orientation of the stacks was such as to also permit the flow of liquid through the plates.

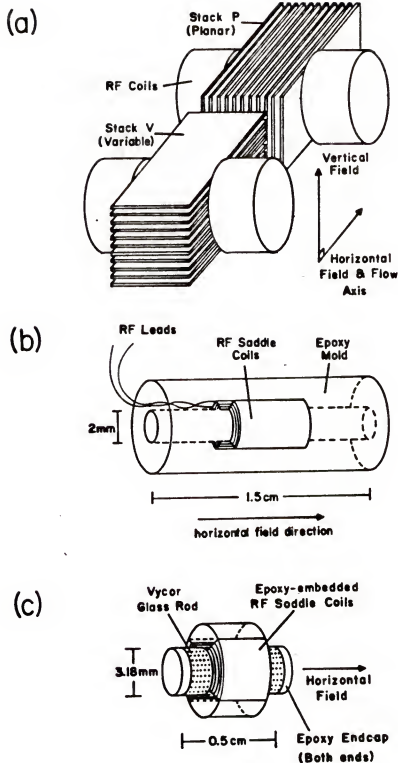


Fig. (3-11). The sample inserts used in each cell: (a) slab geometry insert; (b) 2-mm cylindrical geometry insert; and (c) vycor insert. Note that the magnetic field and flow directions are shown.

Cylindrical Geometry Cell

It was desired to produce a geometry in which the textural interactions could compete in such a way as to substantially alter the observed NMR absorption while being able to extract detailed information from it. This led to the choice of a cylindrical geometry with the cylinder axis along the horizontal Helmholtz field axis.

The sample insert is shown in Fig. (3-11b). It was 0.635 cm in diameter, 1.40 cm in length, with a 2 mm diameter open channel running along the length. Constructed with Stycast 1266 epoxy, the insert had embedded two RF saddle coils to perform NMR, the coils being 50 turns each of #45 AWG Cu wire (0.051 mm diameter, Formvar insulated) with a resistance of 26 Ω and an inductance of 50 μH . They were mounted so that tranverse NMR could be done in any field configuration. This insert was epoxied into the main body at its center. Care was taken to insure that no parallel path around the insert existed so ^3He was only inside the 2 mm channel. In one of the connecting tubes, a filter made of a vycor glass plug was epoxied.

^3He -Vycor Cell

Due to some unusual results obtained in the cylindrical geometry cell we decided to study the NMR and flow properties of liquid ^3He inside vycor glass.

Vycor glass (Corning) is a two-component glass composed of silica-rich and boron-rich phases. In an intermediate manufacturing stage, the boron-rich phase is chemically etched away, leaving a matrix of the silica phase. The matrix is a very tortuous collection of interconnected pores. Measured by various means, the average pore diameter

is 60 Å, other sizes being produced by variation of the final heat treatment during manufacturing. The final composition of the glass is 96% silica, 3% B_2O_3 and 0.5% Al_2O_3 .

Two cells were constructed with a vycor glass insert centrally located. In the first cell after preliminary results were obtained it was realized that the cell was not quite capable of reaching the temperatures required of it. The insert, shown in Fig. (3-11c) was a 0.318 cm diameter vycor rod of length = 0.476 cm. Around the rod, two saddle coils were wrapped to provide for NMR measurements. To insure that no axial crack participated in determining the overall flow characteristics, both ends of the rod were covered with epoxy. The insert was then epoxied into position in the body being careful to prevent any parallel flow channels around the vycor rod from forming. To provide for flow measurements, a sensitive differential pressure gauge (manometer) was mounted in parallel across the vycor rod (this device will be discussed in the next section). Additionally, superfluid filters of Millipore paper (Millipore) were epoxied into the flange elbows to limit fluid movement to the superfluid. This filter paper had pores of average diameter of 0.45 μm .

The design of the second vycor cell shown in Fig. (3-12) was somewhat more involved with two primary changes made. The first change was the addition of a third flange underneath the cell to be mounted to the center Pd heat exchanger. Designed to provide better thermal contact between the Pd exchanger and the cell body, both this center flange and each of the two flange elbows were made of OFHC Cu hard-soldered to Be-Cu bolt circles. Wells were built into the bottoms of each of these three flanges into which fine silver powder (700 Å,

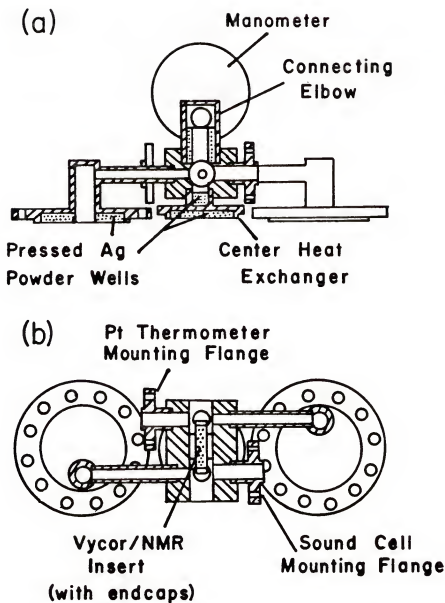


Fig. (3-12). Schematic of the final vycor cell: (a) side cross-section and (b) top cross-section.

Vacuum Metallurgical Co.) was cold-pressed at about 400 bars pressure after the parts were silver electroplated. In each flange well approximately 50% packing of the powder was sought, the two elbows receiving 7.11 gm of silver each, the center flange getting 1.53 gm. To further facilitate thermal contact of the liquid inside the cell body with the exchanger, the top of the center flange contained two smaller cylindrical wells, one on each side of the vycor rod. Into these two 0.476-cm diameter wells silver powder was also pressed, each well containing 0.29 gm of silver. Leaktight connection to the cell body was made by house-keeper seals on each of these two wells. In this way, liquid inside the main body could be in direct contact with the heat exchanger without disturbing the original flow topology.

Each of these two cells contained the Pt thermometry cell previously described, however, only the last cell contained the ^3He sound cell. The last cell also had two Millipore filters although these were mounted closer to the main body, inside it in fact. This minimized the amount of liquid which could only be cooled by the center heat exchanger.

Of prime importance in the flow portion of this experiment was to make certain that the only possible path of the liquid from one side of the cell to the other was through the vycor glass. In each cell, the final test prior to mounting on the cryostat was to verify this. To perform this check, the cells were placed in a bath of liquid ^4He with the volume on one side of the vycor open to the bath, the volume on the other side being kept closed. Using the sensitive differential manometer, the depression of the lambda transition in ^4He was measured. The depression was found to be

$$\delta T_{\lambda} = T_{\lambda, \text{vycor}} - T_{\lambda} \sim -500 \text{ mK} \quad (6)$$

using the onset of pressure fluctuations observed by the manometer as the marker of $T_{\lambda, \text{vycor}}$. (For $T > T_{\lambda, \text{vycor}}$ the two liquid volumes are not well-connected making the differential pressure across the vycor quite susceptible to fluctuations; for $T < T_{\lambda, \text{vycor}}$ the two volumes are well-connected and ΔP becomes quiescent.) Using the results of Ihas and Pobell (1974) this depression corresponded to a typical pore size of 15-20 Å. The cause of this small pore size might be the epoxy endcaps on the vycor, implying a radial pore size dependence, or due to the mild epoxy heat treatment during construction. The test results sufficed in that they proved that no large parallel leak around the vycor existed.

As in the first cell, a double saddle coil was wrapped around the vycor rod. Each coil was 100 turns of 0.025 mm Formvar-insulated Cu wire. The total resistance of the RF coil was 41 Ω and its inductance was 140 μH .

Another development for this last cell was a very small heater to be used inside the cell body to directly heat the liquid. The detailed construction of these heaters, one of which is shown in Fig. (3-13), has been presented elsewhere (Spencer and Ihas, 1986). Two heaters were placed inside the body on each side of the vycor insert.

Picobar Differential Manometer

The differential manometer used in the flow measurements is shown after attachment to the cell in Fig. (3-12) and in greater detail in Fig. (3-14).

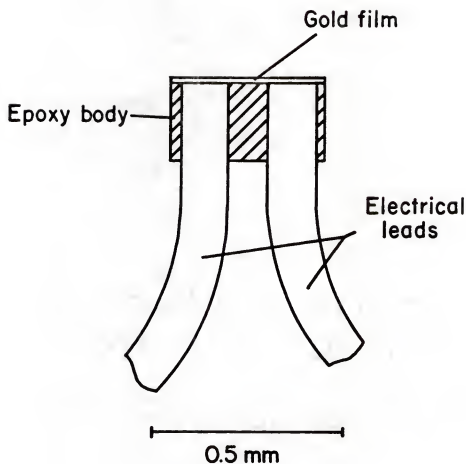


Fig. (3-13). Cross-section of the miniature thin film heater used to heat the liquid in the vycor cell.

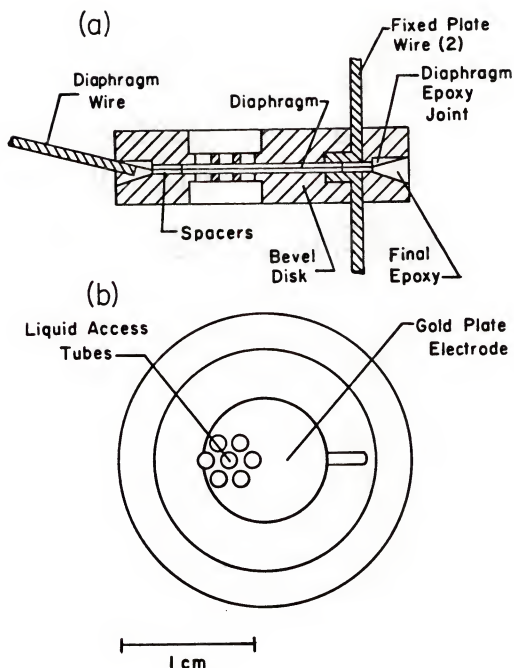


Fig. (3-14). Cross-section of the differential manometer: (a) side section through a diameter; (b) face view of one of the two disks which made up the manometer.

The manometer was a capacitor with one fixed plate electrode and a movable diaphragm for the other electrode. Any change in differential pressure across its two ends caused the diaphragm to move with a corresponding change in its capacitance measured in a bridge circuit. Its greatest sensitivity was due to the method of construction, described in Spencer and Ihas (1984).

The body of the manometer consisted of two halves, each being a 2.54 cm disk of Stycast 1266 epoxy, 0.318 cm thick. One of the disks had a bevel cut into its inner face (i.e., the face that would eventually be on the inside of the manometer) while the other disk had a short step (different versions ranged from 25 μm to 75 μm in height) each feature running completely around the circumference with an inner diameter of 1.98 cm. The stepped disk is used to precisely adjust the diaphragm tension during construction. The bevel of the other disk served as a conduit for the final epoxy joint when the two halves were joined.

To fill the two halves of the manometer, the final design had seven 1.19 mm through-holes in close-packed arrangement in each disk, the holes being 0.25 mm long. At their end these holes opened to a common 0.635 cm diameter entrance port. Housekeeper seals at this port connected each side to an OFHC Cu elbow which led to the main body of the cell. The elbows were silver electroplated and silver powder packed into the vertical members leaving an open I.D. of 0.476 cm. Each elbow was given 0.35 gm of Ag packed to a 50% fraction. The purpose of this powder was to help cool the manometer using the increased surface area.

The first step in the manometer construction was to mount wires in the two disks to be used for electrical leads. A 0.51 mm hole was

drilled through each disk and a snug-fitting wire threaded into the hole where it was then epoxied. After setting, the front surface on the disk was polished in a lapping machine (Minimet by Buehler) to a mirror finish, the final stage using $0.05\text{ }\mu\text{m Al}_2\text{O}_3$ as the abrasive. This left the wire exposed in the face of the disk and dangling out the back side. Measurements of the disk flatness using a He-Ne laser light source ($\lambda = 6328\text{ }\text{\AA}$) to observe Newton's rings (by stretching a Kapton membrane over the disk) indicated a radius of curvature of the polished face greater than 73 m. After polishing, gold electrodes were evaporated onto the faces of the disks, being circular with a 1.03 cm diameter and with a finger extending over to the side to make contact with the in-laid wire.

The most crucial step in the construction was the epoxying of the diaphragm to the stepped disk with the correct tension. To accomplish this a special clamping fixture consisting of two Al rings whose I.D.'s were snug fits to the disks were used. These rings which could be fastened face-to-face served both as a tensionless clamp to hold the Kapton diaphragm material (du Pont), and as positioners for the step disk. To exert the tension desired in the diaphragm, the step disk was first placed in one of the rings, held by set screws, and maneuvered until its polished face was precisely positioned with respect to the face of the ring. Usually the adjustment was such that the lower step was placed in the face of the clamping ring and thus the tension in the diaphragm was due to stretching it to accommodate the short step and mylar spacer. The relative positions of the two planes of these faces were measured by a height indicator (Ralmike's) with a precision of $\pm 2\text{ }\mu\text{m}$. With the placement and therefore the tension fixed, a small amount of epoxy was

applied on the lower (outer) step around its outer circumference. Next, an annular ring of mylar (O.D. = 1.96 cm, I.D. = 1.28 cm, thickness = 25 μm) was laid on the disk face to serve as a spacer. Finally, the Kapton diaphragm (thickness = 8 μm) was laid across the disk and lower clamp ring and clamped by the upper clamp ring. This was allowed to set overnight at room temperature. It was found that curing the epoxy joints at elevated temperatures from this stage to the end resulted in irreversible relaxation of the Kapton diaphragm. A gold electrode was next evaporated onto the diaphragm, contact to the finger being made using a small copper wire and silver conducting paint. After the paint dried, a small dab of epoxy over the paint/wire joint gave the additional strength needed for handling during the final construction phase.

The final step was the joining of the two halves. For this a brass mold was made in two halves with the inside surfaces coated with Teflon. Into each mold-half a prepared disk was placed. The two halves were brought together with a second mylar spacer for the other side of the diaphragm. The mold was locked together and the two manometer halves held by exerting forces from the outside only at the spacer locations to prevent any bowing in the active region of the diaphragm. Epoxy was applied in the bevel groove around the manometer circumference and once again allowed to set at room temperature overnight. After this the two elbows were epoxied into position on the manometer.

The manometer (T5) which was used on the last vycor cell had a step disk with step height of 25 μm and a 25 μm mylar spacer. These provided the tension in the diaphragm given by the strain of stretching as $\delta A/A = 0.009\%$, where A was the initial diaphragm area and δA was the areal stretch of the diaphragm.

The manometers were tested at 300 K on a homemade test stand by putting a known differential pressure across the diaphragm and measuring the response in a capacitance bridge. The maximum sensitivity was around $\Delta P = 0$, while at room temperature all the manometers saturated with a few Torr of differential pressure. However, no sign of saturation of the response was seen at low temperatures even with differentials much larger than this. With a bridge sensitivity in the ratio transformer of $\delta r = 10^{-6}$, T5 had a room temperature sensitivity of $\delta P = 10$ nanobar. Prior to mounting the manometer to the cell, it was leak tested in our 1-K cryostat (Engel et al., 1984). With the temperature below T_λ , the diaphragm was found to be superfluid leaktight, a very important requirement for the experiment.

After T5 was mounted on the cell, the apparatus was tested and calibrated at low temperatures in a glass dewar pair. Oriented in the dewar in such a way as to permit a 35 cm long glass tube (0.635 cm diameter) to be mounted vertically on the Pt thermometer flange, the manometer was calibrated against the fountain pressure of superfluid ^4He . With the open end of the glass tube up and the sound cell flange open directly to the bath, putting heat into the closed space on the Pt thermometer side of the vycor created the temperature gradient needed to drive the effect. The fountain pressure was measured with a laboratory cathetometer to find the level differences between the bath liquid and the liquid in the tube. Simultaneously, the manometer capacitance was monitored in the usual bridge circuit (see Fig. (3-9)). Pressure differences from 18 μbar to 350 μbar were applied. As noted in the vycor cell tests, once superfluid shorted the two sides of the manometer, the signal-to-noise improved by a factor of 100. In

this quiescent mode, the optimized ultimate sensitivity of the manometer (T5) was found to be 59 picobars ($\delta P = 5.9 \times 10^{-11}$ bar = 8.6×10^{-10} psi = 4.4×10^{-8} mm Hg) making it the most sensitive mechanical capacitive manometer in existence. The only differential pressure gauges which better its sensitivity utilize superconducting metal electrodes and rely upon the high sensitivity of a SQUID to sense diaphragm motion (Avenel and Varoquaux, 1985).

Miniature Low Temperature Valves

Besides being able to measure flow properties in a flow experiment perhaps the next most important ability is to be able to say where flow is not happening. The purpose of low temperature valves is to limit motion away from the measurement region. The usual low temperature valves consist of one or more metal bellows which move a valve stem, typically of Teflon, in and out of the valve seat by pressurizing some region of the valve (Roach et al., 1972). While these valves have proven reliable, they have several drawbacks including bulkiness of design, complexity of construction, and sensitivity of the valve stem to deformation requiring care during thermal cycling. Because the vycor flow experiment required at least two such valves, a new design was developed. The construction is detailed elsewhere (Spencer and Ihas, 1985). The miniature cylindrical diaphragm in-line capillary valve is shown in Fig. (3-15). Referring to the figure, the two valves used in the vycor flow experiment had a length $L = 8$ cm, an external body diameter $D_o = 0.39$ cm, and an internal body diameter $D_i = 0.20$ cm. The labels a to f are separate solder joints: b, c, d, and e are hard-soldered; a and f are soft-soldered.

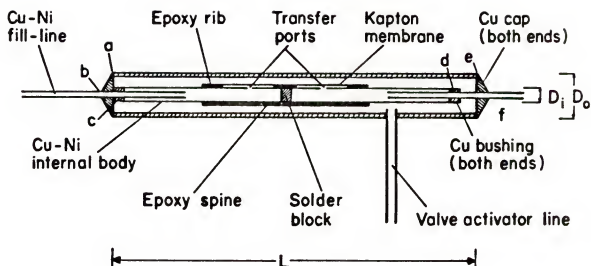


Fig. (3-15). Cross-section of the cylindrical-diaphragm in-line capillary valve, shown in a valve-open mode.

The valve functions by movement of a cylindrical Kapton diaphragm (thickness = 13 μm) which is epoxied in a leaktight manner around the internal body. The diaphragm is held away from the internal body surface by ribs of epoxy, leaktight seals being formed on the outer two ribs, the diaphragm just laying against the central rib. These ribs provide for a definite valving action when the liquid outside the diaphragm is pressurized above the pressure of the liquid inside the internal body. When pressurized, the external liquid squeezes the diaphragm down around the internal body, closing the filling ports and thereby preventing liquid motion through the valve. When the external and internal liquid pressures are equalized, the diaphragm can billow and allow liquid to pass over the central rib and through the valve. These valves are simple to construct with only one machining operation (the rib structure). The volume displaced by one such valve is a factor of 50 to 100 times smaller than that of a typical bellows valve. This allows these valves to be located in out-of-the-way places in the cryostat, being scarcely larger than capillary tubing.

The valves were leak-tested and found to be leak-tight above T_λ with a 1-bar differential pressure across the valve even though the design is not meant to handle such differentials. To close the valve requires about a 10 psi (0.69 bar) over-pressure of the external liquid above the internal sample liquid pressure.

The valves for the two fill lines on the vycor experiment were mounted on the mixing chamber of the dilution refrigerator to keep their operating temperatures above the superfluid transition. An indication of their performance was seen in a decrease in the manometer noise level by a factor of ten when the valves were closed.

CHAPTER IV
SUPERFLUID $^3\text{He-B}$ EXPERIMENTAL RESULTS AND DISCUSSION

Introduction

This chapter presents the results of experiments on the B phase of superfluid ^3He in two confining geometries. The theory pertinent to these systems has been presented in Chapter II, starting at page 10.

In the first experiment to be discussed, superfluid $^3\text{He-B}$ was confined between parallel glass plates forming the liquid into a slab shape. Continuous-wave NMR measurements of the resonance frequency and susceptibility were taken both at relatively high pressure for comparison to the work of others and at low pressure to extend the knowledge of the B phase. The experiment was performed in varying conditions of magnetic field and flow. In addition to the study of the \hat{n} texture in the static case, the flow results allowed comparison to theory concerning the orientational effects of flow.

In the second experiment, superfluid $^3\text{He-B}$ was confined in a cylindrical geometry (diameter = 2 mm) and a magnetic field was directed along the axis. Dramatic effects on the shape of the NMR absorption were observed in this case. A procedure to deconvolute the resonance was developed which allowed for detailed quantitative comparison to the theory of \hat{n} textures.

Finally in concluding remarks of this chapter, several ideas for further experimentation on these systems are presented.

Superfluid $^3\text{He-B}$ in a Slab Geometry

Due to the nature of this cell, a variety of configurations of the competing orientational effects of magnetic field, surface, and flow were possible. To simplify the presentation, the results for static liquid are separated from those of the flowing liquid and presented first. The experiments were performed at pressures of 21.5 bar and 0 bar (saturated vapor pressure) in a magnetic field of 286 G (central sample field) with the Pt thermometry being performed at 250 kHz.

Liquid at Rest

After demagnetization to the temperature region of interest, data-gathering began as the temperature slowly rose under the residual heat leak. The sample magnetic field, persisted very close to the value required for resonance absorption by the liquid, was ramped up and down through the resonance at a frequency of 0.01 Hz. The signal averager (Nicolet 1170) was adjusted to trigger on a positive-going slope for most of this experiment and thereby data was taken generally on the up-sweep. The NMR absorption was collected into the first half of the signal averager memory, the second half collected the current trace of the field sweep. The field sweep trace was required to be able to measure the value of the magnetic field as the ^3He absorption shifted away from the Larmor value. Equally important, due to the presence of a resistive shunt across the superconducting leads of the magnets (for quench protection), an inductive time constant L/R existed for sweeping the fields. Thus, the actual magnetic field on the sample at any given point during a sweep was not given by the value of the current in the sweep transformer at that instant, but rather it was lagging behind the indicated value due to this time constant. To determine the amount

of lag, sweeps in both directions were recorded while in the normal liquid where the Larmor frequency was known. If i_{res} is the true current at resonance in the liquid, i_u and i_d are the values of the current when resonance occurs during the sweep, and L is the lag then

$$i_{\text{res}} = i_u - L = i_d + L \quad (1)$$

from which both the amount of lag and true resonance current can be found as

$$L = (i_u - i_d)/2, \quad (2)$$

$$i_{\text{res}} = (i_u + i_d)/2. \quad (3)$$

Final calibration of the NMR was accomplished by changing the RF drive frequency ν_{RF} and measuring the new position of the normal liquid resonance. Given the resonance currents i_1 and i_2 at frequencies ν_1 and ν_2 , the NMR coil calibration constant κ becomes

$$\kappa = \frac{\nu_1 - \nu_2}{i_1 - i_2} \frac{1}{\gamma} \quad (4)$$

and the Larmor frequency is

$$\nu_0 = \nu_{\text{RF}} - \kappa i_0 \gamma. \quad (5)$$

A typical normal liquid NMR absorption and current sweep trace are shown in Fig. (4-1a,b), taken from the P (planar) stack NMR coil (surface normal

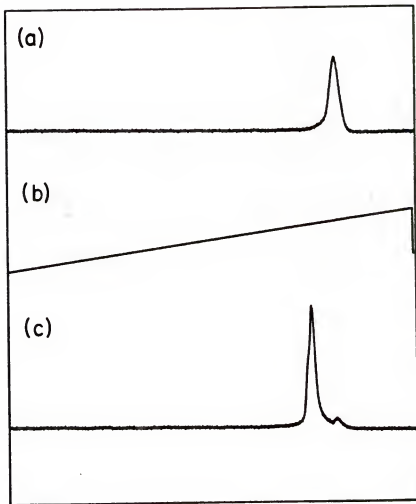


Fig. (4-1). Normal liquid NMR and sweep current: (a) typical normal liquid ^3He resonance in $H_0 = 286$ G near the superfluid transition in P stack at 21.5 bar; (b) trace of corresponding current sweep taken for the resonance in (a), sweep limits were ± 3 amps in a period of 100 sec; and (c) normal liquid ^3He resonance in the V stack at 21.5 bar.

always perpendicular to H_0). In Fig. (4-1c) a normal liquid resonance taken from the V (variable) stack NMR coil (surface normal is vertical so orientation with H_0 is variable) is presented.

At 21.5 bar, corresponding to $T_c = 2.41$ mK, the magnetic field was oriented in the vertical direction making it perpendicular to the surface normal in the P stack (as always) and parallel to the surface normal in the V stack of plates. Presented in Figs. (4-2) through (4-7) are representative results of NMR absorptions in each set of plates at closely corresponding temperatures, with the Larmor frequency marked in each case. In each figure, the absorption of the P stack is on the top, that of the V stack is on the bottom, with the temperatures corresponding to each peak added in the reduced form of $1 - T/T_c$. The most obvious feature of the data in this format is that the absorption in the V stack remained at the Larmor frequency while that of the P stack was shifted farther and farther as the temperature was reduced.

At saturated vapor pressure ($T_c = 1.15$ mK), the magnetic field was in the horizontal direction making it perpendicular to the surface normals of both stacks of glass plates. Representative absorptions for this configuration are shown in Figs. (4-8) through (4-10). In this configuration frequency shifts occurred in both stacks of plates.

The analysis of the NMR frequency shift begins very simply through the use of the calibrations already mentioned. The overall magnitude of the shift is formed by picking out the apparent current at the position of the NMR peak. Using the Pythagorean relation (Chapter II, eq. (45)), the frequency shift may be expressed as

$$(\Delta\nu)^2 = \nu_{RF}^2 - \nu_0^2 = \nu_{RF}^2 - \gamma^2(H_0 + H(t))^2,$$

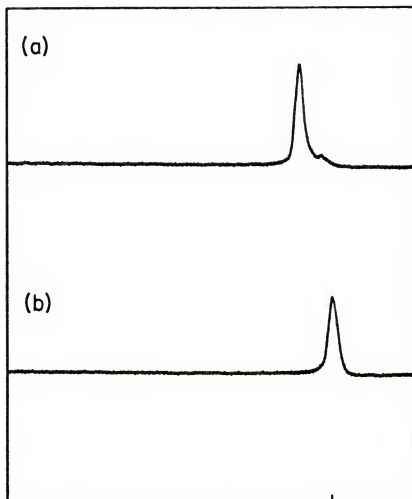


Fig. (4-2). NMR absorption at 21.5 bar and 921 kHz: (a) P stack, $1-T/T_c = 0.0104$; (b) V stack, $1-T/T_c = 0.0124$.

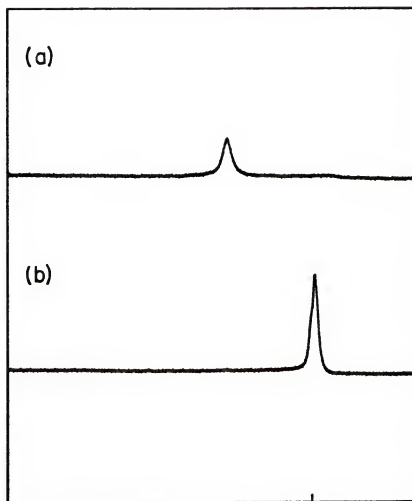


Fig. (4-3). NMR absorption at 21.5 bar and 921 kHz: (a) P stack, $1 - T/T_c = 0.0431$; and (b) V stack, $1 - T/T_c = 0.0389$.

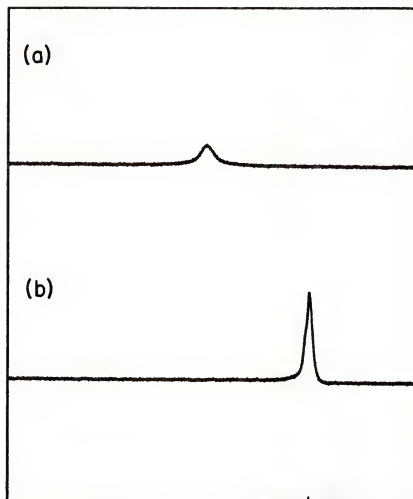


Fig. (4-4). NMR absorption at 21.5 bar and 921 kHz: (a) P stack, $1 - T/T_c = 0.0991$; and (b) V stack, $1 - T/T_c = 0.0866$.

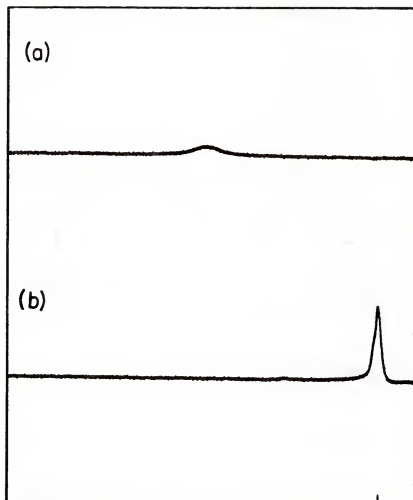


Fig. (4-5). NMR absorption at 21.5 bar and 922 kHz: (a) P stack, $1 - T/T_c = 0.1447$; and (b) V stack, $1 - T/T_c = 0.1323$.

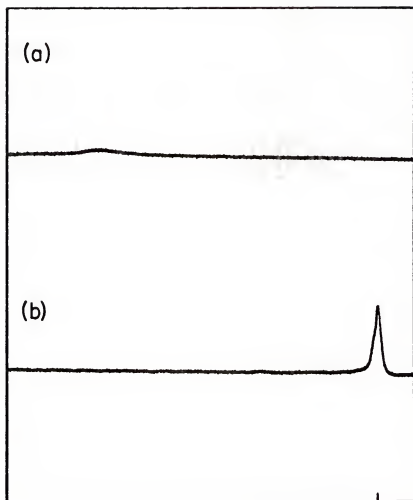


Fig. (4-6). NMR absorption at 21.5 bar and 922 kHz: (a) P stack, $1 - T/T_c = 0.2153$; and (b) V stack, $1 - T/T_c = 0.2111$.

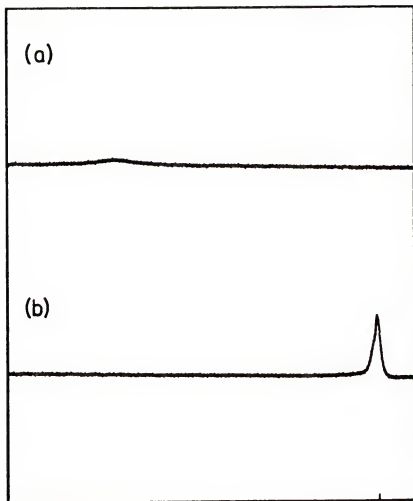


Fig. (4-7). NMR absorption at 21.5 bar and 925 kHz: (a) P stack, $1 - T/T_c = 0.2360$; and (b) V stack, $1 - T/T_c = 0.2381$.

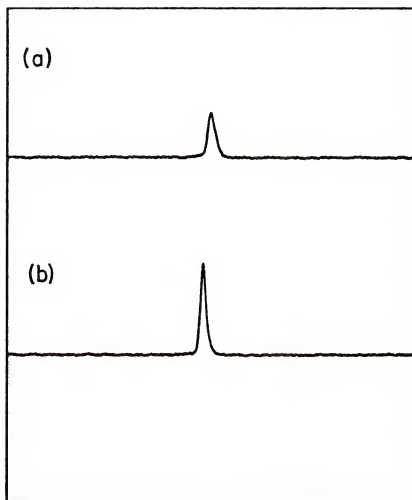


Fig. (4-8). NMR absorption at 0 bar and 923 kHz: (a) P stack, $1 - T/T_c = 0.0227$; and (b) $1 - T/T_c = 0.0161$.

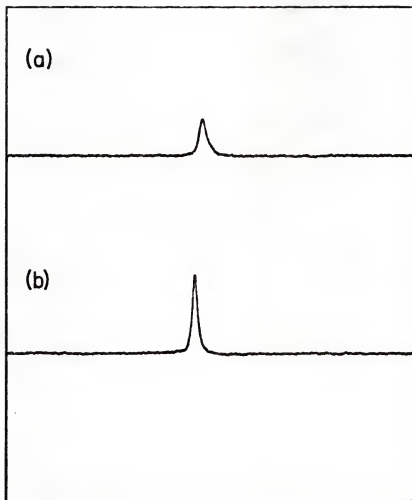


Fig. (4-9). NMR absorption at 0 bar and 923 kHz: (a) P stack, $1 - T/T_c = 0.0688$; and (b) $1 - T/T_c = 0.0551$.

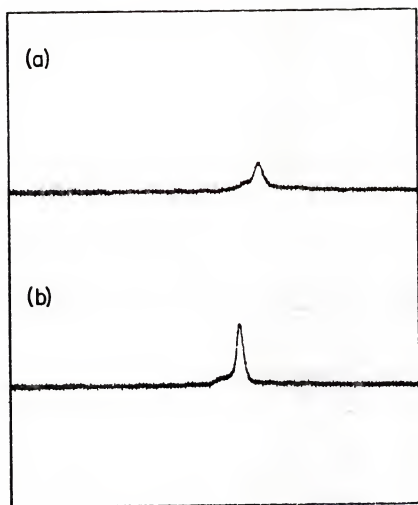


Fig. (4-10). NMR absorption at 0 bar and 929 kHz: (a) P stack, $1 - T/T_c = 0.1627$; and (b) V stack, $1 - T/T_c = 0.1675$.

which finally yields

$$(\Delta\nu)^2 = \nu_{RF}^2 - (\nu_0 + \gamma\kappa i(t))^2 = \Omega_B^2(T) \sin^2\beta. \quad (6)$$

The works of Osheroff et al. (1975) and Ahonen et al. (1976) having established the theoretical expectation that $\beta = \cos^{-1}(1/\sqrt{5})$ in static ${}^3\text{He-B}$ in this system where the surface-field energy F_{SH} dominates, the magnitude of the longitudinal resonance frequency $\Omega_B(T)$ may be determined from our results, including the first measurement of $\Omega_B(T)$ at s.v.p. Conversely, by comparison of our total shifts $(\Delta\nu)^2$ at 21.5 bar to the measurements of Ahonen et al. (1976) at 21.2 bar, we could verify that $\beta = \cos^{-1}(1/\sqrt{5})$. The 21.5 bar results are shown in Fig. (4-11), the s.v.p. results in Fig. (4-12). These are also tabulated in Table (A-1)(Appendix A). The s.v.p. results were presented in Spencer, Ihas, and Alexander (1981). A least squares straight line fit to these results gives:

$$P = \text{s.v.p.} \quad \Omega_B^2(T) = 2.458(1 - T/T_C) \times 10^{10} \text{ Hz}^2 \quad (7)$$

$$P = 21.5 \text{ bar} \quad \Omega_B^2(T) = 14.23(1 - T/T_C) \times 10^{10} \text{ Hz}^2. \quad (8)$$

These can be combined, with the expectation from Fig. (2-8) of a linear pressure dependence, to give

$$\Omega_B^2(T,P) = (2.46 + 0.548P(\text{bar}))(1 - T/T_C) \times 10^{10} \text{ Hz}^2. \quad (9)$$

Some structure can be observed on many of the absorptions. The main reproducible feature is the appearance of a small tail leading from the main peak back toward ν_0 . This tail comes from the fact that the RF

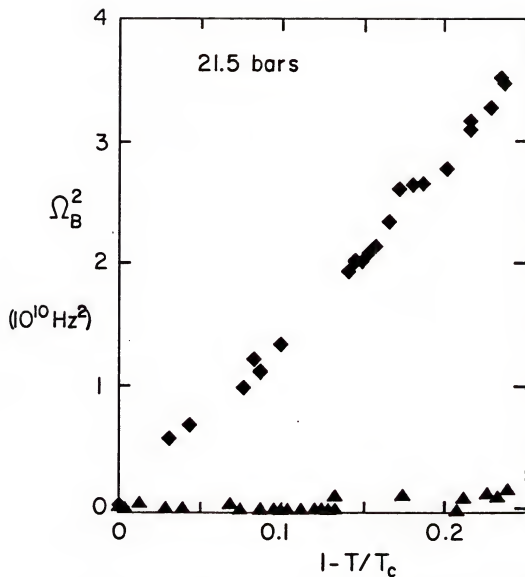


Fig. (4-11). Plot of $\Omega_B^2(T)$ versus $1 - T/T_c$, at 21.5 bar vertical $H_0 = 286$ G). (diamonds) P stack, (triangles) V stack.

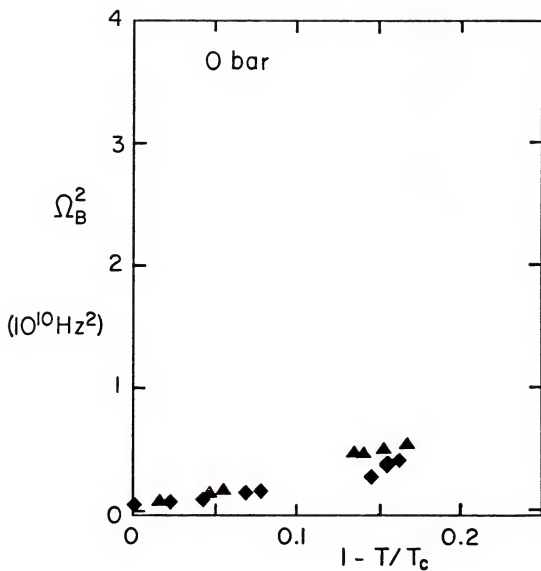


Fig. (4-12). Plot of $\Omega_B^2(T)$ versus $1 - T/T_c$ at s.v.p. (horizontal $H_0 = 286$ G). (diamonds) P stack, (triangles) V stack.

coil can observe some liquid in unconfined regions either near the plate edges or between the two stacks themselves. Measurements of the relative susceptibility (χ_B/χ_N) were made, but because of this tail and the inability in this unsymmetrical geometry to separate the confined liquid signal from the unconfined liquid signal, the susceptibilities deviate from the behavior expected in Fig. (2-1). These results are shown in Fig. (4-13) and also tabulated in Table (A-1).

Qualitative remarks can be made concerning the textural information given by these spectra. First, the fact that some liquid in open regions of the cell is observed to resonate at the Larmor value, ν_o , indicates that there is indeed a force causing \hat{n} to align with \hat{H}_o outside of the surface-dominated region. That force is, of course, the bulk-field energy F_{BH} . Equally pertinent is the fact that, rather than a satellite peak at ν_o , the feature is observed to be a tail going back to ν_o . This indicates that a bending energy is present that prevents sudden (hence zero spectral weight) changes in the direction of \hat{n} . This force is the bulk-bending energy F_{BB} . Features similar to these were seen by Ahonen et al. (1976). Finally, the lack of a frequency shift in the V stack in a vertical magnetic field happens because all three energies (F_{SH} , F_{BH} , F_{BB}) favor alignment of \hat{n} with \hat{H}_o in this case. With the surface normal \hat{s} parallel to \hat{H}_o , F_{SH} is minimized for \hat{n} also being parallel to \hat{H}_o (see equation (2-52)), as F_{BH} is similarly minimized at all times. With a completely uniform texture such as this one ($\hat{n}||\hat{s}||\hat{H}_o$), F_{BB} is identically zero (neglecting edge effects).

Flowing Liquid

A wide variety of pump strokes were performed during the course of these experiments, both short-term strokes from equilibrium and long-term

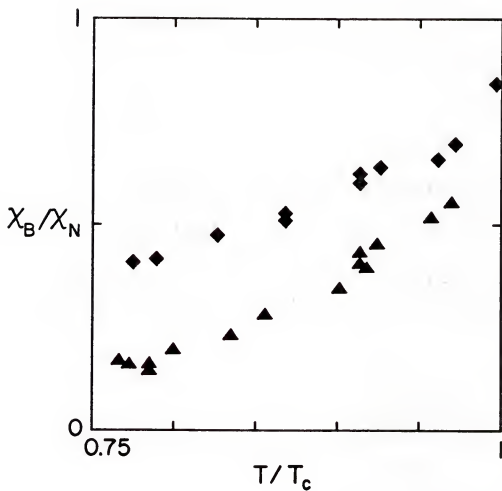


Fig. (4-13). Plot of χ_B/χ_N versus T/T_c at 21.5 bar. (diamonds) V stack, (triangles) P stack.

Table (4-1)
Forces on the \hat{n} Vector due to Orientational Energies
in a Vertical Magnetic Field

Orientational Energy	Configuration	Stack	Direction \hat{n} is Pushed
$F_{SH} \sim -(\hat{s} \cdot \hat{R} \cdot \hat{H})^2$	$\hat{s} \perp \hat{H}$	P	$\theta_H = \theta_S = 63.4^\circ$
	$\hat{s} \parallel \hat{H}$	V	$\theta_H = \theta_S = 0^\circ$
$F_{BH} \sim -(\hat{n} \cdot \hat{H})^2$	$\hat{s} \perp \hat{H}$	P	$\theta_H = 0^\circ, \theta_S = 90^\circ$
	$\hat{s} \parallel \hat{H}$	V	$\theta_H = 0^\circ, \theta_S = 0^\circ$
$F_{BV} \sim -(\hat{n} \cdot \hat{v}_S)^2$	$\hat{v}_S \perp \hat{H}$	Both	P: $\theta_V = 0^\circ, \theta_H = 90^\circ$ V: $\theta_V = 0^\circ, \theta_H = 90^\circ$
$F_{HV} \sim -(\hat{v}_S \cdot \hat{R} \cdot \hat{H})^2$	$\hat{v}_S \perp \hat{H}$	Both	$\theta_H = \theta_{v_S} = 63.4^\circ \neq \theta_S$

term relaxations, with superfluid flow velocities up to 0.484 cm/sec (9.01×10^{-4} cm³/sec = 0.733 g/cm²sec). No effect of the flow was observed on the NMR properties including no alteration of the non-flow frequency shifts, no change of shape of the spectra or appearance of satellite peaks, and no effect on the susceptibility.

Typical flow NMR spectra are shown in Figs. (4-14) through (4-17) with side-by-side comparison to non-flow spectra at similar temperatures. Spectra from both stacks are presented, each in a vertical magnetic field. The superfluid flow velocity in each of these flow spectra averaged $v_S = 0.118$ cm/sec (6.09×10^{-4} cm³/sec = 0.495 g/cm²sec).

To determine what might have been expected in this system assuming all the orientational energies were of equal strength, Table (4-1) has been constructed. Referring to the Table and the discussion of the static liquid NMR absorption structure, immediate remarks concerning the bulk-flow energy F_{BV} can be made. Given the fact that this system is

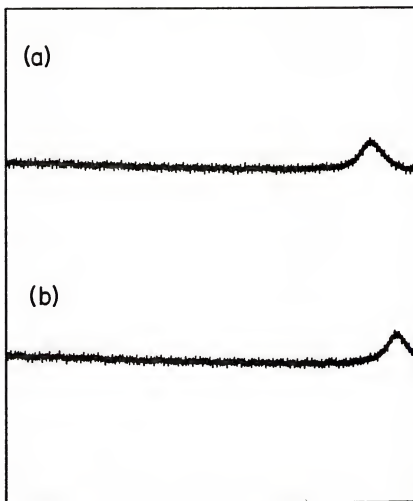


Fig. (4-14). NMR absorption at 21.5 bar and 933 kHz: (a) P stack, $v_s = 0.118$ cm/sec, $1 - T/T_c = 0.1447$; and (b) P stack, $v_s = 0$, $1 - T/T_c = 0.1406$.

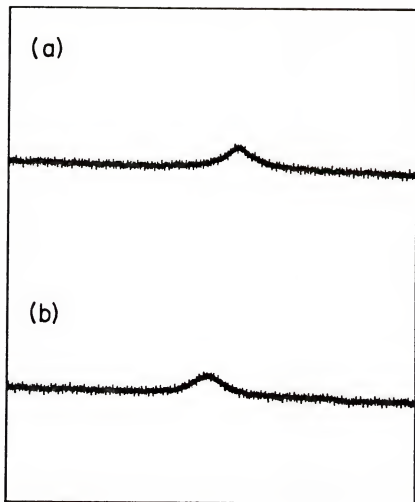


Fig. (4-15). NMR absorption at 21.5 bar and 933 kHz: (a) P stack, $v_s = 0.118$ cm/sec, $1 - T/T_c = 0.1862$; and (b) P stack, $v_s = 0$, $1 - T/T_c = 0.2007$.

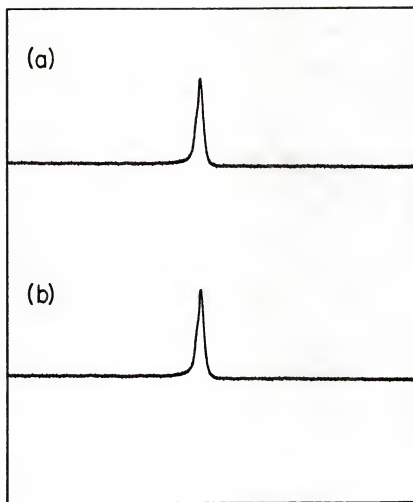


Fig. (4-16). NMR absorption at 21.5 bar and 921 kHz: (a) V stack, $v_g = 0.118$ cm/sec, $1 - T/T_c = 0.0866$; and (b) V stack, $v_g = 0$, $1 - T/T_c = 0.0866$.

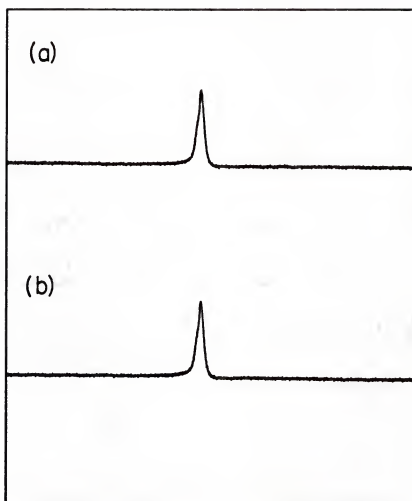


Fig. (4-17). NMR absorption at 21.5 bar and 921 kHz: (a) V stack, $v_s = 0.118$ cm/sec, $1 - T/T_c = 0.1281$; and (b) V stack, $v_s = 0$, $1 - T/T_c = 0.1323$.

surface-dominated and bulk energies appear to be seen only from the plate edges or other unconfined regions, it is not surprising that the bulk-flow energy F_{BV} does not contribute to any major change in the absorptions. However, further limits on its strength can be placed. If, for example, the strength of F_{BV} was comparable to F_{BH} then bending effects similar to those seen in the static liquid spectra would be expected. In this case, the \hat{n} vector in unconfined regions near the plates would bend toward the v_s and further away from H giving a larger frequency shift. In the limit of large flow coupling ($ev_s^2 \gg \alpha H^2$, see equations 2-46 and 2-48) the \hat{n} vector would align with v_s to produce the maximum shift possible at any given temperature, that with $\theta_H = 90^\circ$. As can be seen in the Figs. (4-14) through (4-17) no tail leading to higher frequency shift was observed. To check the possibility that some liquid did shift in this way but not far enough to be clear of the main absorption, static-liquid spectra were subtracted from flowing-liquid spectra at comparable temperatures. No formation of hidden spectral-tails or satellites was found. Another possibility which could reduce the size of flow effects due to F_{BV} is the fact that the velocity in the open regions of the cell is somewhat smaller than that in the slabs. A continuity equation relates the flow velocities in the two regions as

$$A_{\text{bulk}} v_{s,\text{bulk}} = A_{\text{slabs}} v_{s,\text{slabs}}, \quad (10)$$

where the assumption is made that the confining geometry has not substantially altered the superfluid fraction ρ_s/ρ . The cross-section of one slab is $3.38 \times 10^{-3} \text{ cm}^2$ (there being 10 slabs/stack) while the open cross-

section in the bulk region adjoining the slabs is $A_{\text{bulk}} \approx 3 \text{ mm} \times 2.5 \text{ mm} = 0.075 \text{ cm}^2$ giving $v_{s,\text{bulk}} \sim 0.5v_{s,\text{slabs}}$. This reduces the strength by a factor of four.

Now considering the field-flow energy F_{HV} , the two sets of plates must be considered separately. The P stack, which was observed to have a frequency shift at $\theta_{\text{H}} = 63.4^\circ$ in the static case, was observed to have the same shifts during flow. It is necessary to note that while both F_{SH} and F_{HV} would force \hat{n} to the same angle (63.4°) with respect to \hat{H} , F_{SH} forces \hat{n} to be at 63.4° with respect to \hat{s} simultaneously, while for F_{HV} the other simultaneous constraint is $\theta_{\text{V}} = \cos^{-1}(\hat{n} \cdot \hat{\phi}_{\text{s}}) = 63.4^\circ$ which is not the same direction. Thus, in the P stack while one might expect the main peak of the absorption to remain at the static-liquid frequency shift given by $\hat{\alpha}_{\text{B}}^2(T) \sin^2(63.4^\circ)$, there should be a more twisted \hat{n} texture due to the competition between F_{SH} and F_{HV} for alignment of \hat{n} with \hat{s} and $\hat{\phi}_{\text{s}}$ respectively. This would be observed as a change in the overall shape of the absorption around the main peak, which again was not observed. In the V stack the situation will be even simpler to observe. In that configuration (refer to Table (4-1)) F_{SH} causes $\theta_{\text{H}} = \theta_{\text{s}} = 0^\circ$ while F_{HV} should cause $\theta_{\text{V}} = \theta_{\text{H}} = 63.4^\circ$. Therefore, during static-liquid NMR there should be no frequency shift (as observed) while during flowing-liquid NMR a shift from the Larmor value should occur as F_{HV} grows in strength with v_{s}^2 . One might reasonably expect either a tail at the frequency-shifted value or a satellite peak depending on the relative strengths of F_{SH} and F_{HV} . Again, no such result was obtained.

To place the analysis on a more quantitative basis, the surface-field and field-flow energies can be parametrized under the assumption of small bending δ from the observed angle ($\hat{n} \cdot \hat{H} = \cos(1/\sqrt{5})$ in P, $\hat{n} \cdot \hat{H} = 1$

in V). In the P stack, with $\hat{H}||\hat{z}$, $\hat{s}||\hat{x}$, and $\hat{n} = (\cos\alpha\sin\beta, \sin\alpha\sin\beta, \cos\beta)$, the results point to $\beta = 63.4^\circ \pm \delta$, $\alpha = 60^\circ$. The free energy per unit area with no flow in the slabs is (after some algebra)

$$f_o(\hat{n}, T) = -d(\hat{s} \cdot \vec{K} \cdot \vec{H})^2 = -dH^2(4 + 12\delta)/16 \quad (11)$$

with the flowing-liquid energy per unit area being $(\hat{v}_s||\hat{y})$

$$\begin{aligned} f(\hat{n}, v_s, T) &= f_o(\hat{n}, T) - f(\vec{v}_s \cdot \vec{K} \cdot \vec{H}) \\ &= f_s(\hat{n}, T) - 3fv_s^2H^2L(11 - 8\delta)/64 \end{aligned} \quad (12)$$

where an integral has been performed across the slab thickness L assuming no bending (the bending energy in these terms is proportional to δ^2 in lowest order). The corresponding energies in the V stack are $(\hat{s}, \hat{H}||\hat{z})$

$$f_o(\hat{n}, T) = -25dH^2\{(1 + \delta^2/2)^2 - 1/5\}^2/16 \quad (13)$$

and

$$f(\hat{n}, v_s, T) = -15fv_s^2H^2L(6 + \sqrt{20})\delta^2. \quad (14)$$

The greatest constraint put upon F_{HV} from a lack of observed flow effects then comes from the expressions for the P stack. By comparing the static-liquid term which is independent of δ to the corresponding term in the flowing-liquid, an inequality is obtained to be

$$(f/d) \sim 1/(v_c^2L) \ll 1/(2.06v_s^2L) \quad (15)$$

where v_c is a characteristic velocity for F_{HV} which was estimated by Fetter (1976) to be $v_c \sim 0.8$ mm/sec at the PCP. Because our typical velocities were $v_s \geq 0.1$ cm/sec our null results indicate the coupling of the \hat{n} vector to flow is smaller than anticipated since from (15)

$$v_c \gg (2.06)^{\frac{1}{2}} v_s = 0.14 \text{ cm/sec.} \quad (16)$$

Making this value the characteristic velocity reduces the coupling by a factor of 3.06 from the theoretically expected value. Insertion of our highest velocity of 0.484 cm/sec would require a reduction of 36.6 from the theoretical value, but as this data was some of the earliest NMR/flow data somewhat less confidence is attached to it.

Finally, these results should be compared with two other experiments which probed for flow effects in the NMR properties of $^3\text{He-B}$. Flint, Mueller, and Adams (1978) used a double Pomeranchuk cell to provide both the final stage cooling into the superfluid phases (by means of compressional cooling first conceived by Pomeranchuk (1950)) and the flow. The external magnetic field was rotatable with respect to the impressed flow and the flow channels consisted of a 1.5 mm diameter cylinder and two stacks of glass plates with separation of 135 μm as in this experiment. While they did observe flow effects on the NMR spectra in the A phase, no such effects were observed during flow in the B phase including no frequency shift due to flow, no flow-induced susceptibility changes, and no formations of satellite peaks. This work is occasionally called into question because of the presence of solid ^3He in the flow channels evidenced by the large absorption at the Larmor frequency throughout the data. However, the fact that they did observe flow-satellites in the A

phase indicates that they were sensitive to small changes in the NMR absorption even in the presence of the large solid absorption. Hutchins, Brewer, and Kruppa (1985) performed measurements of liquid at 5 bar and in 278 G flowing through a pair of "superleaks" in parallel, each being formed by two parallel plates separated by 100 μm and one being twenty times as long as the other (1 mm, 20 mm). In a separate connecting tube of 2 mm diameter nearer one side of the diaphragm, the transverse NMR coil was wound. The magnetic field was perpendicular to the tube (apparently). The authors claimed that above a temperature-independent critical velocity of $v_c \approx 0.1 \text{ mm/sec}$ a flow-induced frequency shift was observed and they compared this to Fetter's theoretical calculation (Fetter, 1976). The reason for the discrepancy between their result and both that of Flint et al. and this work is not clear. However, one possible source is the rather large noise level on the NMR spectra presented (presumably typical data). Also presented are reasonable normal liquid and non-flowing superfluid spectra but these are signal-noise averaged for an unknown number of eductions. The data which they have analyzed to obtain the flow-induced shifts were not signal-averaged and as a result there appear substantial false satellites and holes in the spectra on the baselines away from the absorptions. Such false structure, if it occurs during the passage through resonance, can produce large changes in lineshape and apparent peak position. If not due to short-term electronic drift, then another candidate might be an instability in their field sweep, the method of generation of the sweep having not been mentioned. Another source for their apparent flow-induced shifts could be the fact that the NMR observation tube is (apparently) asymmetrically located with respect to the flow mechanism (i.e.,

it is on one side of the parallel superleaks). Not knowing the time-scale for the flow production or the thermal properties of their heat exchanger, it is possible to speculate that on a short timescale flow experiment (e.g., minutes) not much normal fluid would flow through the superleaks allowing for a depletion of the superfluid fraction (ρ_s/ρ) on one side of the apparatus and an enrichment of it on the other. The result of this (in essence a thermo-mechanical effect) would be a reduction of the temperature on the superfluid-enriched side of the apparatus. If the NMR tube is present on that side, one would observe an increased frequency shift due to the temperature decrease. Flow in the opposite direction would produce the opposite effect, an increased temperature in the NMR tube and decreased frequency shift. This speculation could be immediately dispensed if it was known that the NMR effects were independent of flow direction. The authors make no statement concerning their data at 5 bar, but at 18.7 bar they report an asymmetry in the NMR shift with respect to flow direction. They do not elaborate on whether this means a reversal of the frequency shift or simply a change in magnitude (which could still be caused by this effect). These considerations certainly lead to a decreased confidence in the results.

One final problem with each of these flow experiments, including the present work, concerns the assumption used by each that the normal liquid fraction of the ^3He sample is made immobile by viscous clamping in the small channels (100 μm up to 1.5 mm). This assumption undoubtedly fails in the 1.5 mm diameter cylinder of Flint et al. As for the parallel plate geometries in each work, the situation is problematic. Evidence will be presented in Chapter V which strongly indicates that

it is very difficult to lock the normal liquid. Mere use of small flow paths is not sufficient to guarantee said result. It is necessary to also account for the timescale of the flow with respect to the timescales of the other measurements. For short-term flow (minutes), the assumption may be correct at least to low order. For long-term flows (on the order of an hour or more) as in many DC-flow experiments there is normal flow which may be characterized as slip in the more open geometries and as viscoelastic in the very restricted geometries. This normal flow affects the flow measurements by decreasing the superfluid velocity. Experiments in which the control parameter is mass current

$$\vec{j} = \rho_s \vec{v}_s + \rho_n \vec{v}_n \quad (17)$$

are susceptible to this problem but it can be controlled by judicious balancing of the timescales as noted.

Superfluid $^3\text{He-B}$ in a Cylindrical Geometry

As has been stated more than once previously, having gained some experience on the slab geometry system which because of its textural complexity was susceptible only to simplified analyses, a new geometry was desired which at once would have a dramatic effect on the NMR properties yet be susceptible by some means to detailed analysis. The result was the cylindrical geometry cell described in Chapter III.

During the course of the experiment, which was begun at low pressures, a large pressure-dependent heat leak into the demag stage was encountered which prevented initial attempts to raise the sample pressure. After that problem was solved, a small leak on the experiment

opened which again prevented the pressure from being increased. As a result, the experiment was performed only at low pressures (0.82 bar and 2.89 bar). Once again the field was held at $H_0 = 286$ G to allow for platinum thermometry at 250 kHz, the field being limited this time to the horizontal direction placing it parallel to and collinear with the axis of the 2-mm-diameter cylinder under NMR observation.

Data Gathering and Calibrations

The method of gathering the NMR data was altered somewhat from that in the slab experiments. Once in the temperature region of interest, after the large demagnetization, the field sweep was executed continuously with a period of 100 sec. Rather than record a single absorption in the entire signal memory (4096 addresses in the Nicolet 1170), the time base of the instrument was set to allow four full field sweep periods (400 sec) to be recorded. Thus, in one memory scan eight spectra were recorded, alternating upsweep and downsweep resonances. In this manner, if the temperature was constant during a particular scan of 400 sec (or changing very slowly) it would later be possible to combine the eight peaks for signal-averaging to improve the result. The signal-averaging was performed by the HP9845A computer using the program called "AVERL" (for average line) which is presented in Appendix B (along with several other data reduction programs to be described when appropriate). If on the other hand the temperature varied substantially during a scan then the eight separate resonances would be preserved for individual analysis thereby avoiding a loss of information by "thermal smearing" if signal-averaging were employed all the time. The choice of four sweep periods was a compromise between the loss of resolution

of individual peaks as their number is increased in the scan and the inconvenience of transferring a small number of lines per scan from the signal averager to the computer. For consistency the first-recorded sweep of a new scan was always a downsweep. Shown in Fig. (4-18) is a typical recorded current trace of the field sweep between $i_{\text{sweep}} = \pm 2.40$ amps amounting to a variation of $\Delta H = \pm 1.65$ G around the persisted Helmholtz field. Also shown is an idealized set of NMR lines to illustrate the usual set-up. To make certain the field sweep was constant, such a current trace was periodically recorded.

The actual normal liquid NMR did not appear as simple as the ideal peaks. Shown in Fig. (4-19) is a real signal-averaged normal liquid NMR line (downsweep) at 2.89 bar and just above the superfluid transition temperature at $\nu_{\text{RF}} = 923$ kHz. The structure (i.e., the side peak) on what should be a symmetric resonance is due to the convolution of the Helmholtz field profile with the RF saddle coil. In the simplest terms, this lineshape can be regarded as the instrument function of this particular NMR spectrometer. If one wishes a physical explanation, it comes from consideration of the fact that the RF coil can sense the precessing ^3He spins for some finite distance along the cylindrical channel along which distance the field is not constant. If H_0 had been constant across the range of the RF coil a symmetric line would result. The on-axis profile of the horizontal Helmholtz field is shown in Fig. (4-20) with the confining geometry of the cell superimposed. The lineshape is given in one dimension by

$$P(\nu) = \frac{1}{\nu} \int dz \delta(\nu - \nu(z)) \quad (18)$$

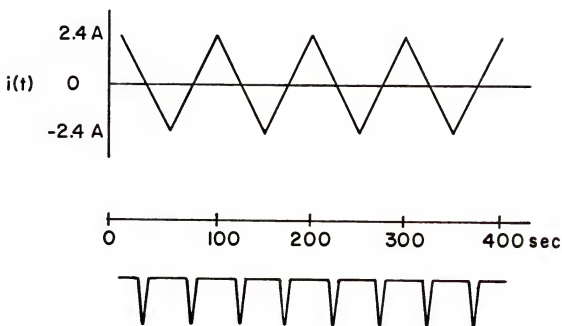


Fig. (4-18). Typical recorded current trace showing the current fed into the field-sweep transformers, amplitude = ± 2.40 amps = ± 1.65 G (about H_0) and period of 100 sec. An idealized set of NMR absorptions is included to illustrate a typical NMR sweep set-up.

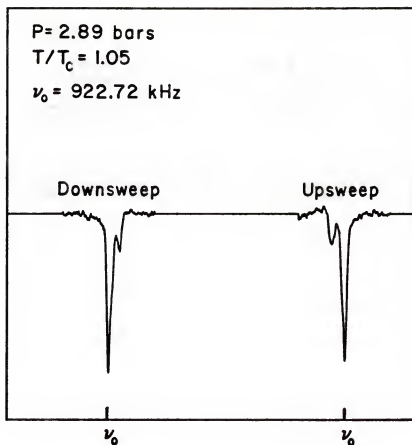


Fig. (4-19). Signal-averaged normal liquid NMR absorption at $T/T_c = 1.05$, $\nu_{RF} = 923$ kHz, $\nu_0 = 922.72$ kHz.

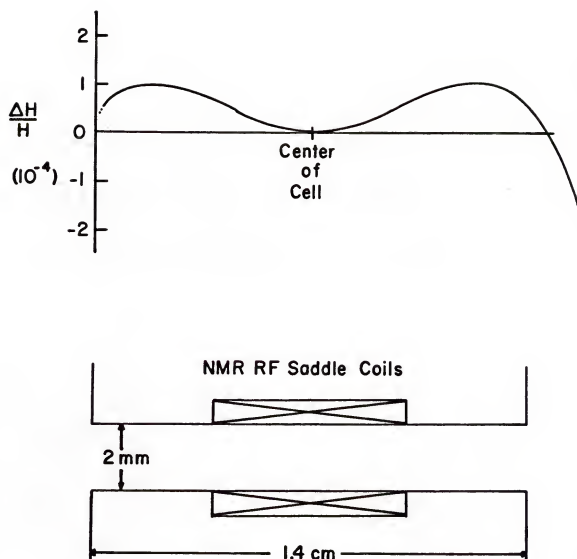


Fig. (4-20). The on-axis profile of the horizontal magnetic field shown in relation to the NMR RF coil and the confining geometry of the cell.

where

$$v(z) = \gamma H_0(z) \approx \gamma (H_0(z) + z \frac{dH_0}{dz}). \quad (19)$$

Using the property of the Dirac delta function that

$$\delta(f(x)) = \left| \frac{df}{dx} \right|^{-1} \delta(x - x_0) \quad (20)$$

where $f(x_0) = 0$, it can easily be shown that the Larmor resonance condition $v_0 = \gamma H_0$ will be satisfied at the positions along the profile where $dH_0/dz = 0$. Of course, the Larmor condition can be satisfied elsewhere along the profile during a sweep but the spectral weight of these positions will be small due to the field gradient whereas at the flat profile regions there will be a local maximum in the number of spins at the proper values of field and frequency. In this way, a small side peak (or shoulder) is formed on the low-field side of the main peak (since the Helmholtz field is larger in the peripheral flat regions than at the center). Effectively, the normal liquid lineshape provides a map of the field within the cylinder.

The normal liquid NMR calibrations were performed in the same manner as in the slab experiment (equations 1-5) by variation of the RF frequency. Shown in Fig. (4-21) is a pair of calibration scans at 0.83 bar in 286 G, Fig. (4-21a) being at 929.5kHz while Fig. (4-21b) is at 927.5 kHz. In this experiment, rather than manually performing the calibration analysis, it was handled by the computer using the program "ANAL" given in Appendix B. The output of "ANAL" included v_0 , κ (sweep current-to-field conversion), the memory locations of each of the eight

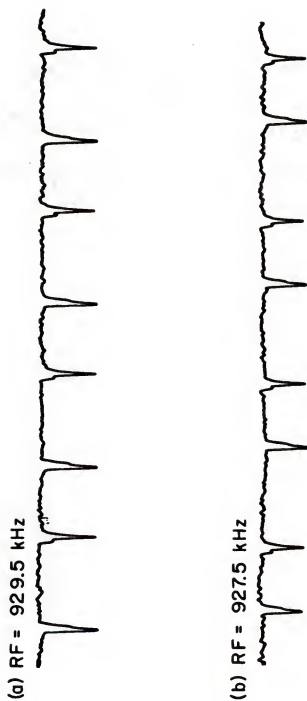


Fig. (4-21). Normal liquid calibrations taken at 0.83 bar and 286 G: (a) RF = 929.5 kHz; and (b) RF = 927.5 kHz.

normal liquid peaks, and the values of the inductive lags of the true current L (the upswing and downswing lags are, in general, not equal but are nearly so).

As discussed in Chapter III, pages 61-63, the thermometry in this cell above T_c was by pulsed Pt NMR while below T_c the maximum frequency shift of the ^3He was used.

Normal Liquid and Superfluid Spectra

The raw normal liquid and superfluid NMR spectra are presented in Figs. (4-22) through (4-24). In contrast to the presentation of the slab geometry NMR data which had been inverted, the data of this experiment were never inverted during storing or analysis and have been left in this form, as absorptions. In the middle of the fifth trace of Fig. (4-23) the gain was reduced to see the entire normal liquid adsorption. If the scan occurred at constant temperature the average reduced temperature T/T_c is given. When the temperature varied substantially during the scan, individual temperatures for each peak are given.

The signal-averaging program "AVERL" used for constant temperature scans performed two operations to average the NMR lines. Using the addresses of the normal liquid peaks (i.e., the Larmor frequency addresses x_i), the program first translated all the downswing (upswing) peaks to the position of the first downswing (upswing) peak adding them together. If the down- and upswing lags were equal, it could then reflect all the upswings about the Larmor address and average them together with the downswings. If the lags were too disparate this operation was not performed. Finally, the signal-averaged peaks were stored on tape for further analysis. The full sequence of NMR anal-

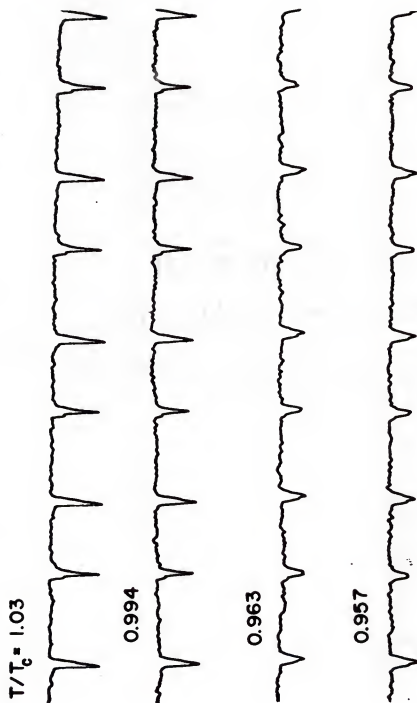


Fig. (4-22). Spectra obtained at 0.83 bar, 286 G, 929.5 kHz.

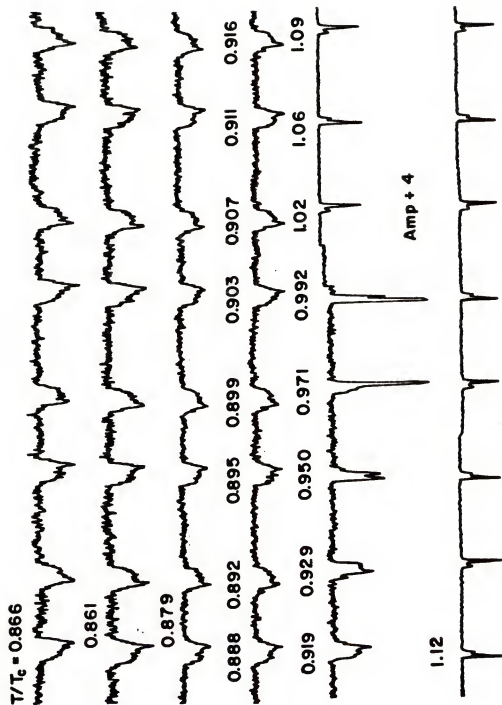


Fig. (4-23). Spectra obtained at 2.89 bar, 286 G, 923 kHz.

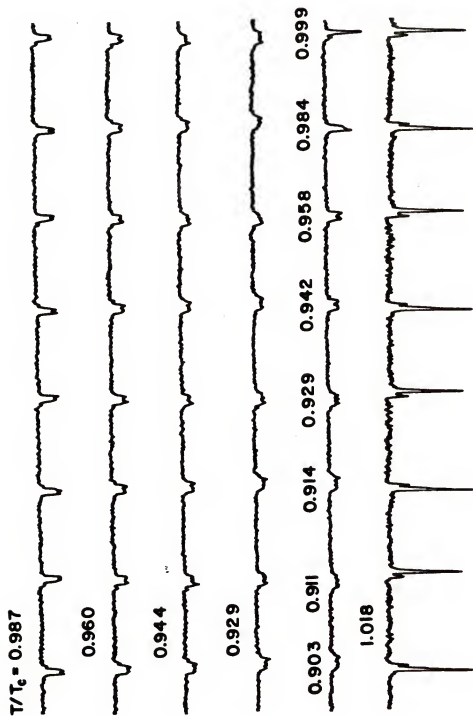


Fig. (4-24). Spectra obtained at 2.89 bar, 286 G, 923 kHz.

ysis is pictorially presented in the form of a flowchart at the beginning of Appendix B.

After averaging in "AVERL" or in the case of non-constant temperature scans in its stead the superfluid NMR line was passed to the program "SIP" (shift-integral program). The program was originally written as a group of separate routines capable of any combination of smoothing, baseline subtraction, measurement of frequency shift of line structure, and measurement of longitudinal resonance frequency Ω_B^2 in any order desired. In its present use it provided the measurement of the maximum frequency shift of an absorption from ν_0 which could be used to obtain the temperature of the ^3He , as described in Chapter III. Once the position of the maximally-shifted absorption was determined, the value of the sweepcurrent was found and equation (6) could be used to establish Ω_B^2 and finally the temperature.

Deconvolution of Superfluid Spectra

As can be seen in the NMR scans, substantial effects on the resonance were achieved. In order to do more than merely measure the maximum frequency shift (not particularly interesting in the wake of the slab geometry experiments) or even measure the spectral weight as a function of frequency shift (more interesting but not directly related to any calculations), a method of deconvolution of the resonances to obtain the \hat{n} texture was sought.

The first step in deriving a deconvolution was the realization, already stated, that the normal liquid NMR lineshape was a map of the static field profile (or a convolution of H_0 with H_{RF}). Equally important was the fact that the frequency shift of the superfluid, caused by

the longitudinal resonance Ω_B^2 , was field-independent. (See equations (37), (40), and (42) in Chapter II.) The immediate conclusion from these points was that, lacking any textural effects on the NMR, the superfluid lineshape would be identical to the normal liquid. For example, in a large bulk sample in which the surface effects were negligible, $\hat{n}(\vec{r})$ would everywhere be aligned with \vec{H}_O yet the resonance frequency would still depend upon the field inhomogeneity through

$$v^2(\hat{n}(\vec{r}), \vec{H}_O(\vec{r})) = v_O^2(\vec{H}_O(\vec{r})) + \Delta v^2(\hat{n}(\vec{r})). \quad (21)$$

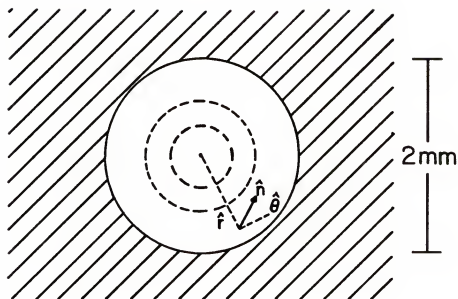
In the present experiment, it was extremely important that the cylinder symmetry of the system had been preserved, particularly through the use of the horizontal Helmholtz field which was coaxial with the cylinder. Breaking this symmetry would have stopped the deconvolution effort at this point since no symmetry arguments could have uniquely established the resulting complex asymmetric texture. Turning on the textural interactions, including F_{BH} , F_{BB} , F_{SD} , and F_{SH} (respectively, equations 46, 47, 50, and 52 in Chapter II) would not alter the symmetry but rather impose it since the boundary conditions at the surface would be determined by the cylindrical wall. Away from the wall the bulk interactions would provide a continuously-applied force on the texture as the cylinder axis was approached. Therefore, with the surface interactions providing the boundary conditions and the bulk interactions constraining the texture throughout the sample volume, it was possible to conclude that the texture would possess cylindrical symmetry. At any point in the liquid the \hat{n} vector was constrained by the local conditions of bending and continuity determined by its proximity

to the wall. As a result, except for the field inhomogeneity, the equipotential surfaces formed by contours of constant constraint force on the texture would be concentric cylinders within the channel, shown in Fig. (4-25). (These contours are equipotential surfaces in the sense that the superfluid attempts to minimize its free energy through variation of the \hat{n} vector field. At any point within the sample, F_{BH} and F_{BB} compete for alignment of \hat{n} and the balance of forces felt by \hat{n} on such a contour is constant. Upon another contour the balance of constraint between F_{BH} and F_{BB} is different resulting in a new equilibrium direction for \hat{n} .) On a given equipotential the field-dependence would be given by the normal liquid lineshape in the limit $v_0 \gg \Delta v$. At this point the \hat{n} vector field could be parametrized as

$$\hat{n}(\vec{r}) = (n_x, n_y, n_z) = (-\cos\alpha(r) \sin\beta(r), \sin\alpha(r) \sin\beta(r), \cos\beta(r)). \quad (22)$$

These considerations provide the deconvolution scheme or conversely explain the shape of the superfluid NMR absorptions. A broadened superfluid NMR line is the algebraic sum of the inhomogeneously-broadened normal liquid absorptions, each equipotential contour resonating at the frequency given by the local texture on that contour. The overall texture in the cylinder is presumed, on the basis of the above, to resemble the flare-out texture introduced by Smith et al. (1977) and discussed in Chapter II, pages 38-41. The surface interactions cause \hat{n} to deviate farthest from \hat{H}_0 at the wall giving the largest shift from v_0 ; moving toward the axis F_{BH} forces increasingly greater alignment mediated by the bending energy F_{BB} giving smaller frequency shifts back toward v_0 .

(a)



$$\hat{n}(r) = (n_r, n_\theta, n_z) = (-\cos\alpha(r) \sin\beta(r), \sin\alpha \sin\beta, \cos\beta)$$

(b)

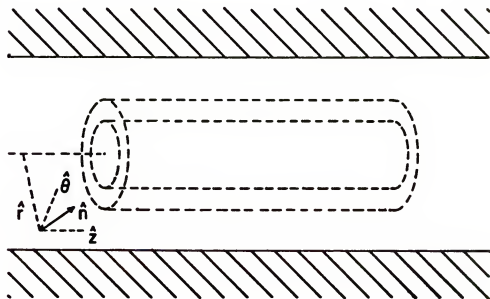


Fig. (4-25). Schematic of the constant constraint contours: (a) end view; and (b) side cross-section. Also shown is the parametrization of $\hat{n}(\vec{r})$.

Armed with these three assumptions (cylindrical symmetry, textural continuity, and inhomogeneous broadening of the Larmor resonance) the superfluid spectra could be deconvoluted in the following manner. First, at the Larmor frequency a signal-averaged normal liquid NMR peak was scaled down to the amplitude of the superfluid line at ν_0 and then the normal peak was subtracted from the superfluid peak. If $P_n(\nu)$ was the normal liquid lineshape and $P_s(\nu)$ was the superfluid lineshape then the remainder was given by

$$R_1(\nu) = P_s(\nu) - S(\nu_0)P_n(\nu), \quad (23)$$

where the scale factor $S(\nu_0) \equiv P_s(\nu_0)/P_n(\nu_0)$ and ν ranged across the frequency equivalent of the field sweep, $\nu \pm \Delta\nu/2$ where $\Delta\nu = \gamma\Delta H$. In this manner an accounting of all spins in the sample resonating at ν_0 was made. The fraction subtracted away

$$f(\nu_0) = 1 - R_1(\nu)/P_s(\nu) = S(\nu_0)P_n(\nu)/P_s(\nu) \quad (24)$$

was recorded. Sequentially the normal liquid peak was translated away from ν_0 to larger frequency shifts centered on ν_k , scaled to the amplitude of the remainder, and subtracted. After k such operations the remainder was

$$R_k(\nu) = R_{k-1}(\nu) - S(\nu_k)P_n(\nu) \quad (25)$$

where $S(\nu_k) = R_{k-1}(\nu_k)/P_n(\nu_0)$ giving the fraction subtracted in this interval as

$$f(v_k) = S(v_k)P_n(v)/P_s(v). \quad (26)$$

Use of the normal lineshape insured that all spins resonating at a given v_k were taken into account. This shift/subtraction process was continued until all the original superfluid signal had been removed, operationally defined by having the integral of the final remainder $R_f(v)$ be a small percentage of the initial superfluid susceptibility, typically 2% or better. An idealized subtraction is shown in Fig. (4-26a). Presented in Fig. (4-26b) are the two deconvolution errors which are most evident. The first, over-subtraction, is caused by using too large a scale factor $S(v_k)$ producing a large negative excursion (upward) in $R_k(v)$ over a small interval. The second, over-translation, is caused by using too large a frequency shift from one interval to the next resulting after subtraction in a positive excursion (downward) in $R_k(v)$ and leaving some of the superfluid susceptibility unaccounted. This deconvolution was performed by "ALGOR" (Appendix B); it included routines to automatically detect these and other errors and avoid them. Knowledge of the center frequency v_k of the deconvolution intervals allowed each subtracted fraction $f(v_k)$ to be associated with a frequency shift $\Delta v_k^2 = v_{RF}^2 - v_k^2$. Use of equation (II-45) and equation (IV-9), giving $\Omega_B^2(T,P)$, allowed the calculation of the angle the texture made with \vec{H}_0 in each interval yielding

$$\beta_k = \sin^{-1} \left(\frac{v_{RF}^2 - v_k^2}{\Omega_B^2(T,P)} \right)^{1/2}. \quad (27)$$

The results given by "ALGOR" were $(\beta_k, f(\beta_k))$, $f(\beta_k)$ being the fraction of superfluid characterized by $\beta_k = \cos^{-1}(\hat{n}_k \cdot \hat{H}_0)$. Actual deconvolutions of superfluid lines at various temperatures are presented in Fig. (4-27).

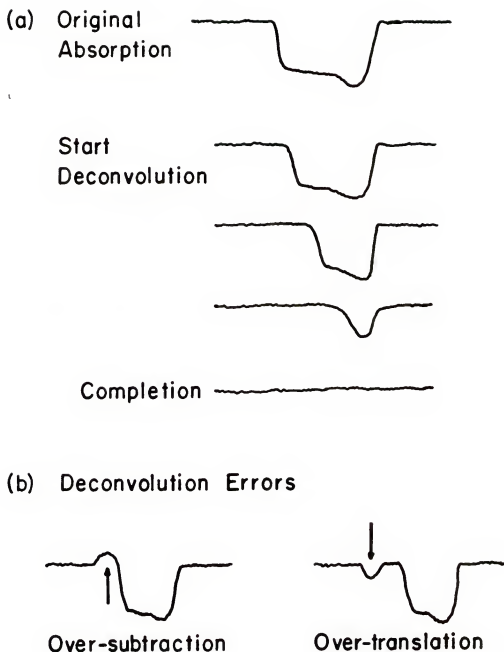


Fig. (4-26). Depiction of the idealized NMR deconvolution process: (a) deconvolution; and (b) possible errors in deconvolution.

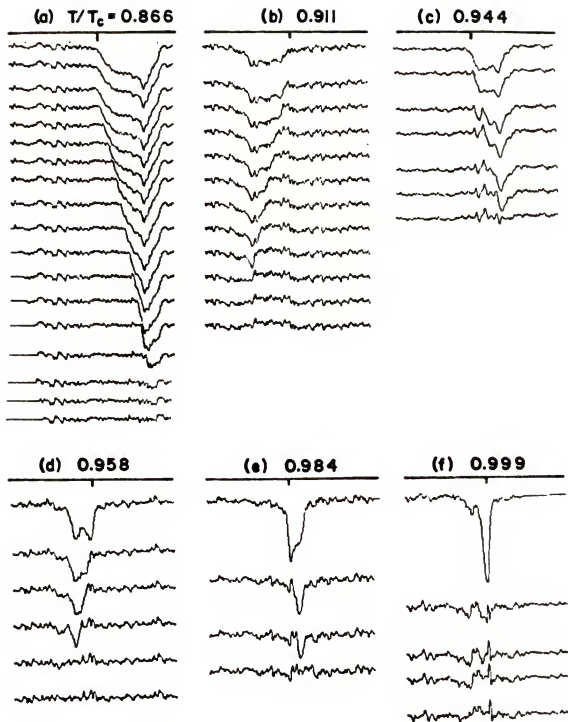


Fig. (4-27). Actual deconvolution of 2.89 bar superfluid peaks at several temperatures: (a) $T/T_c = 0.866$; (b) 0.911; (c) 0.944; (d) 0.958; (e) 0.984; and (f) 0.999. The Larmor frequency is marked on each by a tic-mark.

To begin to obtain the coordinate space picture of the \hat{n} texture, the deconvoluted results from "ALGOR" had to be associated with positions inside the cylindrical sample. Using the considerations already detailed this was accomplished in the following way. The fraction of signal at zero frequency shift (i.e., at the Larmor frequency), $f(0)$, was assumed to occupy a cylindrical subvolume of the total cylindrical sample (most easily visualized by reference to Fig. (4-25)), since alignment of \hat{n} and \vec{H}_0 would occur, if anywhere, near the axis, with the relation

$$f(0) = V_{\text{sub}}/V_{\text{cyl}} = r_o^2/R^2, \quad (28)$$

where R = the radius of the sample = 1 mm and r_o was the radius of this subvolume. Having found $r_o(\beta=0)$, in each successive interval the fraction of signal at that shift was assumed to occupy a cylindrical shell whose volume was related to the total cylindrical volume by that fraction. In the k^{th} interval

$$f(\beta_k) = (r_k^2 - r_{k-1}^2)/R^2 \quad (29)$$

from which the outer radius r_k could be found. This process was continued starting from the cylinder axis and moving toward the wall. It was performed by "SPATEX" (Appendix B) which returned $(r, \beta(r))$. Some values of $\beta(r)$ at various temperatures are shown in Fig. (4-28). At the lowest temperatures \hat{n} requires almost the entire cylinder volume to recover its alignment with the field while just below T_c it quickly bends and is aligned over most of the volume. Note also that the texture does seem to approach the boundary condition given by F_{SH} at the

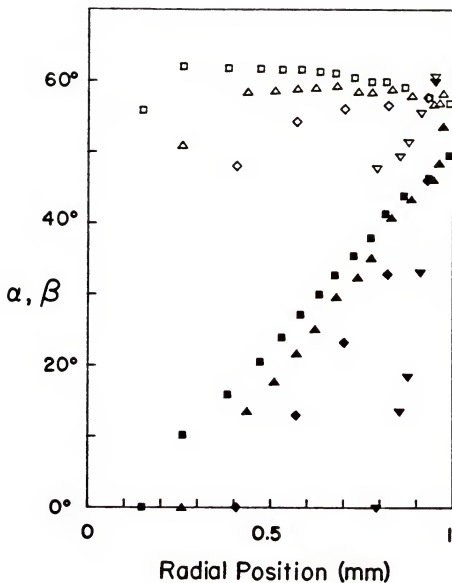


Fig. (4-28). The textural angles $\alpha(r)$ (open symbols) and $\beta(r)$ (closed symbols) inside the cylinder at various temperatures at 2.89 bar. The square symbols are $T/T_c = 0.797$; triangles, 0.906; diamonds, 0.917; and inverted triangles, 0.929. (After Spencer and Ihas, 1982.)

wall that being $\beta(r = 1\text{mm}) = \cos^{-1}(1/\sqrt{5}) = 63.4^\circ$. This is a result obtained from the experiment and was not forced. This is to be compared with the original flare-out texture calculation of Smith et al. (1977) in which the boundary condition selected at the wall was that given by F_{SD} , namely $\beta(\text{wall}) = 90^\circ$. In this sense, the texture found in this experiment is not the originally-proposed flare-out texture, but the name is retained regardless.

To finally reveal the 3-dimensional texture a means of finding the azimuthal angle $\alpha(r)$ was needed. This was achieved by use of the two bulk free-energy terms F_{BH} and F_{BB} which constrained the texture in the cylinder. The texture responded in such a way as to minimize its free energy throughout the sample. Referring to equation (II-46) F_{BH} depended only on $\beta(r)$ which had already been uniquely determined by the NMR deconvolution. Thus, F_{BH} was not subject to any minimization. Only F_{BB} was left to be minimized. Starting from its original form (equation (II-47)) it was cast into cylindrical coordinates which, after regrouping, appeared as

$$F_{BB}(\alpha, T) = \frac{2\pi L}{13} c \int_0^R dr r F(\alpha(r), \beta(r)) = \frac{2\pi L}{13} c I_{BB}(T) \quad (30)$$

where L was the cylinder length and the integrand was

$$\begin{aligned} F(\alpha(r), \beta(r)) = & \beta'^2 \{ (3\sin^2\beta + 2)\cos^2\alpha + 11 - 2\sqrt{15} \cos\beta \sin\alpha \cos\alpha \} \\ & + \frac{2}{r} \beta' \{ (14\sin^2\alpha - 3)\sin\beta \cos\beta - \sqrt{15} \sin\beta \sin\alpha \cos\alpha (\cos^2\beta + 1) \} \\ & - 2\beta' \alpha' \{ 2\sin\beta \cos\beta \sin\alpha \cos\alpha + \sqrt{15} \sin\beta (\cos^2\beta \cos^2\alpha - \sin^2\alpha) \} \\ & + \frac{2}{r} \alpha' \{ (5\sin^2\beta + 14)\sin^2\beta \sin\alpha \cos\alpha - \sqrt{15} \sin^2\beta \cos\beta (\cos^2\alpha - \sin^2\alpha) \} \\ & + \alpha'^2 \{ (5\sin^2\beta + 11)\sin^2\beta \cos^2\alpha + 13\sin^2\beta \sin^2\alpha + 2\sqrt{15} \sin^2\beta \cos\beta \sin\alpha \cos\alpha \} \\ & + \frac{1}{r^2} \{ 5\sin^4\beta \sin^2\alpha + \sin^2\beta (2\cos^2\alpha + 11) - 2\sqrt{15} \sin^2\beta \cos\beta \sin\alpha \cos\alpha \}. \quad (31) \end{aligned}$$

The primes indicate d/dr . Because only 1st derivatives of α and β were involved, only one boundary condition was required for a complete solution. This was the constraint due to F_{SH} at the wall. If $\beta(\text{wall}) = \cos^{-1}(1/\sqrt{5}) = 63.4^\circ$, it is easy to show that $\alpha(\text{wall}) = \cos^{-1}(1/2) = 60^\circ$. To determine $\alpha(r)$, these boundary conditions were inserted and the integral I_{BB} was performed at each interval for which $\beta(r_i)$ was known starting at the wall and moving toward the axis. In each interval the value of I_{BB} was minimized by variation of $\alpha(r_i)$. This was done by "MINI" (Appendix B) which gave the value of $\alpha(r_i)$ which minimized $I_{BB}(r_i)$. It also returned both integrals $I_{BB}(T)$ and the corresponding bulk-field integral $I_{BH}(T)$. The $\alpha(r)$ results are shown in Fig. (4-28). Although $\alpha(r)$ does show some variation across the cylinder (becoming indeterminate when $\beta = 0$) it is surprisingly constant. Prior to this result and lacking any information to the contrary, all calculations assumed that it was constant, $\alpha(r) = \alpha_0$. It does seem that the texture maintains its azimuthal twist at the expense to the radial component. Shown in Fig. (4-29) are plots of the \hat{n} texture at different temperatures. This work provided the first experimentally-derived look at a non-trivial three-dimensional \hat{n} texture in $^3\text{He-B}$.

Free-energy Analysis to find the Magnetic Bending Length

As the temperature of the sample approaches T_c it becomes possible to apply a Ginzburg-Landau expansion of the free-energies to low enough order in $\epsilon = 1 - T/T_c$ to make meaningful results extractable from the experimental deconvolutions. For the runs at 2.89 bar data was taken as the sample approached very close to T_c , permitting this kind of analysis.

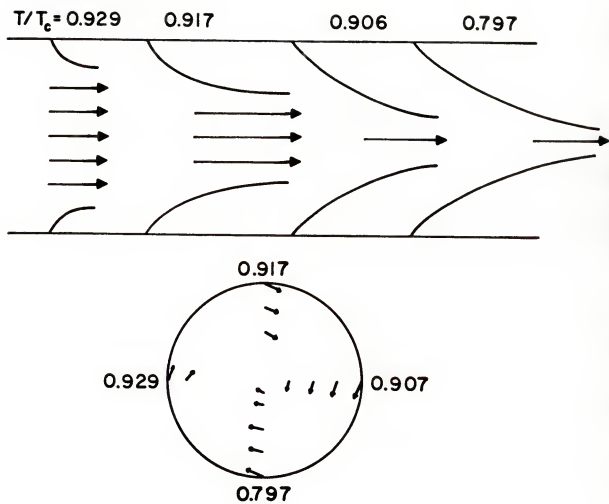


Fig. (4-29). Views of the \hat{n} texture inside the cylinder.

The bulk free-energy per unit length of the sample could be written as

$$(2\pi L)^{-1} \Delta F(\epsilon) = -a(\epsilon)H^2 I_{BH}(\epsilon) + c(\epsilon)I_{BB}(\epsilon)/13 \quad (32)$$

where the axial and angular integrations have been done leaving the radial integrals $I_{BH}(\epsilon)$ and $I_{BB}(\epsilon)$ and where $a(\epsilon)$ and $c(\epsilon)$ were the coefficients of F_{BH} and F_{BB} respectively (equations (II-46) and (II-47)). The temperature dependences of these parameters were written as

$$a(\epsilon) = a_0 - a_1\epsilon \quad \text{and} \quad c(\epsilon) = c_1\epsilon \quad (33)$$

from Brinkman and Cross (1978) and Smith et al. (1977).

As already stated, the program "MINI" performed the radial integrals I_{BH} and I_{BB} as part of the $\alpha(r)$ determination. The results of these integrals are shown in Fig. (4-30). As might have been expected, the bending integral was quite sensitive to the boundary condition at the wall and so in cases where large gradients occurred, perhaps due to the graininess of the deconvolution, points near the wall were smoothed. The data was best fit by

$$I_{BH}(\epsilon) = \int_0^R dr \, r \cos^2 \beta(r) = (0.465 - 1.15\epsilon) \text{ mm}^2, \quad (34)$$

and

$$I_{BB}(\epsilon) = \int_0^R dr \, r F(\alpha, \beta) = 3.53\epsilon^{-1}. \quad (35)$$

The error estimates for the values of these integrals, represented by

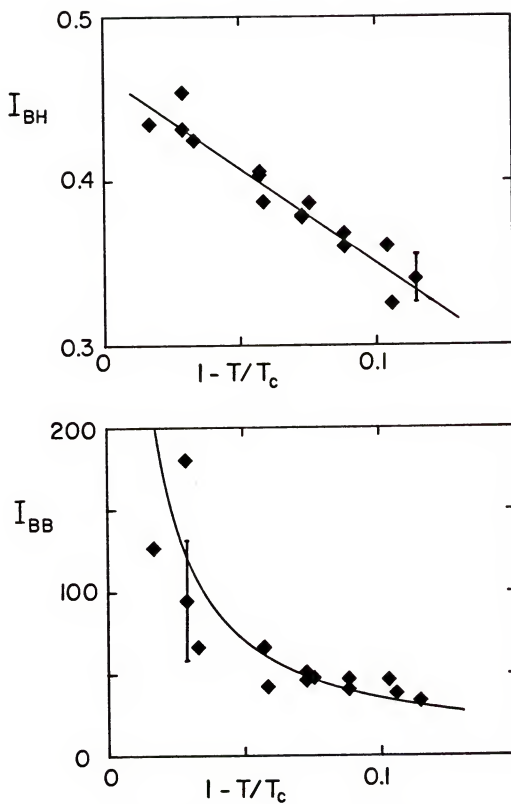


Fig. (4-30). The radial parts of the free-energy integrals I_{BH} and I_{BB} versus $1 - T/T_c$.

the error bars in Fig. (4-30), were derived from considering the baseline noise on the NMR spectra and its contribution to the uncertainty in the deconvolution. If the absolute noise (obtained by taking the absolute values of the deviations from the baseline, integrating along the entire baseline, and finding the average deviation) was n in the scan, then the uncertainty in any given fraction was

$$\delta f = \pm \frac{n}{N_T} \frac{\Delta a}{d} \quad (36)$$

where N_T = true total area of NMR absorption, Δa = width of NMR absorption in addresses in the scan, and d = number of intervals in the deconvolution. This in turn created an uncertainty in the radial position of the deconvoluted interval of

$$\delta r_i = \frac{1 + 1}{2r_i} R^2 \delta f \quad (37)$$

where $R = 1$ mm. Substituting experimental values for these quantities, as $n \sim 5$, $N_T \sim 10^4$, $\delta a = \Delta a/d \sim 8$, gave the uncertainty as

$$\delta r_i = 0.002 \frac{1 + 1}{r_i} \text{ mm.} \quad (38)$$

This value was then propagated through the radial integrals to arrive at the error estimates.

The results (34) and (35) can be converted to give the free-energy densities of the two bulk interactions as

$$f_{BH} = -aH^2(0.93 \pm 0.02 - 2.3\epsilon) \text{ erg/cm}^3 \quad (39)$$

and

$$f_{BB} = (54 \pm 13) c\epsilon^{-1} \text{ erg/cm}^3. \quad (40)$$

To obtain the magnetic bending length, the total bulk free energy $\Delta F(\epsilon)$ was set equal to zero at $T_c(\epsilon=0)$, giving

$$c_1/a_0 = 1.713H^2 \text{ mm}^2 \text{ G}^2. \quad (41)$$

This left the ratio (a_1/a_0) undetermined. Using unpublished results of Osheroff and Brinkman, Smith et al. (1977) quoted estimates of $a(T)/\chi_N$ which were fit (in this work) as $a(\epsilon)/\chi_N = (0.8633 - 1.100\epsilon) \times 10^{-5}$ yielding $(a_1/a_0) = 1.274$. Maki and Nakahara (1983) using the texture plots of Fig. (4-28) as a guide to their calculation of spin-wave satellite frequencies in rotating $^3\text{He-B}$ found the result $(a_1/a_0) = 0.53$ in the Ginzburg-Landau regime (near T_c). A value close to this last may be found in the present analysis but only by extending it far beyond the presumed region of validity. Using the Maxwell relation $S(T) = -(\partial F/\partial T)_V$ and the fact that $S(T=0) = 0$ the result $(a_1/a_0) = 0.627$ was obtained from $\Delta F(\epsilon)$ in (32). This differs from the Maki-Nakahara value by some 15% and is within 2% of being exactly half of the Osheroff-Brinkman value. That an extrapolation of a low-order Ginzburg-Landau expansion to a large value of the expansion parameter ($\epsilon = 1$) should return a result so close to a calculation carried out near T_c is hardly expected. The reason for the factor of two with respect to the Brinkman result is also unclear.

The magnetic bending length was found from these efforts to be

$$R_c H_B = (c/a)^{1/2} = \left(\frac{c_1}{a_o} \frac{\epsilon}{1 - (a_1/a_o)\epsilon} \right)^{1/2} \\ = (37.4 \pm 5) \left(\frac{\epsilon}{1 - 0.627\epsilon} \right)^{1/2} \text{ cm G} \quad (42)$$

at $P = 2.89$ bar and $H_o = 286$ G. This is to be compared with the result found by Osheroff et al. (1975) of $R_c H_B = 36(1 - T/T_c)$ at the melting curve. Shown in Fig. (4-31) is the present result to lowest order in its temperature dependence,

$$R_c H_B = (37.4 \pm 5)(1 - T/T_c)^{1/2} \text{ cm G}, \quad (43)$$

shown as the full curve. Also plotted are discrete values of $R_c H_B$ from this analysis, shown as inverted triangles. The data of Osheroff et al. (1975) is also shown both as its melting curve value and scaled to 2.89 bar using the pressure dependence of the Fermi-liquid parameters as measured by Alvesalo et al. (1981) (see equations (II-46) and (II-47)). Finally, if the scaled results of Osheroff et al. (1975) are used to determine the next order of ϵ in the present expression for the bending length the result becomes

$$R_c H_B = (37 \pm 5)(\epsilon^{1/2} + 0.9\epsilon^{3/2}) \text{ cm G} \quad (44)$$

to compare with the expansion of (42)

$$R_c H_B = (37 \pm 5)(\epsilon^{1/2} + 0.3\epsilon^{3/2}) \text{ cm G}. \quad (45)$$

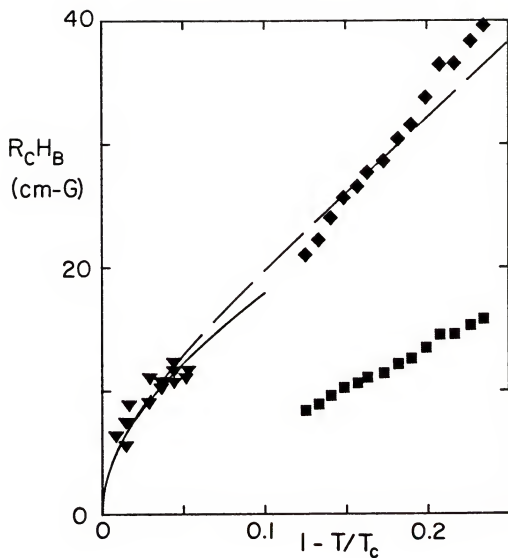


Fig. (4-31). The magnetic coherence length $R_C H_B$. Expression (43) is the full curve while discretized values of $R_C H_B$ obtained at 2.89 bar are the inverted triangles. The melting curve results of Osheroff et al. (1975) are the squares; these same results scaled to 2.89 bar are the diamonds. The broken curve is a fit to both sets of data given by equation (44).

Expression (44) is plotted as the broken curve in Fig. (4-31). The reason for the discrepancy between temperature dependences in these two works may be due to the fact that at the melting curve the B phase does not exist above $T/T_c \sim 0.75$. The present experiment approaches T_c to within $T/T_c > 0.98$.

Work by Others

After the results above were initially published by Spencer et al. (1981, 1982) they were used to analyze a somewhat more complex system, a rotating cylinder of $^3\text{He-B}$ with an axial magnetic field (Ikkala et al., 1982). Maki and Nakahara (1983), as mentioned, parametrized the \hat{n} vector as in (22), wrote the bending and field energies, and solved numerically to find the \hat{n} texture. Their result gave

$$\beta(r) = \beta_1 (r/r_o) \quad (46)$$

with

$$\beta_1 = 1.9(r_o/\xi_H)^{3/2} \exp(-0.93r_o/\xi_H) \quad (47)$$

and

$$\xi_H = (0.7016)R_c H_B/H. \quad (48)$$

This gave a $\beta(r)$ similar to the experimental results of Fig. (4-28) except that in their calculation the azimuthal angle was taken to be strictly constant, $\alpha(r) = \pi/3$. Using this as a basis, they found

answers which fit the rotating data reasonably well. In a similar effort to explain the rotating data, Hakonen and Volovik (1982) performed an Euler-Lagrange analytical calculation to find the static texture with the result that $\alpha(r)$ varied from 60° at the wall to 38° in the bulk liquid. They claimed a more quantitative fit with both this work and the rotating data.

The question of whether $\alpha(r)$ is constant or not at any given temperature can not be decided on the basis of the static texture work. The radial integral I_{BB} is not sufficiently sensitive to $\alpha(r)$ to cause a definitive change if the α -dependence is varied between these two limiting cases, the reason being that the large gradients in $\beta(r)$ dominate the bending integral.

Concluding Remarks and Future Work

In summary, the work of the two B phase experimental cells accomplished the following: (1) extended the measurements of the longitudinal resonance frequency Ω_B to s.v.p. allowing interpolation between these results and high pressure results; (2) found the textural response to flowing superfluid to be smaller than anticipated, perhaps null; (3) devised a means to deconvolute the NMR spectra in a specific geometry, hopefully providing guidance to future efforts in other carefully-selected geometries; (4) experimentally mapped the 3-dimensional \hat{n} texture inside the cylinder disclosing an unanticipated variable twist ($\alpha = \alpha(r)$); (5) used the bulk free-energies to find the magnetic bending length revealing the proper Ginzburg-Landau temperature dependence $\epsilon_c^{1/2}$ near T_c ; and (6) provided intriguing hints that application of Ginzburg-Landau expansions at large expansion parameter values may give reliable results.

Concerning future work in these systems, in many respects holes remain to be filled in the experimental testing of the innumerable theoretical calculations. Methods have been devised for performing both CW (Ehnholm et al., 1979) and pulsed NMR (Friedman et al., 1986) in very low and even zero magnetic field. These methods could be used in each of the two kinds of geometry discussed here. In the slab geometry, low-field NMR ($H_0 \leq 30$ G) could be used to make the textural-flow interactions (F_{HV} and F_{BV}) dominate the system (if they are in fact present). Any effects would be most telling in a vertical magnetic field (in the present slab configuration) because in the V stack of plates the small magnetic interactions would once again produce a uniform texture ($\hat{n} || \hat{s} || \hat{H}_0$). Any bending due to impressed flow would be visible as a decrease in the Larmor susceptibility and/or the appearance of satellites or shoulders on the absorption. In the cylindrical geometry cell, Smith et al. (1977) have predicted the appearance at low fields of a different \hat{n} texture, the so-called "in-plane" texture (occasionally referred to as the "Pan-Am" texture due to its resemblance to that company's logo; this term was originally applied to an A phase \hat{l} texture). The signature of this textural transition should be quite dramatic since the in-plane texture has $\beta(r) = \pi/2$ throughout the cylinder. Therefore, in the flare-out regime at sufficiently low temperature, the CW NMR absorptions would be the pill-box shaped lines seen in this work while at the same temperature in the in-plane regime the entire line would shift to the maximum frequency shift at $\beta = 90^\circ$. The dynamics of the transition have not been worked out but if the transition region is narrow it might be possible to set up a field-sweep situation in which

the \hat{n} texture was in-plane at the low end of the sweep and flare-out at the high end. Using the deconvolution technique presented herein the possibility of studying such a dynamic system directly is very interesting.

CHAPTER V
NMR AND FLOW OF ^3He INSIDE VYCOR GLASS

Introduction

In this chapter are presented the results of the studies of ^3He inside the extremely restricted geometry provided by vycor glass. What theory there is which can be applied to this system has been presented in Chapter II, pages 44-52.

First, CW NMR results obtained in a preliminary cell are presented. In that experiment, a very small frequency shift from the Larmor frequency was measured. Next the susceptibility of ^3He in vycor was measured at 1.10, 3.93, and 5.45 bars in the range from 1 to 200 mK using pulsed NMR.

Finally, the results of the measurements of flow of liquid ^3He through vycor are presented as well as observations of a flow effect on the susceptibility.

Magnetism of ^3He Inside Vycor

Frequency Shift Measurements

The frequency shift of the ^3He resonance away from the Larmor value was measured in a preliminary cell (which was later replaced by the cell of Fig. (3-12)) using CW NMR. The field was swept while persisted in the manner discussed in Chapter IV but the amount of the field sweep was reduced substantially and a field gradient was turned onto the sample. In

this way, it was possible to look at only the peak of the absorption rather than its entire structure. This magnified peak was collected into the memory of a Biomation transient recorder (model 610) and then transferred into the computer (HP9845). Using a parabolic fit, the location of the NMR peak was found and stored. The standard calibration of the data by variation of the frequency of the RF was performed.

The results of the frequency shift measurement at 0.10 bar are shown in Fig. (5-1a). The field was 28.6 mT. The shift of the response was quite small and negative which is the opposite direction from that of the superfluid shift. Shown in Fig. (5-1b) is the data plotted as a function of $1/T^{2.2}$. The straight line is a least squares fit to the shifts. Shown in Fig. (5-2) is this fit (solid line) plotted along with the data of Bozler et al. (1983). The positive frequency shift they measured had the field parallel to the surface normal of the substrate while the negative shift had the field perpendicular to the normal. The reason why these two very different systems can have similar frequency shifts, in particular why the shift in Grafoil with a perpendicular field should resemble the shift in a heterogeneous system like vycor is unclear.

Susceptibility Measurements

The susceptibility measurements were performed in the final vycor cell, shown in Fig. (3-12), by pulsed NMR. As discussed in Chapter III a cancellation bridge circuit was used to prevent the RF pulse from saturating the detection apparatus. Relative susceptibilities were measured by integration of the free induction decay (FID) envelope after the pulse. As seen in Fig. (3-7), mistuning of the bridge permitted more

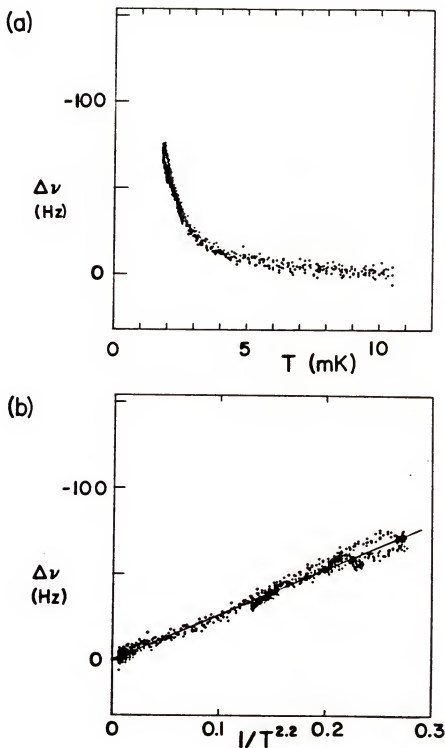


Fig. (5-1). Frequency shift from CW NMR: (a) The frequency shift of ^3He at 0.1 bar and 28.6 mT. The shift is negative with $\nu(T) - \nu_0 < 0$. (b) The frequency shift plotted as a function of $T^{-2.2}$ with the least squares fit shown.

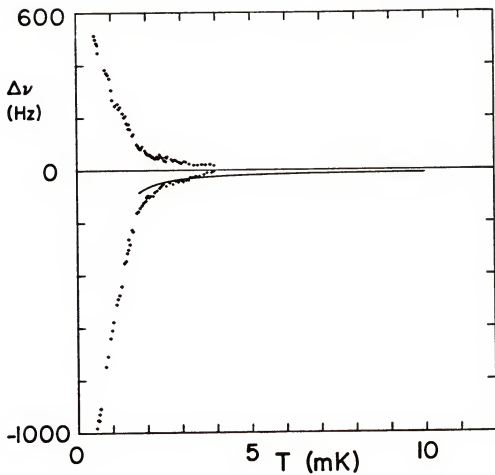


Fig. (5-2). A comparison of the frequency shift measured in vycor (this work, shown as a solid line) with that measured by Bozler et al. (1983) in Grafoil in 16.9 mT.

of the pulse to enter the amplifier chain causing a subsequent dead time of the amplifier. It was found that the FID integral was unaffected as long as the integration was begun after the amplifier recovery. Even so, care was taken to keep the tuning correct. Also, checks of the saturation of the FID integral with respect to the pulse amplitude and length were made and these values were avoided. The data was taken using the program "TIMERS" which is presented in Appendix B. The program took measurements of all required quantities (pump position, manometer differential pressure, sound level, Pt thermometer, and FID) at regular intervals, typically every three minutes, alternating a pulsed Pt NMR for thermometry with a ^3He NMR pulse every six minutes at the lowest temperatures to avoid excess RF heating.

To span the large temperature range, after a demagnetization and flow experiment, the flow was stopped and a final small demag performed to regain the minimum temperature and reduce the heat capacity of the copper bundle. Using the Pt thermometer, the cell was permitted to warm under the residual heat leak. The warming process from 1 to about 20 mK required about three to four days. Around 20 mK, a resistance thermometer, calibrated against a commercial Ge thermometer, was turned on, the heat switch connection to the dilution refrigerator closed and the remainder of the data (20-200 mK) taken by heating the fridge and experiment in steps and waiting for equilibrium to be obtained in the vycor as determined by a constant susceptibility. Signal-averaging was also performed for the data above 20 mK.

The susceptibilities measured at 1.10, 3.93, and 5.45 bars are shown in Figs. (5-3), (5-4), and (5-5), respectively, all scaled to the same power level. The plots are log-log, units of the relative susceptibility

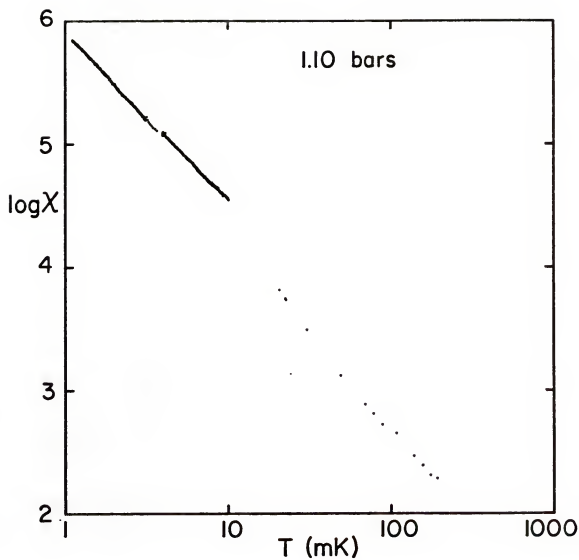


Fig. (5-3). The susceptibility of ^3He at 1.10 bars and 28.6 mT.

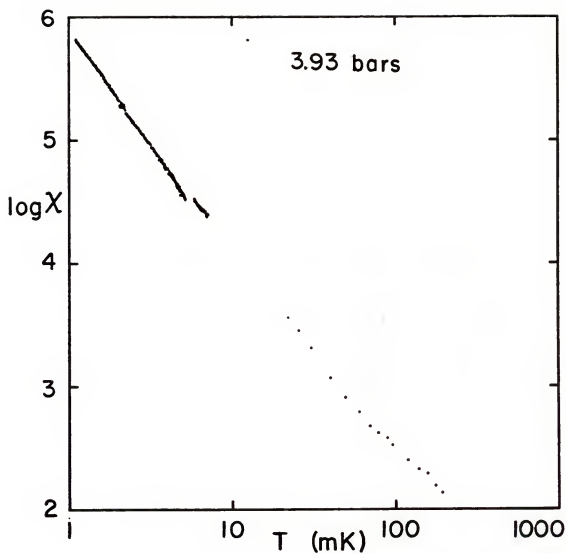


Fig. (5-4). The susceptibility of ^3He at 3.93 bars and 28.6 mT.

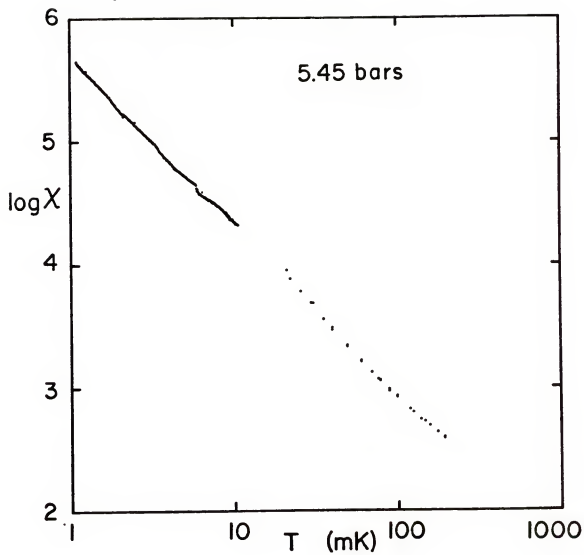


Fig. (5-5). The susceptibility of ^3He at 5.45 bars and 28.6 mT.

being arbitrary. No data appears in the region between 10 and 20 mK because the two thermometers did not agree closely in that region (where each has a decreased reliability). Rather than attempt some averaging of the two values in this region, the χ data collected there was not included in the analysis. In this way, no bias due to the averaging method was introduced into the overall analysis.

To analyze these results, the standard model of the surface ferromagnetism was employed writing

$$\chi(T) = A + B/(T - \theta), \quad (1)$$

where A is the temperature independent part of χ and θ is the Curie-Weiss temperature. To determine A , the high temperature data was used and χ was plotted against $1/T$ giving A in the limit of $1/T \rightarrow 0$ as

$$\chi(1/T \rightarrow 0) = A. \quad (2)$$

Having found A , this was used to isolate the Curie-Weiss term for the low temperature data. Writing $\chi' = \chi - A$, equation (1) becomes

$$\frac{1}{\chi'} = \frac{T}{B} - \frac{\theta}{B}. \quad (3)$$

For each pressure, the lowest temperature data ($T < 5$ mK) written as χ' was fit to a linear function of T allowing the Curie-Weiss temperatures to be obtained from the intercept. These results are given in Table (5-1). There seemed to be no consistent variation of θ with pressure as can be seen in the Table. However, if only the 1.10 and 5.45 bar

Table (5-1)
The Curie-Weiss Temperatures and Power Law
Exponents of the Susceptibility of ^3He in
Vycor Measured over the Range of 1 to 200 mK

P (bar)	T range (mK)	θ (mK)	p
1.10	1.25-193	0.573	-1.31
3.93	1.04-193	0.546	-1.71
5.45	1.09-193	0.646	-1.36

data are considered (these are thought to be the best data) then the increase in θ with pressure seen by Ahonen et al. (1976) is reproduced. Also, since the calibration of the Pt thermometer depended upon the choice of the superfluid transition, a dependency of these results upon that choice was checked using the three existing versions of the superfluid phase diagram (the scales are the La Jolla, Helsinki, and Greywall). The values of T_c used to obtain the results in Table (5-1) were those of the La Jolla group. Substitution of either Greywall's values or those of the Helsinki group changed the temperature calibration by 3% and 5%, respectively, which would change the Curie-Weiss θ 's by a similar amount.

Another interesting find was the fact that χ could be fit over the entire 200 millidegree temperature range using a power law. The fits at 1.10 and 5.45 bar were particularly good giving exponents, p , which were virtually the same value of -1.3. These exponents are presented in Table (5-1). It should be remembered that the thermometer above 20 mK was a calibrated resistance thermometer and that no juggling of the data was performed to make the low and high T data lie on the same line. Due to the difference between the slopes, there is a cross-over of the susceptibilities of these two pressures between 10 and 20 mK. At the

lowest temperatures, the 1.10 bar susceptibilities were larger than those at 5.45 bar. The 3.93 bar data did not fit into this scheme as well due to the fact that its power law exponent was substantially different (being -1.7). With this exponent, the 3.93 bar data spanned the difference between the 1.10 and 5.45 bar values making it difficult to draw conclusions about the effect of pressure upon χ .

These results seem to fit well within the existing body of data on ^3He magnetism in confined geometries.

Flow of ^3He through Vycor Glass

The most extraordinary results of this experiment were the flow measurements taken with ^3He in vycor. It should be remembered, as already mentioned in Chapter III, that before the experiment was performed this cell was tested in liquid ^4He to make certain that no parallel leak around the vycor rod existed. This test will be used later as further evidence in the explanation of the flow character. Additionally, as will be discussed later, a flow effect on the NMR of the confined ^3He was observed providing direct evidence of the liquid flowing through the vycor. It will be speculated that an interaction between the flow and the surface magnetism is responsible for the unusual flow behavior.

Flow Methods and Expectations

The flow experiment was performed at 0.14, 1.10, and 5.45 bars with most of the data being taken around the bulk transition temperature, although later a study at 20 mK was done. When the experiment began it was hoped that a superfluid transition in the vycor would be observed.

Such a state presumably being a very delicate situation, the first few demagnetizations at 0.14 and 1.10 bar were limited to low mass currents. As evidence mounted that no such state seemed to exist, the variety of flows attempted was increased.

The pump position was regulated as discussed in Chapter III using the output of the pump sensor bridge to drive the heater-controller which in turn provided current to the ^4He bomb. By changing the value of the ratio transformer in this bridge, thereby causing an off-null bridge output, the controller either increased the bomb current (for a forward stroke from mechanical pump equilibrium) or decreased the current (for a backward relaxation toward mechanical pump equilibrium). In this way differential pressure steps were applied to the two sides of the vycor cell causing flow to occur. The response of the liquid to these steps was monitored by the manometer, the capacitance of which was observed in a separate bridge circuit.

As mentioned earlier in this chapter, the program "TIMER5" was responsible for taking and storing the data. Both the pump position and manometer response were measured every three minutes. Data could be taken no faster than this because of the constraints of the NMR FID analysis which the computer performed at every other datum (alternate data points contained the pulsed Pt thermometry as mentioned).

Another complication to the flow measurement was the presence of the Millipore filter at each entrance to the flow cell. In the case of a vycor superfluid state these filters would have been necessary in order to observe pure superflow (as was originally hoped). With no such state in the vycor, they became an additional factor to be aware of in the experiment. Shown in Fig. (5-6) is the anticipated sequence of obser-

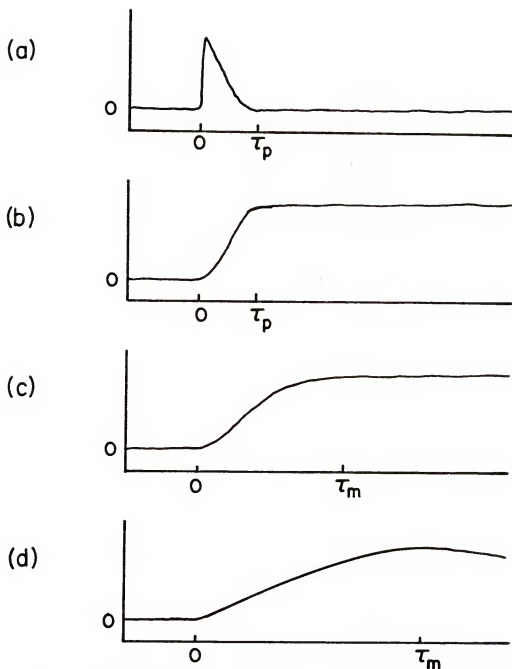


Fig. (5-6). Possible manometer responses: (a) A typical pump stroke showing the initial regulation and the regulation after the stroke to the new position; (b) Expected response of the manometer assuming no Millipore filters and no flow through the vycor; (c) Expected manometer response with filters in place but no vycor flow; (d) Observed short time scale manometer response indicating flow.

vations under a variety of situations which might have been obtained in this experiment. In Fig. (5-6a), an actual pump stroke is shown. Initially the position was regulated, then at $t = 0$ the bridge null was changed causing the output to jump to a new position after which the regulation system drove the pump to its new null. This occurred in a time $\tau_p \sim 5$ to 30 sec depending upon the size of the change in null (typically the ratio transformer was changed by $\Delta r = \pm 1$ to $\pm 2 \times 10^{-5}$). In Fig. (5-6b) is shown the manometer response to the pump stroke as it would appear with no Millipore filters and also no flow through the vycor. In Fig. (5-6c), once again it is assumed that there is no vycor flow (and thus the manometer does not relax) but now it is assumed that the filters are in place. Due to the compressibility of the liquid, the finite time which it requires to pass through the filters, and the possibility of flexing of the filters, the response of the manometer would be slower in developing, and slower in reaching its final state. Finally, in Fig. (5-6d) is shown the actual result. A slower response time τ_m was observed as postulated. For a pump stroke time $\tau_p = 24$ sec a manometer response time $\tau_m = 100$ sec was observed. The difference between this actual observation and that shown in Fig. (5-6c) was the relaxation of the manometer seen subsequently.

One other difficulty in the mechanics of the experiment was found after gaining some experience with the apparatus. That difficulty was the multiplicity of time scales displayed by the experiment. As just shown, part of the response to a perturbation occurred in the period of a few tens of seconds. As will be shortly seen, there were also intermediate and long time scales to be accounted. The kinds of data taken were a compromise in order to discern the complete range of behaviors being displayed.

Flow Measurements

Through the course of this flow experiment, many pump strokes were performed. Shown in Fig. (5-7) is a typical sequence of manometer responses. This set was obtained at 1.10 bar and 6.24 mK over a 12 hour period. In Fig. (5-8), a second set of flows is shown still at 1.10 bar but taken during warming from 0.711 to 1.285 mK ($T_c = 1.301$ mK) with an elapsed time of 48 hours.

These two sets of flows illustrate the typical feature of all the flows at all temperatures (1 to 20 mK). The short time scale behavior after a stroke (periods ≤ 100 sec) has been detailed including the initial manometer response and the compressibility/filter flex complication. In the intermediate time scale (periods ≤ 1 hour) many flows displayed an initial relaxation (or $\dot{\Delta P}$ in Figs. (5-7) and 5-8)) higher than the steady-state (sometimes much higher). Finally, in the long time scale the relaxation approached a steady-state value. Most surprisingly, the long term relaxations were not exponential in shape.

Returning for the moment to the intermediate time scale, many but not all of the flows showed the high initial relaxation. Due to its appearance this feature was named the flow cusp, no relation to the mathematical definition of a cusp being implied. At first this cusp was thought to be caused by flexing of the Millipore filters. Considering this process, as the pump is stroked the volume available for the liquid on one side of the cell outside the filters is reduced, that on the other side of the cell being increased. As the filters flex, they sweep out a volume $\Delta V_f < \Delta V_p$ where ΔV_p is the change in the pump volume on one side. This is due to the compressibility of the liquid. So the initial manometer response to the stroke would indicate a smaller ΔP

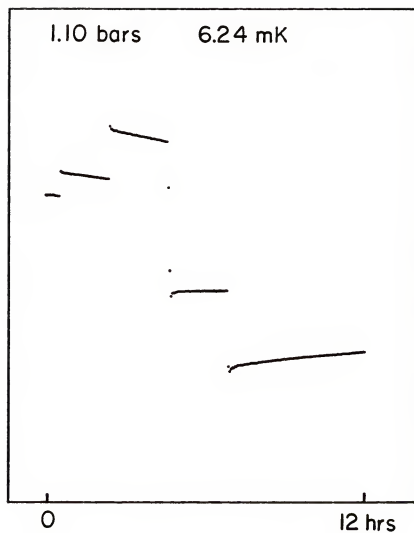


Fig. (5-7). A series of manometer responses taken at 6.24 mK and 1.10 bar over a period of about 12 hours.

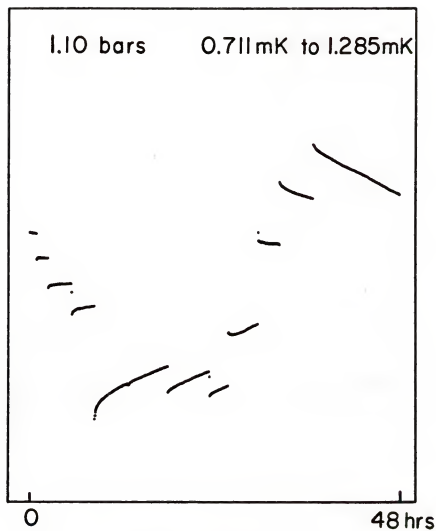


Fig. (5-8). A series of manometer responses taken during warming from $T = 0.711$ mK to $T = 1.285$ mK at 1.10 bar over a period of about 48 hours.

than actually applied. As time passes (seconds) and the liquid flows through the filters, more and more of the applied ΔP is felt by the manometer while the filters relax to their equilibrium positions. This process is seen in the small positive slope of the manometer response in Fig. (5-6d) after time τ_p . The full ΔP of the stroke is not built-up until τ_m after which it relaxes as liquid traverses the vycor. This being the flex process it is easy to see that it is not capable of producing the cusps since they are in the wrong direction (i.e., they are further from $\Delta P = 0$ than the rest of the relaxation). Having ruled this process out as the source of the cusps and there being no other obvious source in the apparatus, it is believed that they reflect a true high initial mass current in the vycor. The problem remains to explain why they do not always appear and why there seems no correlation between their appearance and either the total differential pressure (i.e., total distance from $\Delta P = 0$) or the size of the stroke (i.e., $\Delta P(0^+) - \Delta P(0^-)$ where the stroke occurs at $t = 0$).

Before proceeding to further considerations, the method of analysis of the flows is presented. Shown in Fig. (5-9) is a series of idealized manometer responses to pump strokes with the pertinent variables labeled. The $\Delta P = 0$ voltage is called V_{eq} , the values of the manometer immediately before and after the i^{th} stroke are called $V_i(0^-)$ and $V_i(0^+)$, respectively, and the manometer response (or flow) as a function of time is called $V_i(t)$. With these definitions it is easy to see that the pressure change due to a stroke is

$$\Delta P_i = k\Delta V_i = k(V_i(0^+) - V_i(0^-)), \quad (4)$$

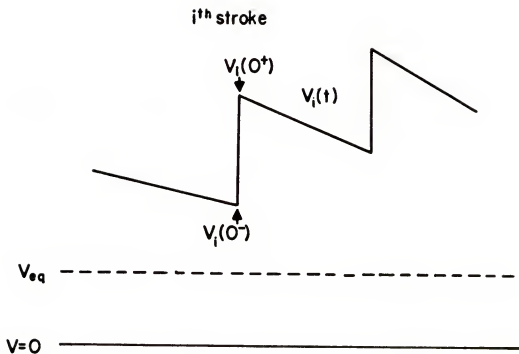


Fig. (5-9). A set of idealized manometer responses (in volts) to illustrate the method of analysis.

where k is a calibration constant determined from the pump properties. The differential pressure during the flow is

$$\Delta P_i(t) = k(V_i(t) - V_{eq}) \quad (5)$$

and the rate of decay of the pressure head is

$$\frac{d}{dt} \Delta P_i(t) = \dot{\Delta P}_i(t) = k\dot{V}_i(t). \quad (6)$$

The constant V_{eq} , which gives the flow equilibrium region where $\Delta P = 0$, can be determined either graphically using flow sets similar to Figs.(5-7) and (5-8) by looking for a region where the the slope of the flows is zero or numerically using flow pairs in the following manner. The assumption is made that

$$\Delta P_i(t) = k(V_i(0^+) - V_{eq})f(t) \quad (7)$$

where all the time-dependence is contained in $f(t)$. Next the ratio of the initial slopes of a pair of strokes is written as

$$R = \frac{\dot{V}_i(0)}{\dot{V}_j(0)} = \frac{(V_i(0^+) - V_{eq})\dot{f}_i(0)}{(V_j(0^+) - V_{eq})\dot{f}_j(0)}. \quad (8)$$

Finally, the assumption is made that the time-dependence of the strokes is the same allowing cancellation of the two $f(0)$ functions. For this to be identically true it requires that the two flows which are compared traverse the same differential pressure region and not be too far apart in time to avoid any history dependence in the flows. The equation is

then solved for V_{eq} to yield

$$V_{eq} = \frac{V_1(0^+) \dot{V}_j(0) - \dot{V}_1(0) V_j(0^+)}{\dot{V}_j(0) - \dot{V}_1(0)}. \quad (9)$$

To apply this technique, first all the flows (in voltage output from the manometer bridge circuit) were fit as functions of the time. To avoid the necessity of using high order polynomials to fit the cusp curvature (which was not always present), all the cusps were left off the fits. This generally required not using the first 5 to 10 points of a relaxation (15 to 30 minutes of the total flow time). In this way, looking at the intermediate to long time scales, fits of fourth order in time or less gave good results. The number which was used for $\dot{V}_1(0)$ was taken to be the coefficient of the first order term of the fit (i.e., the coefficient of the linear term). This gave the effect of extrapolating the fit to the time of the stroke ($t = 0$) rather than using the slope at the beginning of the fit after the cusp ($t > 0$). For a given series of flows, pairs of related flows were then used in equation (9) to find V_{eq} for that series. The validity of this method was confirmed by the result that virtually any pair of flows in a series gave the same value for V_{eq} . Some noise would appear due to the failure of the time dependence assumption.

To determine the amount of pressure applied by a pump stroke, the compressibility was used as

$$\begin{aligned} \Delta P_1(0) &= -\frac{1}{\beta} \frac{\Delta V_1}{V} = 4 \frac{C_s}{V} \frac{\delta V}{\delta C} \frac{1}{\beta} \frac{\Delta r}{r_1 r_f} \\ &= k(V_1(0^+) - V_{eq}), \end{aligned} \quad (10)$$

where β was the compressibility, ΔV_1 was the change in volume on one side of the pump with V being the volume of one side, C_s was the standard capacitor in the pump bridge, $\delta V/\delta C = 0.10703 \text{ cm}^3/\text{pf}$ from the pump tests, and r_i , r_f , and Δr were the initial, final, and change in the pump ratio transformer which caused the stroke. All these numbers were either already known or were measured during the pump tests. This equation gave the calibration constant k .

Also, the actual mass current could be related to ΔP . For a given stroke, the amount of liquid which had to flow to relieve the ΔP was that amount which occupied the displaced volume ΔV , thus

$$J(t) = \frac{d}{dt} \frac{\Delta V}{v} = - \frac{\beta V \Delta \dot{P}(t)}{v} \text{ moles/sec,} \quad (11)$$

where v was the molar volume. Use of equation (10) allowed $J(t)$ to be written in terms of measured quantities.

The first use of this analysis was to plot $J(0)$ against $\Delta P(0)$. In an ordinary viscous fluid this plot would of course be a straight line with the impedance being the inverse of the slope. When plotted there was sufficient scatter in the points to mask any temperature dependence. These results for 1.10 and 5.45 bar are shown in Figs. (5-10) and (5-11), respectively. In each plot, data at all temperatures is plotted; also note that the scales are different. The scatter also masked any curvature of the data meaning that the best fit to each set was a straight line. The slopes are presented in Table (5-2). As can be seen from the table, there did seem to be a measurable effect of pressure on these slopes. It indicated that a given differential pressure produced a higher initial current as the pressure was reduced.

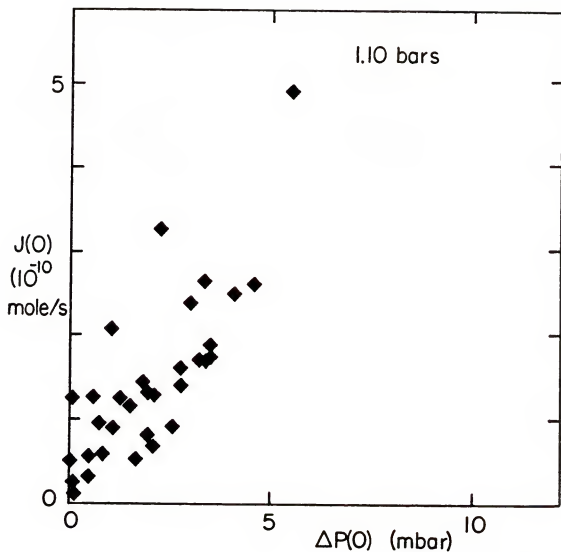


Fig. (5-10). Plot of initial current $J(0)$ versus initial differential pressure $\Delta P(0)$ for $0.711 \text{ mK} \leq T \leq 6.24 \text{ mK}$ at 1.10 bar.

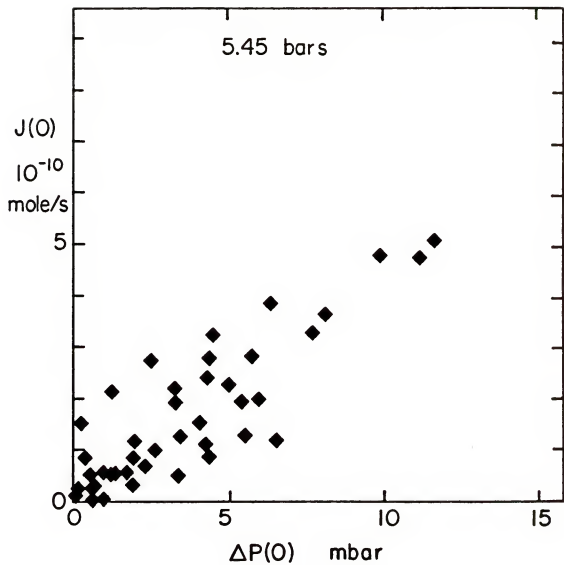


Fig. (5-11). Plot of initial current $J(0)$ versus initial differential pressure $\Delta P(0)$ for $1.4 \text{ mK} \leq T \leq 21.0 \text{ mK}$ at 5.45 bar.

Table (5-2)
Slopes of the Best Fits to $J(0)$ versus $P(0)$

P (bar)	$J(0)/P(0)$ (10^{-9} moles/sec bar)
1.10	80
5.45	61

Having obtained the fits of $\Delta P_1(t)$ with time, it was possible to see how the mass current depended on differential pressure. This method (taking derivatives of the fits of $\Delta P_1(t)$) avoided the need to take derivatives by differences of data points which might have introduced scatter into the results. The net effect of this method was to smooth the data. This produced the most striking result of this experiment. The plots of mass current J_1 as a function of differential pressure ΔP_1 are shown in Figs. (5-12) and (5-13) at the pressures of 1.10 and 5.45 bar, respectively. All the low temperature data have been grouped together for a given pressure due to a lack of any discernable temperature dependence in the character of the flows over small temperature variations. The higher temperature data, 21.0 mK, at 5.45 bar has been separated out and is shown in Fig. (5-14). Notice that the scales are different on the plots. Also, data only occupies the 2nd and 4th quadrants due to the nature of the relaxation; if $\Delta P > 0$ then $J \sim \dot{\Delta P} < 0$ and vice versa.

What might have been anticipated on a plot of this sort was that the fits all fell on or near a single smooth curve which went through the origin. Looking at Fig. (5-7) or (5-8) the flows certainly appear to be relaxing back to equilibrium. As previously discussed, the initial currents $J_1(0)$ and pressure heads $\Delta P_1(0)$ do lie on a straight line. Some of the shorter flows appear as misshapen points while others which were

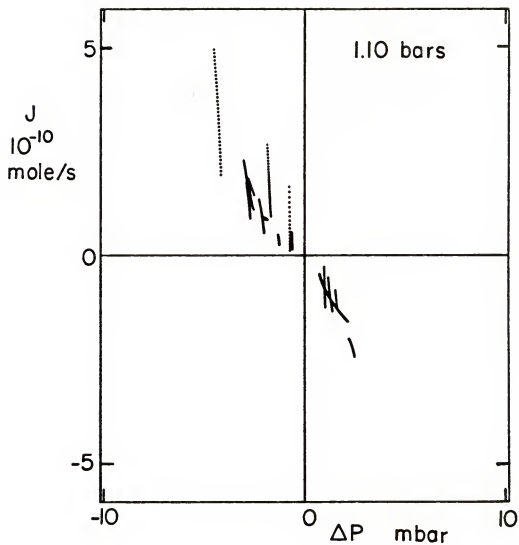


Fig. (5-12). Mass current J_i versus differential pressure ΔP_i for $0.711 \text{ mK} \leq T \leq 6.24 \text{ mK}$ at 1.10 bar.

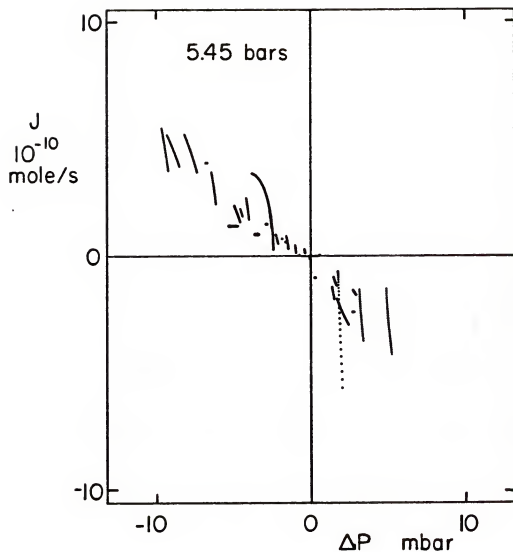


Fig. (5-13). Mass current J_i versus differential pressure ΔP_i for $1.136 \text{ mK} \leq T \leq 1.638 \text{ mK}$ at 5.45 bar.

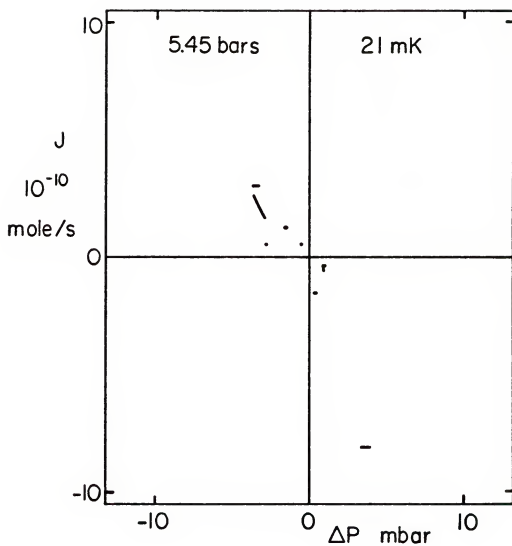


Fig. (5-14). Mass current J_i versus differential pressure ΔP_i at 21.0 mK and 5.45 bar.

best fit by linear functions of time giving a constant upon differentiation appear as horizontal lines. But beyond that short-to-intermediate time scale behavior, many of the flows do not come close to approaching the origin. Many flows (both long- and short-term flows; witness the flows whose individual points are visible) quickly approach a near-vertical slope with no hope of passing through the origin without a large, unobserved change in curvature.

This repeatedly observed behavior is certainly beyond explanation by appeal either to simple Newtonian viscous flow or even to Knudsen flow. In each of these, the mass current is directly proportional to the differential pressure. While the short time scale behavior follows this proportionality, at some point after the flow begins, the current deviates from it and quickly goes to a very small (or zero) value.

This behavior is characteristic of viscoelastic fluids, as discussed in Chapter II. If the viscosity of a fluid depends upon the state of stress the fluid undergoes, then it is possible for the fluid to support a non-zero stress (differential pressure in this case) while not flowing.

Leaving aside for the moment the perplexing questions regarding the nature of viscosity in a fluid system smaller than the pertinent mean free paths in the fluid, if the assumption of viscoelasticity is used as a working hypothesis then the first question to be addressed is the class of which this system (^3He in vycor) is a member. At this point it is to be remembered that the fits plotted in Figs. (5-12) and (5-13) did not include the initial high currents of the flow cusps, but rather only fit the steady-state currents after the cusps. So in the cases where the conditions were correct to observe a cusp, the overall behavior

of the flow was an initial high current immediately after changing the state of stress on the fluid followed by a more or less rapid approach of the current to zero as the stress (ΔP) decreased. This is also the behavior observed in shear-thinning fluids.

In the simplest form of viscoelastic behavior, a minimum differential pressure (or minimum yield stress) is needed to create flow. In this experiment, although some flows did approach the equilibrium closely, no region near $\Delta P = 0$ was found in which the mass current was strictly zero. Taking the minimum differential pressure which was applied as the upper limit for this yield pressure gives it as $\delta P_{\text{yield}} \leq 184 \text{ } \mu\text{bars}$ measured at 5.45 bars (the corresponding value at 1.10 bars was 283 μbars but this difference was not necessarily meaningful; it was just a different minimum applied differential pressure).

An additional complication to the explanation was the presence of an apparent history-dependence to the flows. This can be seen in both Figs. (5-12) and (5-13) in the way that some individual flows intersect each other with different slopes. Thus, even though they pass through the same region of $\Delta P - J$ space they behave differently. Other flows, however, lie right on top of each other as can be seen in these figures. The behavior was not even this simple as can be easily seen. Not only was no yield pressure found but rather than relax back toward the region where the yield pressure might be expected to reside ($|\Delta P| < \delta P_{\text{yield}}$) the mass current seemed to go to zero (by extrapolation to $J = 0$) at any value of ΔP . The more correct way to describe this observation might be to say that the fluid stopped flowing after either a certain elapsed time since the stroke or after some fraction of the new total differential pressure had been relieved. Either of these two alternatives could be

explained if the long-term steady-state condition of the system which stops the current (or reduces it) was temporarily upset by changing the stress state. It might then require a finite time to recover from the change and bring the current to a halt (or to a much lower value). It is not clear whether this last feature should be regarded as a dependence of the individual flow on the total system history or instead as a time-dependence of each relaxation, independent of the other relaxations.

The higher temperature experiment at 21 mK was separated from the others in Fig. (5-14) for the reason that the one long-term flow which was observed had a slope which extrapolated close to $\Delta P = 0$. This was the only long-term flow observed which did not clearly go to zero at finite ΔP . If taken as a real difference then this would indicate that the fluid is acting in a more ordinary manner, perhaps exhibiting simple Knudsen flow.

Another interesting feature of the long-term flows was the fact that they were not exponential relaxations, at least at low temperatures. Shown in Fig. (5-15) are long-term flows at 1.10 bars. The wiggles in each trace were due to liquid helium transfers in other cryostats affecting the recovery system of our cryostat. The flow cusp is visible at the beginning after which the relaxations continue to show some curvature which is fit by a cubic polynomial in time. Exponential fits of $\Delta P(t)$ had chi-squared values worse by a factor of 2 to 5. Similar long-term flows taken at 5.45 bars are shown in Fig. (5-16) which appear almost linear in time after the cusp. In fact, there is some curvature and each are fit by a quadratic in time. In this case, exponential fits are worse by a factor of 30 to 50 in chi-squared. It was also observed that as the temperature increased the exponential fits became better. At 21

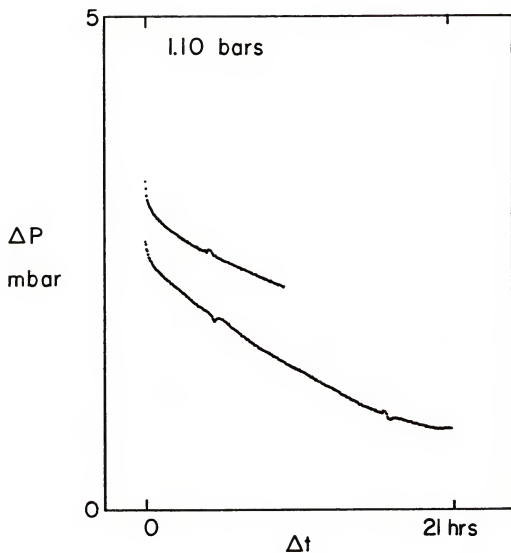


Fig. (5-15). Long-term flows taken at 1.10 bar and $T = 0.753$ mK (upper trace) and $T = 1.235$ mK (lower trace).

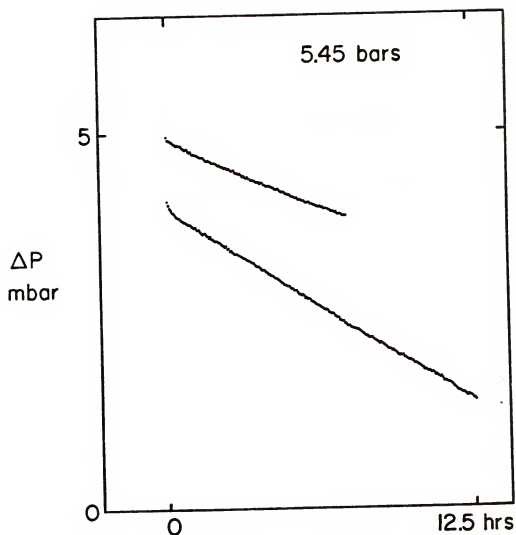


Fig. (5-16). Long-term flows at 5.45 bar and $T = 1.62$ mK.

mK, exponential fits were essentially as good as polynomials. This again indicated that the fluid began to behave more normally as the temperature was increased.

It should be noted that there is sufficient noise in the data and in some cases a sufficient paucity of the right kind of data that these apparent trends with temperature might not be real. Nevertheless, the trends do seem to be in the same direction.

Flow/NMR Interactions

One final, very interesting effect was observed. At low temperatures where the susceptibility was highest, the presence of fluid flow was found to decrease the susceptibility. Shown in Fig. (5-17) is a series of increasing flows (caused by increasing the differential pressure regularly) and the relative susceptibility. This was taken at 1.23 mK and 5.45 bars although the effect was seen at other (low) temperatures and pressures. As the susceptibility decrease became pronounced, the flow was stepped down to near zero beginning at $t = 510$ min while the recovery of the susceptibility was followed.

The observation of this kind of effect was welcomed not just because it added another interesting twist to the experiment but also for a more basic reason. This effect provides direct proof that the fluid is in fact flowing through the vycor rather than around it by means of an unknown parallel path. The regions of the cell containing bulk liquid were essentially unaffected by the flows in this series as evidenced by the bulk liquid thermometers (Pt NMR and ^3He ultrasound) remaining essentially constant.

The simplest explanation of this phenomenon is that the flow is causing local heating inside the vycor and the decrease of the suscep-

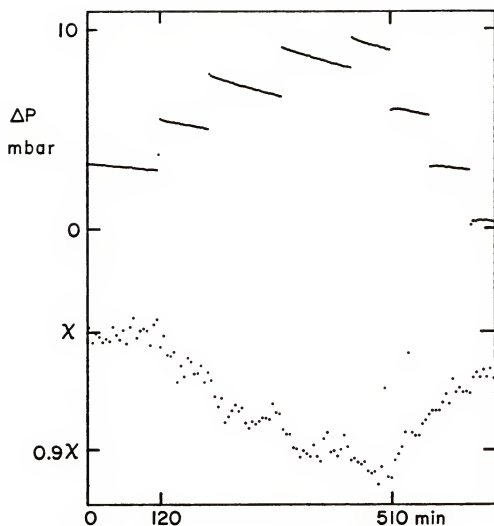


Fig. (5-17). The effect of flow (upper trace) on the NMR susceptibility (lower trace) at 1.23 mK and 5.45 bar. The flow was stopped at $t = 510$ min and the NMR recovery was observed.

tibility merely reflects an increased temperature of the confined ^3He . A more exotic explanation is that the flow is somehow directly affecting the surface magnetism in the vycor.

It is possible to estimate the orders of magnitude of the heat required for this depression as well as the power provided by the flow. The maximum depression of the susceptibility was 13% which would require a temperature increase of about 9% using the power law for χ at this pressure (Table (5-1)). The temperature rise would then have been $\delta T = 0.115 \text{ mK}$ at 1.23 mK . This depression occurred over a time of 390 min. So, using the assumptions of a 50% filling factor of ^3He inside the vycor and no thermal contact with any other system (including the vycor matrix or bulk liquid), a lower limit to the required additional heat leak due to flow is found to be $\dot{Q} \geq 0.4 \text{ pW}$. The energy per unit time available in the flowing liquid was $\Delta P \dot{V}$ where \dot{V} was the volumetric flow. Using the highest flow rate in this series, an upper limit is established as $P_{\text{max}} \leq 15 \text{ pW}$.

By noting the response of the susceptibility at the times when the flow was being reduced, some idea of the time constant for re-equilibration at the new reduced current can be obtained. In each of the three downward ΔP steps, the susceptibility responded by increasing in a very short time. The response to a decreased current began within one data point ($\Delta t \leq 6 \text{ min}$) and then plateaued within three data points ($\Delta t \leq 18 \text{ min}$). If the depression was due to simple heating, this recovery time indicates that the confined liquid is in reasonable thermal contact with some other bath (certainly over a period of 510 min), most likely the bulk liquid. This result would require the additional flow heat leak to be much larger, a rough estimate being $\dot{Q} \sim 7 \text{ pW}$. This is half the total energy per unit

time available in the flow. It seems unlikely that fully half of the flow energy was being expended in some kind of heating process in the vycor.

In either case these calculations can not definitively rule in favor of one explanation over the other.

Speculations on the Viscoelasticity of Confined ^3He

Until now observations of the flow behavior have been merely reported with few comments on the cause of the behavior. It is now time to consider such things. (It is hoped that the reader will give allowance for the fact that these are only speculations.)

The safest comment that can be made regarding the flow of ^3He in vycor is that it certainly is not simple. A wide range of behavior was displayed. Due to the difficulty of establishing a clear relation between individual flows the only remaining correlation which did not seem to fail was that between the appearance of given flow characteristics and the elapsed time from the beginning of a given flow. For example, flow cusps were only observed immediately after a stroke; or during unperturbed flow (unperturbed by unwanted extraneous forces) the mass current was a monotonically decreasing function of time from the stroke. Also, no minimum yield pressure was found to which all strokes relaxed before stopping. As mentioned, this last could be regarded as either a history dependence or an elapsed-time dependence. Finally, the very short time scale behavior did seem to be simple, either Newtonian viscous or Knudsen.

These characteristics can be used to eliminate the various candidate flow types discussed in Chapter II. First, the overall long-term flow

is not the simple viscous type (at the low temperature). Although the $(\Delta P(0), J(0))$ points lie on a straight line which passes through the origin, the total relaxation quickly deviates from this (over a small ΔP range) and the proportionality $J \propto \Delta P$ fails. For this same reason Knudsen flow can be eliminated. It has been suggested (J. T. Tough, private communication) that these results might be understood as due to the presence of vortices in the vycor rod. While it is possible that the decay of the differential pressure might be affected by vortices, the vortices require fluid motion in order to persist. In an open-ended geometry such as this cell, if there is fluid flow to sustain the vortex structure then the differential pressure will continue to decay and eventually reach $\Delta P = 0$, passing through the origin of the J versus ΔP graph. An even more serious problem for this explanation will be discussed later. Regarding the change in the relaxation after the flow cusp as a change in the effective viscosity of the system means the flow is non-Newtonian.

A simpler explanation of the complicated flow results might be to postulate the existence of a parallel leak around the vycor glass with a much different flow impedance. Arguing against this is the fact that the construction of the cell was specifically designed to avoid such a leak and even more importantly the superleak test (i.e., the measurement of the depression of the lambda point δT_λ , discussed in Chapter III) found no evidence of such a leak. Also, the flow effect on the magnetism clearly indicated liquid flow in the vycor.

All of these flow observations have been seen before in other types of materials and all fall within the realm of fluids exhibiting viscoelastic behavior. The initial high relaxation of the cusp followed by

a slower relaxation is what is expected of a shear-thinning fluid. In many other cases, however, such fluids do continue to relax until the entire shearing stress is relieved and many have a minimum yield stress which is zero. Confined liquid ^3He is quite different in this respect. Because of the apparent dependence of the flow upon time after the stroke, this system might be regarded as thixotropic. But again, in many other cases thixotropic fluids continue to relax until the shear stress is relieved. In the cases where the limiting value of the shear stress is non-zero, the material is regarded as a solid rather than a fluid. Of course, to some extent the designation of fluid or solid is dependent upon the length of time one is willing to wait. In the present work, the relaxations did certainly appear to be getting quite small although none was followed to $J = 0$. The shear-thinning hypothesis can also explain the apparent Newtonian behavior of the short time scale extrapolated flow (i.e., $J(0) \propto \Delta P(0)$). Ostwald (1924) postulated the existence of a Newtonian region above the shear-thinning region at high shear stress values and this has been observed in other materials.

So, the present picture of ^3He in vycor glass is that of a hysteretic thixotropic system at low temperatures ($T \leq 6 \text{ mK}$) perhaps approaching a Newtonian or Knudsen system at higher temperatures ($T \sim 20 \text{ mK}$). It should be emphasized that it is not being claimed that ^3He is a viscoelastic fluid but only that its flow behavior in vycor appears to fall within the range of behaviors displayed by the class of viscoelastic fluids.

If the viscoelastic hypothesis is correct then a major unanswered question is, of course, the source of this behavior. Taking the apparent temperature dependence to be real provides an immediate clue. If one

observes extraordinary flow in confined ^3He at very low temperature, is there any other extraordinary low temperature characteristic simultaneously present? The answer is yes and surface ferromagnetism is the effect. It might be argued that in the absence of the surface ferromagnetism, Knudsen flow should have resulted in this system. This is in fact the result of calculations performed by several workers which was discussed in Chapter II. The only wall interactions included were specular or diffuse quasiparticle reflection. In the presence of the magnetism this result might be altered. Recall the result of Okuda et al. (1985) in which the ferromagnetism only appeared at film thicknesses greater than 5 layers. This means that inside the vycor, a substantial fraction of all the atoms in the pores are participating in the magnetism. (In 60 Å pores, 94% of the atoms are within 6 atomic diameters of the wall.) It is these same atoms which are taking part in the flow. Thus, an obvious candidate for the origin of the viscoelasticity is the surface ferromagnetism. Although the mechanism is not understood, the interaction between the ferromagnetism and the flow must be affecting each. (Not necessarily to the extent seen in Fig. (5-17) which could still be heating.) This mechanism might also provide the answer to the question alluded to earlier, namely the nature of viscosity in a system whose characteristic dimensions are smaller than the quasiparticle mean free path. In this case, the ordinary definition of viscosity certainly fails, but the magnetic/flow interaction might provide a vehicle with which to define an effective viscosity. As stated, with no magnetism the flow is Knudsen. But with magnetism there exists the possibility that the magnetic/flow interaction acts in such a manner as to reduce the current, thereby slowing the flow and supporting a finite ΔP .

This would be observed in the experiment as a decrease in $\Delta\dot{P}$, and therefore could be interpreted as a change in an effective viscosity in the confined ^3He . As with other thixotropic systems, the time-dependence (after each stroke) might be attributed to the breakdown of some structure caused by the perturbation of the stroke. The structure broken down in this case would be the previously established steady-state configuration of the magnetic surface layers. As time passes after the stroke, a new equilibrium is approached and eventually it brings the current to a very low value. It should be remembered that the differential pressures which are apparently being supported (by extrapolation to $J = 0$) are on the order of 1 mbar. This pressure gradient across the vycor rod will induce a small susceptibility gradient. Whether the existence of such a gradient in χ can reduce the current by some means is not known.

The breakdown and rebuilding of the steady-state surface ferromagnetic structure might also provide a means to explain the apparent hysteresis in the system. If the perturbation caused by each new pump stroke is sufficient to upset the previous steady-state configuration in the vycor then with each stroke (regardless of total ΔP) the effective viscosity immediately afterward is lowered. As time passes and the steady-state is re-established, the effective viscosity increases and the current decays away at finite ΔP . The result of this would be that the system has no minimum yield ΔP to start flow; rather all strokes upset the magnetic/flow interaction and all strokes can be brought to a halt independent of ΔP .

If on the other hand the temperature dependence seen in this work is not real, this would presumably present problems for the surface

ferromagnetism as the origin of the viscoelasticity since the magnetism is quite temperature dependent. There appear to be few other candidates for the cause of the viscoelasticity. However, if one further speculation is permitted, it should be recalled that many viscoelastic fluids derive this property from the presence of extended objects either in the fluid or constituting the fluid (e.g., various polymer melts and quicksand). At first glance no such structures exist in the very clean and homogeneous ^3He liquid. But below 100 mK in bulk liquid, ^3He is regarded as being composed of dressed particles, the so-called quasiparticles (see Chapter II, page 10). To the extent that these may be regarded as extended objects (due to the full many-body interaction), the quasiparticles might upon confinement to the pores of vycor begin to behave viscoelastically.

If due to surface ferromagnetism or quasiparticles, the viscoelastic hypothesis could be tested by adding ^4He to the ^3He in an attempt to affect the surface magnetism. More directly, the ^3He could be replaced completely by liquid ^4He and the experiment repeated. This has effectively already been done in this cell during the fountain pressure calibration of the manometer in a ^4He bath (see Chapter III). Both above and below the lambda point (the superfluid transition in ^4He at 2.17 K) differential pressures across the vycor rod were observed as level differences and with the manometer. No non-zero ΔP was observed below T_λ unless a fountain pressure was generated by a heat input. Above T_λ , all remanent differential pressures caused by external perturbations were observed to decay to zero in short periods. Using the density of liquid ^4He , it is easy to calculate that a 1 mbar pressure gradient would have resulted in an easily observed level difference of 7 cm. The con-

clusion from this test is that ^4He does not display the apparent viscoelasticity seen in ^3He . It also dispells any doubts in the flow-measuring apparatus, primarily the manometer, since the expected simple Knudsen behavior was seen in ^4He . Finally, this test appears to refute the possibility of a vortex origin for the flow properties for if ^3He vortices were causing that behavior, the same would occur in ^4He through its vortices.

Concluding Remarks and Future Work

The results of this experiment ranged from the expected to the completely unexpected. The main results included: (1) measurement of the magnetic susceptibility χ of confined ^3He at low pressures; (2) observation of the Curie-Weiss behavior of χ at very low temperatures with Curie-Weiss temperatures of about 0.6 mK; (3) observation of a complex flow behavior of ^3He that can be classified as thixotropic with hysteresis; (4) observation of an interaction between the flowing fluid and the surface magnetism perhaps due to local heating or to direct flow interaction with the surface magnetism; and (5) observation of an apparently ordinary flow behavior of liquid ^4He in the same vycor cell. Once again it should be emphasized that the association of the ^3He flow behavior with viscoelasticity is merely a means of classifying the flow. As discussed, the prime candidate for the origin of most, if not all, of the flow behavior is the surface ferromagnetism.

The flow behavior observed here, having not been reported by other experimenters and having not been anticipated theoretically, should be studied further. In regard to the present results, tests to check whether the apparent hysteresis is real should be made. On the assump-

tion that it is real, the experimental situation could be rather complex and conclusive answers difficult to obtain.

The results of the ^4He test of the cell indicate not only that the apparatus is functioning properly, but also that it is something in the nature of ^3He which causes the viscoelasticity. Adding ^4He to the ^3He sample would not only allow further tests of the surface ferromagnetism but could also decide between the two viscoelastic models suggested here. If the surface magnetism is responsible, then addition of ^4He might be expected to drastically alter the flow behavior. On the other hand, a small percentage of ^4He should not affect the ^3He quasiparticles substantially. Unfortunately, due to its topology, the present cell is not well-suited to this experiment as it would be difficult to guarantee where the ^4He actually was located.

Another point to be made is that if the magnetism is responsible for the flow results, it is not necessarily true that viscoelasticity would be observed in other confined geometries. As noted, in the extremely small pores of vycor at least 90% of the ^3He atoms are participating in the surface magnetism. This may be a crucial point to establishing the viscoelasticity. In other larger geometries, the viscoelastic behavior should be expected to be reduced as a higher percentage of the atoms are not participating in the magnetism and are free to flow as a Knudsen system.

Also, if one is interested in surface magnetism, it is not obvious that flow experiments are the most efficient means of studying it.

Finally, there are two general conclusions to be drawn from this experiment. The first is that ^3He in vycor appears to provide a reasonably good in-situ low temperature NMR thermometer. At least to the temp-

eratures measured in this experiment (~ 0.5 mK) no saturation of the susceptibility was observed. Also, the confined liquid responded quickly to temperature changes of the cell, which is good considering that the liquid in the center of the vycor rod was almost 2.5 mm away from bulk liquid. Also, the vycor being an insulator removes problems of eddy-current heating. Of course, before such a thermometer could be trusted a considerable amount of calibration with respect to pressure, temperature, and magnetic field would need to be performed. The second remark relates to the hope of observing pure superflow in order to check for dissipation. Such experiments, indicating dissipationless superflow, have already been made in closed geometry systems (e.g., toroids). But since a superfluid is a macroscopic quantum system, a closed geometry such as a torus forces the phase of the order parameter to be single-valued. In an open geometry such as a pipe this constraint is no longer required. So, open geometry experiments might show a different behavior of the superflow. In an open geometry experiment to see dissipationless flow it is necessary to prevent the normal liquid from flowing. This is usually (thought to be) accomplished by means of filters such as Millipore. The assumption is made that the normal liquid is locked by its viscosity in the pores of the filter. However, this experiment indicates that the normal liquid always flows regardless of the type of filter. Although the flow results were quite unusual and the long-term flow appeared to come nearly to a halt, on shorter time scales the liquid did flow. Using filters other than vycor might remove the complex viscoelastic behavior but it would only be replaced by Knudsen flow, not by an immobile normal liquid. It is not clear how this might be accounted for in an open geometry superflow experiment, but it is clear that this question must be addressed in such attempts.

CHAPTER VI

CONCLUDING REMARKS

This work has presented the expectations, supporting theories, methods, and results of three experiments performed on ^3He at very low temperatures. In character the experiments covered a wide range from safe (the B phase slab experiment) to reasonable (the B phase cylinder experiment) and finally to speculative (the vycor experiment).

The same can be said for the results of the experiments. The slab geometry results in the liquid at rest are simple extensions to low pressure of work performed by others at the higher pressures. The data are important in that they permit interpolation of the longitudinal resonance frequency, $\Omega_B^2(T,P)$, for use as an in-situ ^3He thermometer. The results of the slab flow experiment are interesting because of the apparent lack of a flow effect on the NMR in conflict with the theoretical anticipation. The results of the cylindrical geometry experiment and the means developed to obtain them are quite interesting and important. The dramatic alteration of the NMR lineshapes below T_c and the fact that it could be deconvoluted and compared to theory gives hope of mapping other, perhaps more complex, n textures. As mentioned earlier, there are many calculations of such textures, theory having outpaced the experiments in this respect. As a single 3-dimensional n texture study can not provide a complete understanding of the textural interactions, more efforts in this direction are needed. Finally comes the $^3\text{He/vycor}$

experiment that ranged from expected results to the serendipitous. The magnetism studies of ^3He in vycor fit nicely into the existing knowledge of ^3He magnetism in confined geometries. However, serendipity was encountered in the flow experiment in this system. That the surface magnetism of ^3He might drastically affect the flow properties in vycor now seems obvious having looked into the back of the book, but it was not so prior to the flow experiments. Continued study of this effect may provide important clues to the elusive answers long sought in these systems.

APPENDIX A

TABULATION OF DATA OF THE B PHASE SLAB EXPERIMENT

Table (A-1)
Frequency Shifts and Susceptibilities of the
B Phase in a Slab Geometry (in 286 G with no flow)

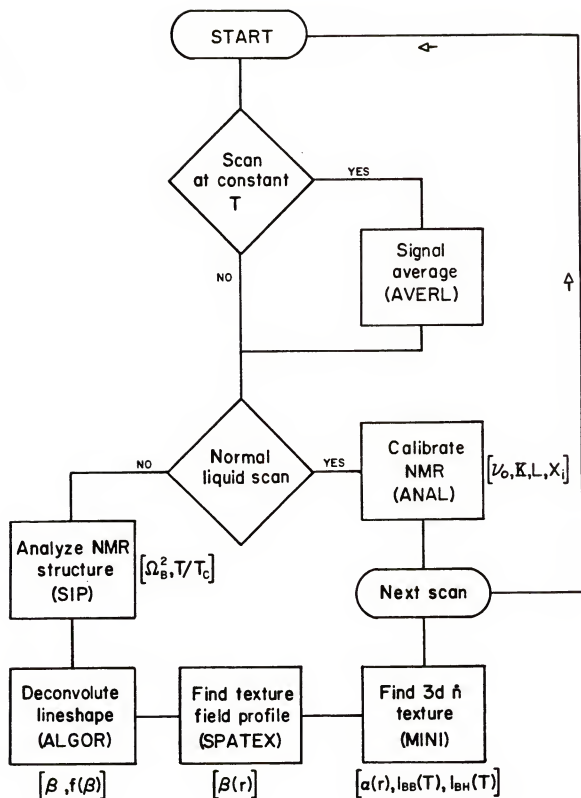
P = 21.5 bar and T _c = 2.41 mK				
	1 - T/T _c	($\Delta\nu$) ² (10 ¹⁰ Hz ²)	Ω_B^2 (10 ¹⁰ Hz ²)	χ_B/χ_N
P stack, $\sigma_{p \perp} H_O$	0.0306	0.4420	0.553	0.5545
	0.0431	0.5320	0.6650	0.5172
	0.0763	0.7760	0.9700	0.4527
	0.0825	0.9629	1.204	0.3958
	0.0866	0.8770	1.096	0.4327
	0.0866	0.8840	1.105	0.4059
	0.0991	1.058	1.323	0.3454
	0.1406	1.536	1.920	---
	0.1447	1.600	2.000	0.2816
	0.1655	1.864	2.330	0.2312
	0.2007	2.210	2.763	0.1964
	0.2153	2.467	3.084	0.1461
	0.2153	2.524	3.155	0.1624
	0.2277	2.613	3.266	0.1613
	0.2339	2.808	3.510	0.1700
	0.2360	2.771	3.464	---
V stack, $\sigma_v H_O$	0.0036	-0.0107	---	0.8403
	0.0285	-0.0094	---	0.6939
	0.0389	-0.0107	---	0.6572
	0.0680	0.0166	---	---
	0.0742	-0.0172	---	0.6376
	0.0866	-0.0172	---	0.6216
	0.0866	-0.0199	---	0.5994
	0.1323	-0.0159	---	0.5250
	0.1323	0.0680	---	0.5077
	0.1738	0.0730	---	0.4718
	0.2111	0.0550	---	0.4142
	0.2256	0.0840	---	0.4062
	0.2319	0.0630	---	---
	0.2381	0.110	---	---

Table (A-1) (continued)

P = 0 bar and T _c = 1.15 mK				
	1 - T/T _c	(Δv) ² (10 ¹⁰ Hz ²)	Ω _B ² (10 ¹⁰ Hz ²)	χ _B /χ _N
<hr/>				
P and V	0.0161	0.0449	0.0563	0.9896
stacks,	0.0227	0.0553	0.0691	0.8433
σ _P [⊥] H ₂ O and	0.0427	0.0737	0.0921	0.8066
	0.0466	0.0858	0.1073	0.8498
σ _V [⊥] H ₂ O	0.0551	0.1022	0.1278	0.8411
	0.0688	0.1043	0.1304	0.7741
	0.0780	0.1145	0.1431	0.7607
	0.1351	0.2991	0.3739	---
	0.1409	0.2950	0.3688	0.5611
	0.1456	0.2589	0.3236	0.5514
	0.1532	0.3175	0.3969	0.5290
	0.1551	0.2937	0.3671	0.5852
	0.1551	0.2814	0.3518	0.5863
	0.1561	0.2927	0.3659	0.6118
	0.1561	0.2937	0.3671	0.6150
	0.1627	0.3162	0.3953	0.5011
	0.1675	0.3430	0.4288	0.5454

APPENDIX B
DATA-GATHERING AND ANALYSIS PROGRAMS

This appendix contains the data-gathering and analysis program listings used in this work. The flow chart presents the order in which programs were used to analyze the \hat{n} -texture experiments starting with "AVERL" and ending with "MINI". The last listing is "TIMER5" which was used in the ^3He -vycor experiment.



```

10  ! ****PROGRAM: AVERL **** Last checked and/or revised: 13 Sept 1984
20  !      This program reads a data file and averages the NMR lines
30  !      in it. It separately averages the down and up sweeps, which
40  !      you can (if you wish) then average together for one averaged line.
50  PRINTER IS 16
60  PRINT CHR$(129);"" ! Inverse video.
70  DISP "This program is now set to average all 4 up sweeps and all 4 downs."
80  DISP "It may be necessary to change this. Watch out!"
90  PRINT CHR$(128)
100 BEEP
110 PAUSE
120 COM Peaks(7),INTEGER Nic(4087),Reflec(4087),Aver1(4087),Down(4087),Up(4087)
,Nic1(4087)
130 INPUT "Which file is to be averaged (T15)?",File$
140 ASSIGN #1 TO File$&"T15"
150 READ #1;Nic(*)
160 REWIND "T15"
170 GOTO 290
180 Avg=Avg1+Avg2=0
190   FOR I1=0 TO 149
200     Avg1=Avg1+Nic(I1)
210   NEXT I1
220   FOR I2=2000 TO 2199
230     Avg2=Avg2+Nic(I2)
240   NEXT I2
250 Avg=.5*(Avg1/150+Avg2/200)
260   FOR I3=0 TO 4087
270     Nic(I3)=Nic(I3)-Avg
280   NEXT I3
290 BEEP
300 PAUSE
310 Loop:1
320 DISP "Enter the addresses of the normal liquid peaks, in order."
330 MAT INPUT Peaks
340 INPUT "Enter the linewidths to be averaged, D=(Xmax-Xmin), suggest 150.",D
350 !
360 ! *****AVERAGE DOWN SWEEPS*****
370 !
380 MAT Down=ZER
390   FOR Line=0 TO 6 STEP 2
400     Addmin=Peaks(Line)-.75*D
410     Addmax=Peaks(Line)+.75*D
420     Displa=Peaks(Line)-Peaks(0)
430     FOR Addr=Addmin TO Addmax
440       Down(Addr-Displa)=Down(Addr-Displa)+Nic(Addr)
450     NEXT Addr
460   NEXT Line
470 MAT Down=Down*(.25)
480 PRINT CHR$(130) ! Blinking.
490 PRINT "Matrix Down complete"
500 BEEP

```

```

510 !
520 ! *****AVERAGE UP SWEEPS*****
530 !
540 MAT Up=ZER
550   FOR Line1=1 TO 5 STEP 2
560     Addmin=Peaks(Line1)*.75*D
570     Addmax=Peaks(Line1)*.75*D
580     Displa=Peaks(Line1)-Peaks(1)
590     FOR Addr1=Addmin TO Addmax
600       Up(Addr1-Displa)=Up(Addr1-Displa)+Nic(Addr1)
610     NEXT Addr1
620   NEXT Line1
630 MAT Up=Up/(3)
640 PRINT "Matrix Up complete"
650 PRINT CHR$(128) ! Clears the blinking.
660 BEEP
670   FOR M=0 TO 4095 ! This adds the 2 matrices and stores them in Nic.
680     Nic(M)=Up(M)+Down(M)
690   NEXT M
700   FOR M1=122 TO 347
710     Nic(M1)=Nic(M1)-Avg
720   NEXT M1
730 M=1
740 GOSUB Plot
750 !
760 ! *****REFLECT UP SWEEPS*****
770 !
780 Reflectup:! This section reflects the up sweeps about the Larmor address.
790 N=Peaks(1)
800 Imin=Peaks(1)*.75*D
810 Imax=Peaks(1)*.75*D
820   FOR I=Imin TO Imax
830     Reflec(2*N-I)=Up(I)
840   NEXT I
850 PRINT "Reflectup complete"
860 BEEP
870 Y=0
880 INPUT "Do you wish to try to add the up and down averages? (yes=1)",Y
890 IF Y=1 THEN GOSUB Addupdown
900 GOSUB Baseline
910 GOSUB Plot
920 EXIT GRAPHICS
930 GOSUB Autotransfer
940 PRINTER IS 16
950 PRINT LIN(5)
960 PRINT TAB(20);CHR$(129);"***** END PROGRAM *****"
970 PRINT CHR$(128)
980 END
990 !
1000 Addupdown:! Adds the averaged up to the averaged down, translating the
1010 ! up sweep to the down sweep position.
1020 !
1030 Displa=Peaks(1)-Peaks(0)
1040 Jmin=Peaks(1)*.75*D
1050 Jmax=Peaks(1)*.90*D
1060   FOR J=Jmin TO Jmax
1070     X=J-Displa
1080     Averi(X)=Down(X)+Up(J)
1090   NEXT J
1100 MAT Averi=Averi*(.5)
1110 DISP "Edit lines 950-970 and 1150 using correct matrix name (Nic or Averi)."
1120 BEEP
1130 PAUSE
1140 GOSUB Plot
1150 PRINT "Addupdown complete"
1160 BEEP
1170 !
1180 Autotransfer:! This section creates a file on a blank tape to hold the
1190 ! averaged line, for transfer to SIP1.
1200 !

```



```

1210 DISP "You must insert into T14 a blank tape."
1220 BEEP
1230 PAUSE
1240 MASS STORAGE IS "T14"
1250 CREATE "Nic",1,16352
1260 ASSIGN #2 TO "Nic"
1270 MAT PRINT #2;Nic1
1280 PRINTER IS 16
1290 BEEP
1300 CAT
1310 REWIND
1320 RETURN
1330 !
1340 Plot:!
1350 !
1360 PLOTTER IS 13,"GRAPHICS"
1370 GCLEAR
1380 GRAPHICS
1390 LIMIT 0,175,0,149
1400 LOCATE 10,90,10,110
1410 FRAME
1420 SCALE 0,1000,-2000,2000
1430 MOVE 0,100
1440   FOR K=0 TO 1000   ! Only draw the interesting section.
1450   IF M=1 THEN DRAW K,Nic(K)
1460   IF M=2 THEN DRAW K,Nic1(K)
1470   NEXT K
1480 M=M+1
1490 RETURN
1500 Baseline:! This averages the baseline on either side of the averaged peak
1510   ! and then subtracts this average from the entire peak.  If there
1520   ! is no baseline on one side then you choose which side.
1530   Yes=0
1540   INPUT "Are there baselines on both sides? (yes=1).",Yes
1550   IF Yes=1 THEN GOTO 1610
1560   Side=2
1570   INPUT "Which side, high field (0) or low (1)?",Side
1580   DISP "Change the limits if necessary."
1590   BEEP
1600   PAUSE
1610   FOR L=0 TO 1
1620     Avg1=0
1630     Imin=Peaks(L)-.75*D
1640     Imax=Imin+49
1650     FOR I=Imin TO Imax   ! 50 addresses.
1660       Avg1=Avg1+Nic(I)
1670     NEXT I
1680     Avg1=Avg1/50
1690     AvgR=0
1700     Jmax=Peaks(L)+.75*D
1710     Jmin=Jmax-49
1720     FOR J=Jmin TO Jmax
1730       AvgR=AvgR+Nic(J)
1740     NEXT J
1750     AvgR=AvgR/50
1760     Mid=(Imin+Imax)/2   ! Middle of leftmost averaging interval.
1770     Diff=Jmin-Imin   ! Run
1780     FOR K=Imin TO Jmax
1790       IF Yes<>1 THEN GOTO 1820
1800       B=Avg1+(AvgR-Avg1)*(K-Mid)/Diff   ! Sloping baseline, y=mx+b.
1810       GOTO 1840
1820       IF Side=0 THEN B=Avg1
1830       IF Side=1 THEN B=AvgR
1840       Nic1(K)=Nic(K)-B   ! Subtracts the baseline.
1850     NEXT K
1860   NEXT L
1870   RETURN

```

```

10  ! ****Program: ANAL ****
20  ! This program first finds the peaks of the normal He-3 NMR and
30  ! then uses them to compute the lag of the sweep coils, to be later
40  ! used in the frequency shift calculation.
50  PRINTER IS 16
60  DISP "This must be done for 2 different RF frequencies in order to"
70  DISP "calibrate the normal liquid."
80  OPTION BASE 0
90  DIM Desc$[50]
100 INPUT "Give description of experiment.", Desc$
110 PRINTER IS 0
120 PRINT Desc$
130 COM C(7), Rescur(7), Sup(7), INTEGER Nic(4087), Curr(4087), Rect(4087), Tnnour(40
140 G=3.2435 ! G= gyromagnetic ratio for He-3, in kHz/Gauss.
150 INPUT "Which tape drive? L/R", Drive$
160 IF Drive$="L" THEN MASS STORAGE IS ":T14"
170 IF Drive$="R" THEN MASS STORAGE IS ":T15"
180 INPUT "Which file contains the current sweep?", File1$
190 ASSIGN #1 TO File1$
200 READ #1; Curr(*)
210 REWIND
220 Y=0
230 DISP "Recall that the Nicolet is triggered on a 'real' current downsweep,"
240 DISP "so verify that recorded current scan is a downsweep ."
250 INPUT "Does current sweep need to be inverted? (yes=1)", Y
260 IF Y=0 THEN GOTO 300
270 FOR K=0 TO 4087
280 Curr(K)=-1*Curr(K)
290 NEXT K
300 BEEP
310 INPUT "Which of the 2 RF's is the operating freq? First(1) or second(2)?", X
320 OUTPUT 0 USING "+,K"; CHR$(27)&"&n41c4s102t42u24u10W"
330 OUTPUT 0 USING "+,K"; CHR$(27)&"&n100c60p61u110u110W"
340 FOR M=1 TO 2
350 INPUT "RF frequency (kHz)=", R(M)
360 INPUT "Which file contains the normal liquid sweeps?", File2$
370 PRINT "Normal spectra used: "; File2$; " Current file: "; File1$
380 ASSIGN #2 TO File2$
390 READ #2; Nic(*)
400 REWIND
410 BEEP
420 PRINT "RF frequency #"; M; " !="; R(M); "kHz"
430 |
440 | *****Find the NMR peaks*****
450 |
460 FOR I=0 TO 3570 STEP 510
470 Ko=I
480 Maxnm=Nic(I)+Nic(I+1)+Nic(I+2)
490 FOR J=I+1 TO I+510
500 Nmr=Nic(J)+Nic(J+1)+Nic(J-1)

```

```

510     IF Maxnmr<=Nmr THEN GOTO 540
520     Maxnmr=Nmr
530     Ko=J
540     NEXT J
550     Maxnmr=Maxnmr/3
560     Hm=.5*Maxnmr
570     Pos(I/510)=Ko
580     IF (X=2) AND (M=1) THEN GOTO 630
590     IF (X=2) AND (M=2) THEN GOTO 620
600     IF (X=1) AND (M=2) THEN GOTO 630
610     IF (X=1) AND (M=1) THEN GOTO 620
620     Posit(I/510)=Ko !Stores desired values for auto-transfer to SIP1.
630     !
640     ! *****Halfwidth*****
650     !
660     DIM Coord(1)
670     I1=I
680     FOR J1=0 TO 1
690         FOR J2=I1+1 TO I1+510
700             Nmr=Nic(J2)
710             IF ABS(Nmr-Hm)<=100 THEN GOTO 730
720         NEXT J2
730         BEEP
740         Coord(J1)=J2 ! Address positions of the half maximums.
750         I1=Ko ! This begins the inner loop at the NMR peak to get other halfmax.
760     NEXT J1
770     DIM Fuhm(?)
780     Fuhm(I/510)=ABS(Coord(0)-Coord(1)) ! Full-width at half-maximum.
790     PRINT "      Peak #";I/510+1;"at address#";Pos(I/510);" FWHM=";Fuhm(I/510)
800     BEEP
810     C(I/511)=Curr(Pos(I/510)) !Apparent current at the resonance.
820     NEXT I
830     GOSUB Correction
840     PRINT "      Actual current counts at resonance (with lag accounted for):"
850     FOR L=0 TO 7 ! Calculates the current at each resonance.
860         Recur(L)=Curr(Pos(L))+Trulag(L)*(-1)^L
870         PRINT "      ";Recur(L)
880     NEXT L
890     Avgcur=SUM(Recur)/8 !Average actual current counts at the peak.
900     Nu(M)=Avgcur
910     PRINT "      Average current counts at this frequency=";Avgcur
920     Avglag=SUM(Trulag)/8
930     PRINT "      Overall average lag=";Avglag
940     Aughu=SUM(Fuhm)/8
950     Aughu=DROUND(Aughu,2)
960     PRINT "      Normal liquid <FWHM=";Aughu;"addresses"
970     IF (X=1) AND (M=1) THEN Fuhm=Aughu
980     IF (X=2) AND (M=2) THEN Fuhm=Aughu
990     NEXT M
1000    Deltac=Nu(2)-Nu(1) !Difference in peak current counts for the 2 RF's.
1010    Deltaf=R(2)-R(1) !Difference in the 2 RF's.
1020    Coilk=Deltaf/(G*Deltac) !Constant for conversion of current into field.
1030    PRINT LIN(1)
1040    PRINT "Coil constant,K=";Coilk;"Gauss/count"
1050    Nuo=R(X)-G*Nu(X)*Coilk ! Frequency of the normal liquid (unshifted).
1060    PRINT "Larmor frequency of the normal liquid, !0=";Nuo;"kHz"
1070    OUTPUT 0 USING "+,K";CHR$(27)&"E"
1080    PRINTER IS 16
1090    !
1100    ! ***** Automatic data transfer to SIP1 *****
1110    !
1120    At=0
1130    INPUT "Manual input to SIP(0) or auto-transfer(1)?",At
1140    IF At=0 THEN GOTO 1310
1150    DISP "You must insert into the drive a tape which is not full."
1160    BEEP
1170    PAUSE
1180    CREATE "Curr",1,16352
1190    ASSIGN #3 TO "Curr"
1200    MAT PRINT #3;Curr

```

```

1210 CREATE "Array",2,32
1220 ASSIGN #4 TO "Array"
1230 MAT PRINT #4,1;Posit
1240 MAT PRINT #4,2;RelIag
1250 CREATE "Consts",4,8
1260 ASSIGN #5 TO "Consts"
1270 PRINT #5;Coilk,Nuo,R(X),Fuhs
1280 BEEP
1290 CAT
1300 REWIND
1310 PRINTER IS 16
1320 PRINT LIN(2)
1330 PRINT TAB(25);CHR$(129);"          END PROGRAM          "
1340 PRINT CHR$(128)
1350 END
1360 !
1370 ! *****
1380 !
1390 Correction: ! This subroutine calculates the true lags for the up and
1400             ! down sweeps assuming they're NOT equal.
1410     IF M=2 THEN GOTO 1880     ! Don't need to repeat GRAPHICS on second
1420                               ! frequency calibration.
1430     PLOTTER IS 13,"GRAPHICS"
1440     GCLERR
1450     LIMIT 0,184,0,149
1460     LOCATE 10,120,10,90
1470     FRAME
1480     SCALE 0,4087,-3000,3000
1490     AXES 100,250,0,0,10,2,3
1500     FOR I=0 TO 4087
1510         DRAW I,Curr(I)
1520     NEXT I
1530 ! !!!Digitize the turnaround points.
1540     DISP "Digitize the turnaround points of the current sweep."
1550     BEEP
1560     PAUSE
1570     FOR J=0 TO 8
1580         DIGITIZE X(J),Y(J)
1590         PRINT "Interval #";J+1;TAB(20);"Turnaround address=";X(J)
1600     NEXT J
1610     FOR I1=0 TO 8
1620         Begin=MAX(0,X(I1)-30)
1630         End=MIN(X(I1)+30,4087)
1640         Max=ABS(Curr(Begin))
1650         FIXED 0
1660         PRINT "Max=";Max;TAB(20);"BEGIN=";Begin;"END=";End
1670     STANDARD
1680     FOR I2=Begin TO End
1690         IF ABS(Curr(I2))<=Max THEN GOTO 1720
1700         Max=ABS(Curr(I2))
1710         Trnpos=I2
1720     NEXT I2
1730     Trnouv(I1)=Trnpos
1740     PRINT "Interval #";I1+1;TAB(20);"Exact turnover address=";Trnouv(I1)
1750     BEEP
1760     PAUSE
1770     NEXT I1
1780     FOR K7=0 TO 7
1790         D1=Trnouv(K7+1)-Trnouv(K7)
1800         Sup(K7)=D1
1810         D2=Trnouv(K7+2)-Trnouv(K7+1)
1820         PRINT "Sweep length=";D1;"addresses"
1830     NEXT K7
1840     DISP "To change any of the sweep lengths, execute Sup(*)=____."
1850     PAUSE
1860     PRINT "Correct sweep interval lengths (in addresses). "
1870     MAT PRINT Sup;
1880     FOR K5=0 TO 6 STEP 2
1890         S=MAX(Sup(K5),Sup(K5+1))/MIN(Sup(K5),Sup(K5+1)) !Scale factor
1900         PRINT "Proper scale factor=";S

```

```

1910 Sumlag=ABS(C(K5)-C(K5+1))  ! =sum of the two lags.
1920 PRINT "C(0)=";C(K5),"C(1)=";C(K5+1),"SUM OF 2 LAGS=";Sumlag
1930 PAUSE
1940 IF Sup(K5)>Sup(K5+1) THEN GOTO 1980
1950 Trulag(K5+1)=Sumlag/(1+S)
1960 Trulag(K5)=S*Trulag(K5)
1970 GOTO 2000
1980 Trulag(K5)=DROUND(Sumlag/(1+S),2)
1990 Trulag(K5+1)=DROUND(S*Trulag(K5),2)
2000 PRINT "Interval #";K5+1;TAB(20);"True lag=";Trulag(K5);"addresses"
2010 PRINT "Interval #";K5+2;TAB(20);"True lag=";Trulag(K5+1);"addresses"
2020 IF (X=1) AND (M=1) THEN GOTO 2060
2030 IF (X=1) AND (M=2) THEN GOTO 2080
2040 IF (X=2) AND (M=1) THEN GOTO 2080
2050 IF (X=2) AND (M=2) THEN GOTO 2060
2060 Rellag(K5)=Trulag(K5)  !Stores desired values for auto-transfer to SIP1
2070 Rellag(K5+1)=Trulag(K5+1)
2080 PAUSE
2090 NEXT K5
2100 RETURN

```

```

10  ! ****Program: SIP ****
11  ! Last check and/or revision: 13 Sept 1984
12  ! This program reads the He-3 NMR data and computes frequency shifts
13  ! (S) and integrals (I).
14  COM Linavg(1),Baslin(8),Avg(8),Truclt(7),C(7),Fssq(7),Intlim(15),Line(15)
15  COM Descpt$(25),INTEGER Curr(4087),Nic(4087),Pos(7),Rect(4087),Trnouv(8)
16  COM Np(7),Totsum(20),Fqyshf(20),Angle(20),INTEGER Trulag(7)
17  G=3.2435
18  BEEP
19  INPUT "Assign tape drive to be used: left(L) or right(R).",Drive#
20  IF Drive#="L" THEN MASS STORAGE IS "T14"
21  IF Drive#="R" THEN MASS STORAGE IS "T15"
22  INPUT "Manual input(0) or auto-transfer from ANAL(1)?",At
23  IF At=0 THEN GOTO 440
24  !
25  ! ***** AUTO-TRANSFER FROM ANAL *****
26  !
27  ASSIGN #1 TO "Curr"      ! Current sweep
28  MAT READ #1;Curr
29  ASSIGN #2 TO "Array"     ! Normal peak positions & lags
30  MAT READ #2,1;Pos
31  MAT READ #2,2;Trulag
32  ASSIGN #3 TO "Consts"    ! Coil constant, normal frequency, Rf, FWHM
33  READ #3;Ck,Nuo,Rf,Avghu
34  PRINTER IS 0
35  PRINT "Normal liquid peak addresses:"
36  MAT PRINT Pos
37  PRINT "Lag in each interval (current counts):"
38  MAT PRINT Trulag
39  Sumd=Sumu=0
40  FOR I=0 TO 6 STEP 2
41    Sumd=Trulag(I)+Sumd
42    Sumu=Trulag(I+1)+Sumu
43  NEXT I
44  Lagd=Sumd/4      ! Average of lags in the 4 down sweeps.
45  Lagu=Sumu/4      ! Average of lags in the 4 up sweeps.
46  PRINT "Average down lag=";Lagd,"Average up lag=";Lagu
47  PRINT "Coil constant=";Ck;"gauss/current count"
48  PRINT "Normal liquid frequency=";Nuo;"kHz"
49  PRINT "Rf frequency=";Rf;"kHz","(FWHM)";Avghu;"addresses"
50  MAT PRINT Curr
51  REWIND
52  GOTO 580
53  ! *****
54  PRINT "Insert into the drive the tape containing the most recent sweep, then press CONT."
55  BEEP
56  INPUT "Which file on the tape contains the current sweep?",File#
57  ASSIGN #1 TO File#
58  READ #1;Curr(*)
59  REWIND
60  INPUT "Does the current sweep need to be inverted? (yes=1)",In

```

```

510 IF In=0 THEN GOTO 560
520 FOR H=0 TO 4087
530 Curr(H)=-1*Curr(H) !This inverts the Nic curr counts to be the same
540 ! as the real current (i.e. positive count=positive current).
550 NEXT H
560 INPUT "Input parameters for ANAL(K in Gauss/count,RF in kHz,Nuo in kHz,Lag
s in counts,<FWMH> in addresses,qtrs to be plotted),Ck,Rf,Nuo,Lagd,Lagu,Fwhm,0
570 INPUT "Enter the addresses of the normal liquid peaks, in order.",Np(*)
580 PRINTER IS 16
590 PRINT "Insert into the drive the tape containing the files you wish to exam
ine."
600 BEEP
610 INPUT "Which file do you wish to examine?",File2$
620 Averg$="N0"
630 ASSIGN #4 TO File2$
640 READ #4;Nic(*)
650 REWIND
660 IF File2$(">")Nic96" THEN GOTO 690
670 IF File2$="Nic96" THEN Averg$="Averaged"
680 INPUT "What is the name of this averaged file?",File2$
690 BEEP
700 Basmooth=0
710 Endsmooth=4087
720 GOSUB Smooth
730 BEEP
740 ! This section draws the file on the CRT for digitizing.
750 PRINTER IS 16
760 PLOTTER IS "GRAPHICS"
770 GCLEAR
780 FRAME
790 Y=1900
800 SCALE 0,1021,-2000,2000
810 AXES 100,500,0,2000,5,1,3
820 FOR I1=0 TO Q-1
830 Y=Y-750
840 MOVE 0,Y
850 Jmin=1022+I1
860 Jmax=Jmin+1021
870 FOR J=Jmin TO Jmax
880 DRAW J-Jmin,Nic(J)+Y
890 NEXT J
900 NEXT I1
910 MOVE 750,-200
920 LOG 2
930 CSIZE 5
940 LABEL USING "K";File2$
950 PRINT "To see the file execute GRAPHICS on key #2."
960 PRINTER IS 0
970 IF Averg$="Averaged" THEN PRINT TAB(10);File2$; " Signal averaged"
980 IF Averg$(">")Averaged" THEN PRINT TAB(10);File2$
990 PRINTER IS 16
1000 !
1010 ! *****PROGRAM BRANCH SECTION***** !
1020 !
1030 BEEP
1040 WAIT 300
1050 BEEP
1060 DISP "The following subroutines are presently available in SIP:"
1070 DISP "1 Satellite--allows digitizing of the NMR spectrum & calculates"
1080 DISP " the frequency shift in kHz squared."
1090 DISP "2 Longitudinal--uses the max freq shift as measured in 'Satellite'"
1100 DISP " to calculate the long. freq. shift for He3-B, "
1110 DISP " assuming you know the chi (arccos(n.H)) which"
1120 DISP " produces it. Presently set for X=63.4 deg."
1130 DISP "3 Findmax--locates the peaks of the NMR and calculates the frequency"
1140 DISP " shifts of them. Not particularly useful for texture-"
1150 DISP " smeared spectra, but good for sharp NMR lines."
1160 DISP "4 Maninteg--allows for integration of the spectra by manually"
1170 DISP " digitizing the region to be integrated as well as the"
1180 DISP " baseline to be averaged for drift."
1190 DISP "5 Autointeg--automatically integrates the NMR by quarters (1023 "
1200 DISP " addresses)."
```

```

1210 DISP "Select which subroutine you wish to use by number. To stop the"
1220 DISP "program, type 0 (zero). For a new file, type 6."
1230 INPUT Choice
1240 IF Choice=1 THEN GOSUB Satellite
1250 IF Choice=2 THEN GOSUB Longitudinal
1260 IF Choice=3 THEN GOSUB Findmax
1270 IF Choice=4 THEN GOSUB Maninteg
1280 IF Choice=5 THEN GOSUB Autointeg
1290 IF Choice=6 THEN GOTO 580
1300 IF Choice=0 THEN GOTO 1320
1310 GOTO 1010 ! Returns to branch beginning unless ordered to stop.
1320 PRINTER IS 16
1330 PRINT TAB(20);CHR$(129);"          END PROGRAM          "
1340 PRINT CHR$(128)
1350 END
1360 ! *****
1370 Smooth: ! Smooths the entire file three times.
1380   FOR I=1 TO 3
1390     Base=Nic(Bsmooth)
1400     Nic(Bsmooth)=Nic(Bsmooth)*2/3+Nic(Bsmooth+1)/3
1410     FOR J=Bsmooth+1 TO Endsmooth-1
1420       Base1=Base/4+Nic(J)/2+Nic(J+1)/4
1430       Base=Nic(J)
1440       Nic(J)=Base1
1450     NEXT J
1460     Nic(Endsmooth)=Nic(Endsmooth)*2/3+Base/3
1470   NEXT I
1480   RETURN
1490 Findmax: ! Finds the NMR peaks, converts to true field and calculates
           ! the frequency shifts.
1500 PRINT "Peak #:      Apparent address #:"
1510   FOR L=0 TO 3500 STEP 500
1520     Ko=L
1530     Max=Nic(L)+Nic(L+1)+Nic(L+2)
1540     FOR Z=L+1 TO L+499
1550       Nmr=Nic(Z)+Nic(Z+1)+Nic(Z-1)
1560       IF Max<Nmr THEN GOTO 1590
1570       Max=Nmr
1580       Ko=Z
1590     NEXT Z
1600     Max=Max/3
1610     Pos(L/500)=Ko
1620     PRINT "      ";L/500+1;"          ";Pos(L/500)
1630     BEEP
1640     C(L/500)=Curr(Pos(L/500)) !Current counts at apparent address,
1650     NEXT L
1660     FOR K1=0 TO 3500 STEP 1000 !Steps 900 thru 950 correct for lag.
1670       Trucnt(K1/500)=C(K1/500)+Lagd !Correction for downsweep lag.
1680     NEXT K1
1690     FOR K2=500 TO 3500 STEP 1000
1700       Trucnt(K2/500)=C(K2/500)-Lagu !Correction for upsweep lag.
1710     NEXT K2
1720     PRINT "Peak #      Frequency shift sqrd      Current at resonance"
1730     PRINT "              (kHz squared)              (in counts)"
1740     FOR K3=0 TO 7 !Compute the frequency shifts.
1750       Fssq(K3)=Rf+2-(Nuo+G+Ck*Trucnt(K3))^2
1760       PRINT "      ";K3+1;"          ";Fssq(K3);"          ";Trucnt(K3)
1770     NEXT K3
1780     RETURN
1790 Maninteg: ! This allows you to manually set the limits of integration
1800 ! and the limits for the baseline average by plotting the NMR lines on
1810 ! the CRT and then digitizing the limits into the memory for later use.
1820 PRINT "Decide how many peaks can't be used because of drift problems."
1830 PRINTER IS 0
1840 INPUT "How many NMR peaks can be integrated?";Dim
1850 REDIM Intlim(2*Dim-1),Line(2*Dim-1)
1860 MAT Intlim=ZER
1870 MAT Line=ZER
1880 PRINTER IS 16
1890 PRINT "Digitize now by moving the cursor to the desired position and pressi
ng CONT."
1900 PRINTER IS 0

```



```

1910 PRINT "(X,Y) coordinates as digitized from CRT:"
1920 PRINT "(NOTE: X coordinates are the integration limits.)"
1930 FOR N=0 TO 2*Dim-1
1940 INPUT "In which quarter is the peak (Type 1,2,3 or 4, then press CONT)?",
Q
1950 DIGITIZE X,Y
1960 X=X+(Q-1)*1000
1970 Intlim(N)=X
1980 Line(N)=Y
1990 PRINT X,Y
2000 NEXT N
2010 PRINTER IS 16
2020 PRINT "You may now integrate the peaks using the X-limits just digitized."
2030 PRINTER IS 8
2040 Int=8
2050 INPUT "Which peak do you wish to integrate? (1 through 8, or 0=stop)",P
2060 IF P=0 THEN GOTO 2260
2070 Xo=Intlim(2*P-2)
2080 Xf=Intlim(2*P-1)
2090 IF Nic(Xo)=0 THEN GOTO 2210
2100 IF Nic(Xo)>0 THEN GOTO 2120
2110 IF Nic(Xo)<0 THEN GOTO 2170
2120 FOR B1=Xo TO Xf
2130 Diff=Nic(Xo)
2140 Nic(B1)=Nic(B1)-Diff
2150 NEXT B1
2160 GOTO 2210
2170 FOR B2=Xo TO Xf
2180 Diff=-Nic(Xo)
2190 Nic(B2)=Nic(B2)+Diff
2200 NEXT B2
2210 FOR A=Xo TO Xf
2220 Int=Int+Nic(A)
2230 NEXT A
2240 PRINT "Integral of peak #:";P;"=";Int
2250 GOTO 2040
2260 INPUT "Do you wish to update the current or RF coil calibrations? (1=yes,0=
no)",Update
2270 IF Update=1 THEN GOTO 440
2280 GOTO 580
2290 RETURN
2300 Autointeg: ! This averages the baseline between peaks in a single quarter
2310 ! and then integrates that quarter by halves(upsweep & down).
2320 PRINTER IS 16
2330 FOR M1=0 TO 8
2340 PRINT "Digitize the 2 points for the baseline average."
2350 FOR M=0 TO 1
2360 DIGITIZE X1,Y1
2370 Linaug(M)=X1
2380 NEXT M
2390 Counts=0
2400 Begin=Linaug(0)
2410 End=Linaug(1)
2420 FOR Addr=Begin TO End
2430 Counts=Counts+Nic(Addr)
2440 NEXT Addr
2450 Baslin(M1)=Counts/(End-Begin)
2460 Aug(M1)=ABS(Baslin(M1)) !This is the average baseline between peaks.
2470 NEXT M1
2480 FOR I0=0 TO 7 !This loop averages the augs on either side of peak.
2490 Aug(I0)=(Aug(I0)+Aug(I0+1))*5
2500 NEXT I0
2510 ! Find the endpoints of the current sweep for integration limits.
2520 FOR I1=0 TO 4087
2530 Rect(I1)=ABS(Curr(I1)) ! This rectifies the current to find the peaks
2540 ! easier.
2550 NEXT I1
2560 FOR I2=250 TO 3250 STEP 500
2570 Max=Rect(I2)
2580 FOR I3=I2 TO I2+499
2590 IF Rect(I3)<Max THEN GOTO 2620
2600 Max=Rect(I3)

```

```

2610      Trnpos=I3
2620      NEXT I3
2630      Trnouv=((I2+250)/500)=Trnpos! Trnouv=turnover point for the sweep.
2640      NEXT I2
2650      Trnouv(0)=0
2660      Max1=Rect(3750)
2670      FOR I4=3750 TO 4085
2680      IF Rect(I4)<=Max1 THEN GOTO 2710
2690      Max1=Rect(I4)
2700      Trn1=I4
2710      NEXT I4
2720      Trnouv(0)=Trn1
2730      ! Now use these points as limits of integration for the individual qtrs
2740      I5=0
2750      Sum=0
2760      FOR I6=Trnouv(I5) TO Trnouv(I5+1)
2770      AVer=Avg(I5)
2780      Recnic(I6)=ABS(Nic(I6))-Aver !This rectifies the NMR peak for simpli-
2790      ! city and subtracts the average baseline.
2800      Sum=Sum+Recnic(I6) ! Performs the integration.
2810      NEXT I6
2820      PRINTER IS 0
2830      PRINT "Peak #";I5+1;"integral=";Sum
2840      IF I5=7 THEN GOTO 2870
2850      I5=I5+1
2860      GOTO 2750
2870      PRINTER IS 16
2880      PRINT "All integrals for this file done."
2890      RETURN
2900      Satellite: ! This calculates the frequency shift of the satellite chosen.
2910      Stop=0
2920      PRINT "Digitize the satellite or shoulder which you wish to see."
2930      PRINT "Execute 'Stop=1' to exit this mode."
2940      PRINTER IS 0
2950      OUTPUT 0 USING "+,K";CHR$(27)&"&n52c60p110q20r41s170T"
2960      PRINT USING "7X,31A,10X,24A";"Satellite shifts (kNz)=:";"Current counts &
address"
2970      INPUT "Describe which peak,which satellite,etc,then press CONT.",Descrpt#
2980      IF Stop=1 THEN GOTO 3120
2990      INPUT "Which quarter?",Qtr
3000      INPUT "Upsweep (0) or downsweep (1)?",Sweep
3010      GRAPHICS
3020      DIGITIZE X2,Y2
3030      X2=X2+(Qtr-1)*1022
3040      IF Sweep=0 THEN GOTO 3070
3050      Trucur=Curr(X2)+Lagd
3060      GOTO 3080
3070      Trucur=Curr(X2)-Lagu
3080      Fssq=Rf^2-(Nu0+G*Gk+Trucur)^2
3090      Rnd=DROUND(X2,4)
3100      PRINT Descrpt#;" ";TAB(30);Fssq;TAB(50);Trucur;TAB(60);Rnd
3110      GOTO 2970
3120      OUTPUT 0 USING "+,K";CNR$(27)&"E"
3130      RETURN
3140      Longitudinal: !
3150      PRINTER IS 0
3160      PRINT "B PHASE LONGITUDINAL RESONANCE FREQUENCY"
3170      PRINT "*(Calculated from maximum shifted edge of each peak)"
3180      OUTPUT 0 USING "+,K";CHR$(27)&"&n77c70r104s104t104u50v154W" !0mega replace
s ?
3190      OUTPUT 0 USING "+,K";CHR$(27)&"&n45c161q160t110u160v110W" !Sub B replaces
%.
3200      OUTPUT 0 USING "+,K";CNR$(27)&"&n52c60p110q20r41s170T" !Super 2 replaces *
3210      OUTPUT 0 USING "+,K";CNR$(27)&"&n166c144t44u50v68W" !Nu replaces u.
3220      OUTPUT 0 USING "+,K";CHR$(27)&"&n108c70p41u40v40W" !Sub L replaces 0
3230      OUTPUT 0 USING "+,K";CNR$(27)&"&n41c61q60t110u110v110W" !Sub o replaces !
3240      PRINT LIN(1);"%*+5u![(X*-1)/(X*-5)] ; X=u0/u!";LIN(1)
3250      PRINT "u!= resonance frequency of maximum shifted signal in this peak"
3260      PRINT "%*= longitudinal resonance frequency of this peak"
3270      PRINT "u0= Larmor frequency"
3280      INPUT "Enter file #",Name$
3290      PRINT Name$
3300      PRINT "Peak#";TAB(20);"u! (kNz)";TAB(35);"%* (kNz*)"

```

```

3310 INPUT "Enter peak # & max shift squared(kHz^2) from Findsat.",Pk,Fssq
3320 Resfreq2=Nuo^2+Fssq
3330 Resfreq=Resfreq2^.5
3340 X=Nuo/Resfreq
3350 Long2=5*Resfreq2*(X^2-1)/(X^2-5)
3360 Long=Long2^.5
3370 PRINT USING "3X,D,13X,3Z,DDD,6X,4Z,DDD";Pk,Resfreq,Long2
3380 INPUT "More peaks in this file, yes(1) or no(0)?",More
3390 IF More=1 THEN GOTO 3310
3400 INPUT "More files to do, yes(1) or no(0)?",Moref
3410 IF Moref=1 THEN GOTO 3280
3420 OUTPUT 0 USING "+,K";CHR$(27)&"E" ! Clears the character definitions.
3430 PRINTER IS 16
3440 RETURN

```

```

10  ! ****Program: ALGORH ****
20  ! Last checked and/or revised: 17 Sept 1984
30  ! This program asks for a superfluid NMR file (Nic) and a normal
40  ! liquid file (Norm), then scales the first normal peak height
50  ! to the height of the first superfluid peak at whichever address
60  ! you choose. Next, it subtracts the normal peak from the superfluid
70  ! peak, storing the result (R1 & R2). Then, you locate the addresses
80  ! of the high field edges of R1 and Norm to find D, which allows you
90  ! to shift the normal peak to successively lower fields and continue
100 ! the subtraction until R1=0, within noise (hopefully).
110 DISP "This program performs the deconvolution algorithm to analyze the"
120 DISP "superfluid NMR spectra. It asks you where to translate the normal"
130 DISP "liquid spectrum and what the scale factor should be at that address."
140 DISP "It will also search for errors either in the result or in the orders"
150 DISP "which you give to it. Good luck. Pausing...."
160 PAUSE
170 COM INTEGER Nic(4087),Norm(4087),Curr(4087),R1(4087),R2(4087),Pk(7)
180 G=3.2435 ! Gyromagnetic ratio.
190 Error=Errcount=Errign=0
200 PRINTER IS 0
210 OUTPUT 0 USING "+,K";CHR$(27)&"&n100c302q44r30s20t60u110v206W"! Chi
220 OUTPUT 0 USING "+,K";CHR$(27)&"&n126c144s44t44u50v60W"! Nu
230 OUTPUT 0 USING "+,K";CHR$(27)&"&n41c61q60t110u10v110W"! Sub o
240 OUTPUT 0 USING "+,K";CHR$(27)&"&n46c110p111u150v130W"! Sub N
250 OUTPUT 0 USING "+,K";CHR$(27)&"&n45c134p124q124r135S"! Super 10
260 OUTPUT 0 USING "+,K";CHR$(27)&"&n44c60p110q20r41s170T"! Super 2
270 OUTPUT 0 USING "+,K";CHR$(27)&"&n77c70p50q70r1S"! Super o
280 INPUT "Give today's date.",Dates
290 INPUT "Which tape drive? L/R",Tapes
300 IF Tapes="L" THEN MASS STORAGE IS ":T14"
310 IF Tapes="R" THEN MASS STORAGE IS ":T15"
320 INPUT "Which file contains the current sweep?",File1$
330 ASSIGN #1 TO File1$
340 READ #1;Curr(*)
350 REWIND
360 Y=0
370 INPUT "Does the current sweep need to be inverted? (yes=1).",Y
380 IF Y=0 THEN GOTO 420
390 FOR I=0 TO 4087
400 Curr(I)=-1*Curr(I)
410 NEXT I
420 INPUT "Which file contains the normal liquid NMR lines?",File2$
430 ASSIGN #2 TO File2$
440 READ #2;Norm(*)
450 REWIND
460 Daver1=250
470 INPUT "Which superfluid file do you wish?",File3$
480 ASSIGN #3 TO File3$
490 READ #3;Nic(*)
500 REWIND

```

```

510 INPUT "Enter the Larmor frequency addresses.",Pk(*)
520 INPUT "Have assumed the width from 'AVERL' is 250. Change if needed.",Dave
r1
530 INPUT "Downsweep (0) or upsweep (1)?",Sup
540 Min=Pk(Sup)*.75+Dave1 ! Beginning address of averaged file.
550 Max=Pk(Sup)+.75+Dave1 ! End address of averaged file.
560 INPUT "In which peak are you interested?",P
570 Trans=Pk(P-1)-Pk(Sup)
580 INPUT "Is a scale factor correction between normal & superfluid required?
Y/N",Q$
590 IF Q$="N" THEN Mult=1
600 IF Q$="Y" THEN INPUT "Give multiplier.",Mult
610 Maxval=0
620 FOR I=Min TO Max
630   Pos=I+Trans
640   IF Pos>4007 THEN Pos=4007
650   R1(I)=Nic(Pos)
660   Norm(I)=Norm(I)*Mult
670   IF ABS(R1(I))<Maxval THEN GOTO 700
680   Maxval=ABS(R1(I))
690   Maxadd=I
700 NEXT I
710 INPUT "Enter: Rf,Larmor freq,longitudinal freq squared,coil constant,lag,F
WMH.",Rf,Nuo,Lfss,Ck,Lag,FuHm
720 Int=1 !This is the first interval,incremented every pass thru Calculation.
730 GOSUB Smoother
740 ! *****
750 X=0 ! Variable to be used when plot fills up the first column.
760 PLOTTER IS "GRAPHICS"
770 GRAPHICS
780 GCLEAR
790 FRAME
800 SCALE 0,1021,-1500,1500
810 AXES 100,500,0,1500,5,1,3
820 MOVE Min,1400
830 FOR I3=Min TO Max
840   DRAW I3,R1(I3)+1400 ! If a sub is bad, this redraws the previous plot.
850 NEXT I3
860 EXIT GRAPHICS
870 ! *****
880 GOSUB Baseline
890 GOSUB Integration
900 Addold=Pk(Sup) ! First check is relative to Larmor position.
910 DISP "First subtract., try matching to Larmor address without translation."
920 DISP "Match either at the peak edges or the peaks themselves for best resul
ts."
930 DISP "On subsequent passes, be sure to update S and D."
940 BEEP
950 PAUSE
960 EXIT GRAPHICS
970 BEEP
980 DISP "Position of maximum=";Maxadd
990 INPUT "Enter address to translate to. (Continue at 950)",Place
1000 S=R1(Place)/Norm(Pk(Sup)) ! Scale factor at this address
1010 D=ABS(Place-Pk(Sup)) ! Amount of translation
1020 DISP "Values: translation=";D;" scale factor=";S
1030 Q$="Y"
1040 INPUT "Are these values acceptable? Y/N",Q$
1050 IF Q$="N" THEN GOTO 900
1060 Addnew=Pk(Sup)+(1-2*Sup)*D ! Address of the point being matched to the Lar
mor freq.
1070 Start=Addold ! Previous matched address is used for check.
1080 End=Addnew
1090 Newsun=0 ! This will be the integral of the remaining peak after sub.
1100 MAT R2=ZER ! Zeros the R2 array since it was used in Smoother.
1110 FOR I4=Min TO Max
1120   IF I4<D THEN I4=D
1130   IF Sup=0 THEN Pos=I4-D
1140   IF Sup=1 THEN Pos=I4+D
1150   R2(I4)=R1(I4)-S*Norm(Pos)
1160   V=R2(I4)
1170   IF V>Rugbas THEN V=0 ! Prevents oversub from under estimating remaind
er
1180   IF ABS(V)<Rugbas THEN V=0 ! Ignores baseline noise
1190   Newsun=Newsum+V
1200   IF (I4<Start) OR (I4>End) THEN GOTO 1220

```

```

1210 Check=Check+R2(I4)
1220 NEXT I4
1230 Sign=SGN(Check)
1240 Check=ABS(Check/Sums)
1250 IF R2(Addnew)=0 THEN GOTO 1280
1260 IF R2(Addnew)>0 THEN Error=1
1270 GOSUB Progerror
1280 Pen=1
1290 GOSUB Graphics
1300 INPUT "Is this subtraction adequate? Y/N",Q$
1310 IF Q$="Y" THEN GOTO 1360
1320 Pen=1 ! Sets PENUP to erase this latest plot.
1330 GOSUB Graphics
1340 Pen=1
1350 GOTO 980 ! Returns to subtraction routine to try again.
1360 GOSUB Calculation
1370 Maxval=0
1380 FOR J=0 TO 4087
1390 R1(J)=R2(J)
1400 IF ABS(R1(J))<=Maxval THEN GOTO 1430
1410 Maxval=ABS(R1(J))
1420 Maxadd=J
1430 NEXT J
1440 PRINTER IS 0
1450 IF Int>1 THEN GOTO 1600
1460 INPUT "Is this an average file? Y/N",Y$
1470 IF Y$="N" THEN GOTO 1530
1480 IF Sup=0 THEN Choice$="Down Sweep"
1490 IF Sup=1 THEN Choice$="Up Sweep"
1500 INPUT "Give file name.",Name$
1510 PRINT Name$;TAB(10);Choice$;TAB(50);Date$
1520 GOTO 1540
1530 PRINT File$;TAB(10);"Peak #";P
1540 IF Times=0 THEN GOTO 1570
1550 PRINT USING "K,Z.4D,10X,K";"@/0$=",Susc,"Not smoothed here."
1560 GOTO 1580
1570 PRINT USING "K,Z.4D,10X,K,DZ,K";"@/0$=",Susc,"Smoothed ",Times," times"
1580 PRINT "Interval #";TAB(15);"Center address";TAB(35);"V!";TAB(45);"@";TAB(50)
; "Fraction";TAB(60);"Freq shift";TAB(71);"Ignored"
1590 PRINT TAB(61);"(10% Hz)";TAB(72);"Errors"
1600 IF Errign>0 THEN GOTO 1630
1610 PRINT USING "6X,2D,10X,4D,10X,3Z.DDD,4X,2D.D,K,4X,D.DDD,6X,Z.DDD";Int,Addne
w,No,Angle,"?",Frac,Fss
1620 GOTO 1660
1630 PRINT USING "6X,2D,10X,4D,10X,3Z.DDD,4X,2D.D,K,4X,D.DDD,6X,Z.DDD,3X,K";Int,
Addnew,No,Angle,"?",Frac,Fss,Errs
1640 Error=0 ! Re-sets parameter to zero for next subtraction
1650 Errign=0 ! Re-sets flag to zero for next error-free printout
1660 Int=Int+1
1670 INPUT "Are there more subtractions to be done on this peak? Y/N",Q$
1680 IF Q$="Y" THEN GOTO 980
1690 Sub=(Sums-Newsum)/Sums ! Fraction which has been subtracted.
1700 IF (Sub)=.9) AND (Sub=1) THEN GOTO 1740
1710 IF Sub<.9 THEN Error=2
1720 IF Sub>1 THEN Error=3
1730 GOSUB Progerror
1740 PRINTER IS 0
1750 PRINT USING "K,Z.DDD";"Fraction of integral subtracted=",Sub
1760 Abssum=Rssum+Possum=0
1770 FOR J1=Min TO Max
1780 Rssum=Rssum+R1(J1)^2
1790 Abssum=Abssum+ABS(R1(J1))
1800 IF R1(J1)<0 THEN GOTO 1820
1810 Possum=Possum+R1(J1)
1820 NEXT J1
1830 Errabs=Abssum/ABS(Sums) ! Absolute estimate of error.
1840 Errrms=SQR(Rssum)/ABS(Sums) ! RMS estimate of error.
1850 Errpos=Possum/ABS(Sums) ! Over-estimate of integral at each interval.
1860 PRINT USING "K,Z.DDD";"RMS fractional remainder=";Errrms
1870 PRINT USING "K,Z.DDD";"Absolute fractional remainder=";Errabs
1880 PRINT USING "K,Z.DDD";"Overestimate of signal (cum. all subs)=";Errpos
1890 PRINT USING "K,DD";"# of errors encountered=",Errcount
1900 INPUT "Are there more peaks in this experiment to be done? Y/N",Q$

```

```

1910 Errcount=Errign=0
1920 IF Qs="Y" THEN GOTO 470
1930 PRINTER IS 16
1940 OUTPUT 0 USING "+,K";CHR$(27)&"E"
1950 PRINT TAB(20);CHR$(129);"      END PROGRAM      ";CHR$(128)
1960 END
1970 Graphics:| This plots the subtracted peaks.
1980 GRAPHICS
1990 PEN Pen
2000 IF Pen=-1 THEN DISP "PENUP, ready to erase...."
2010 IF Pen=1 THEN DISP "PENDOWN, ready to draw...."
2020 DISP "Last Y position=";Ypos
2030 INPUT "Give Y position (between 1500 and -1500).",Ypos
2040 IF Ypos>-1500 THEN GOTO 2070
2050 Xo=500+(1-2*Sup)
2060 GOTO 2020
2070 MOVE Min+Xo,Ypos
2080 FOR J1=Min+Xo TO Max+Xo
2090 DRAW J1,R2(J1-Xo)+Ypos
2100 NEXT J1
2110 EXIT GRAPHICS
2120 RETURN
2130 Calculation:| This calculates the texture.
2140 PRINTER IS 0
2150 Rem=Neusum/Sig ! Fraction of signal remaining after this subtract.
2160 IF Rem>0 THEN GOTO 2240
2170 IF Rem=0 THEN GOTO 2190
2180 IF Rem<0 THEN GOTO 2220
2190 BEEP
2200 DISP "Fraction subtracted=100%"
2210 GOTO 2240
2220 Error=3
2230 GOSUB Progerror
2240 Frac=(Sig-Neusum)/Sums ! Fraction of signal contained in the sub.
2250 IF Check<.025*Frac THEN GOTO 2290
2260 IF Sign=1 THEN Error=8
2270 IF Sign=-1 THEN Error=9
2280 GOSUB Progerror
2290 Sig=Neusum ! Updates Sig to the new integral.
2300 Curr=Curr(Addnew)+(1-2*Sup)*Lag ! Only down sweeps being calculated
.
2310 A=Nuo+G*Gk*Current ! Freq at interval center.
2320 IF A<Rf THEN GOTO 2350
2330 Error=4
2340 GOSUB Progerror
2350 Fs=SQR(Rf^2-A^2) ! Freq shift at interval in kHz.
2360 Lfs=SQR(Lfss)
2370 Sine=Fs/Lfs ! Sine of angle between N and H.
2380 DEG
2390 Angle=ASN(Sine) ! Angle between N and H.
2400 IF Angle<63.4 THEN GOTO 2430 ! 63.4 deg is thought to be wall angle.
2410 Error=5
2420 GOSUB Progerror
2430 No=SQR(Fs^2+Nuo^2) ! Freq at interval center.
2440 Fss=Fss+2*IE-4 ! Switches to units of 10^-10 Hz^2.
2450 Addld=Addnew ! Updates the Addld variable for next check
2460 RETURN
2470 Baseline:| This averages the baseline on either side of the averaged peak
2480 | and then subtracts this average from the entire peak. If there
2490 | is no baseline on one side then you choose which side.
2500 INPUT "Are there baselines on both sides? Y/N",Qs
2510 IF Qs="Y" THEN GOTO 2570
2520 Side=2
2530 INPUT "Which side, high field (0) or low (1)?",Side
2540 DISP "Change the limits if necessary."
2550 BEEP
2560 PAUSE
2570 Aug1=Augr=Augbas=0
2580 Imin=Pk(Sup)*.75*Daver1
2590 Imax=Imin+49
2600 FOR I=Imin TO Imax ! 50 addresses.

```

```

2610      Avg1=Avg1+R1(I)
2620      NEXT I
2630      Avg1=Avg1/50
2640      Jmax=Pk(Sup)+.75+Daver1
2650      Jmin=Jmax-49
2660      FOR J=Jmin TO Jmax
2670          Avg=Avg+R1(J)
2680      NEXT J
2690      Avg=Avg/50
2700      DISP "Baseline avgs: left=";Avg1;" right=";Avg
2710      INPUT "Does a baseline average need to be done? Y/N",Q$
2720      IF Q$="Y" THEN GOTO 2780
2730      Tilt=ABS((Avg1-Avg)/Norm(Pk(0)))
2740      IF Tilt<=.005 THEN GOTO 2880 ! Allows for 0.5% tilt w.r.t. normal peak
2750      Error=6
2760      GOSUB Progerror
2770      GOTO 2880
2780      Mid=(Jmin+Jmax)/2 ! Middle of leftmost averaging interval.
2790      Diff=Jmin-Jmin ! Run
2800      FOR K=Jmin TO Jmax
2810          IF Yes<1 THEN GOTO 2840
2820          B=Avg1+(Avg-Avg1)*(K-Mid)/Diff ! Sloping baseline, y=mx+b.
2830          GOTO 2860
2840          IF Side=0 THEN B=Avg1
2850          IF Side=1 THEN B=Avg
2860          R1(K)=R1(K)-B ! Subtracts the baseline.
2870      NEXT K
2880      FOR J1=Jmin TO Jmax
2890          Avgbas=Avgbas+ABS(R1(J1))
2900      NEXT J1
2910      Avgbas=Avgbas/50 ! Average baseline scatter which will be ignored.
2920      IF Q$="N" THEN GOTO 2940
2930      GOTO 760
2940      RETURN
2950      Integration: ! This integrates the normal and superfluid peaks.
2960      Sumn=Sums+Susc=M=0
2970      FOR I1=Min TO Max
2980          V=Norm(I1)
2990          IF ABS(V)<Avgbas THEN V=0 ! Ignores baseline scatter.
3000          IF V>Avgbas THEN V=0 ! Ignores large positive excursions.
3010          Sumn=Sumn+V
3020      NEXT I1
3030      FOR I2=Min TO Max
3040          V=R1(I2)
3050          IF ABS(V)<Avgbas THEN V=0
3060          IF V>Avgbas THEN V=0
3070          Sums=Sums+V
3080      NEXT I2
3090      Susc=Sums/Sumn ! Relative susceptibility.
3100      IF Susc<1 THEN GOTO 3130
3110      Error=7
3120      GOSUB Progerror
3130      Sig=Sums ! Sig will be updated each pass thru Calculation.
3140      RETURN
3150      Smoother: ! This smooths only the superfluid file N times.
3160      DISP "The program assumes that the normal file has already been"
3170      DISP "smoothed in 'AVERL'"
3180      INPUT "Has the superfluid file already been smoothed in 'AVERL'? Y/N"
3190      ,Y$
3200      IF Y$="N" THEN GOTO 3220
3210      Times=0 ! Sets Times=0 for I/O puposes.
3220      GOTO 3370
3230      INPUT "How many times do you want to smooth?",Times
3240      IF Times=0 THEN GOTO 3370
3250      PRINTER IS 16
3260      FOR N=1 TO Times
3270          FOR K1=Min TO Max
3280              R2(K1)=(R1(K1-1)+R1(K1)+R1(K1+1))/3
3290          NEXT K1
3300          FOR K2=Min TO Max
3310              R1(K2)=R2(K2)

```



```

3318             NEXT K2
3320     IF N=1 THEN GOTO 3350
3330     PRINT USING "K,DZ,K";"Smoothed ",N," times"
3340     GOTO 3360
3350     PRINT "Smoothed 1 time."
3360     NEXT N
3370     RETURN
3380 Progerror:
3390     ! This routine is executed if a program error is detected
3400     ! manually. It allows the operator to immediately select
3410     ! the place to back-track to in the program.
3420     Errcount=Errcount+1 ! Updates error counter
3430     Errign=0 ! Re-sets ignored error flag to zero
3440     PRINTER IS 16
3450     BEEP
3460     WAIT 250
3470     BEEP
3480     PRINT TAB(25);CHR$(129);"          ERROR DETECTED          "
3490     PRINT CHR$(128)
3500     PRINT TAB(10);CHR$(129);"          Program error detected in algorithm."
3510     PRINT CHR$(128)
3520     PRINT CHR$(129);"Error:"
3530     IF Error=0 THEN DISP "UNDIAGNOSED."
3540     IF Error=1 THEN DISP "INCORRECT SUBTRACTION, R2#0."
3550     IF Error=2 THEN DISP "FRACTION SUBTRACTED LESS THAN 90%."
3560     IF Error=3 THEN DISP "FRACTION SUBTRACTED GREATER THAN 100%."
3570     IF Error=4 THEN DISP "IMAGINARY FREQUENCY SHIFT DUE TO TRANSLATION SEL
ECTED."
3580     IF Error=5 THEN DISP "X>63.4 DEGREES."
3590     IF Error=6 THEN DISP "SUBSTANTIAL BASELINE TILT."
3600     IF Error=7 THEN DISP "X/Xn>1"
3610     IF Error=8 THEN DISP "TRANSLATION TOO SMALL, OVER-SUBTRACTION."
3620     IF Error=9 THEN DISP "TRANSLATION TOO BIG, SIGNAL LEFT BEHIND."
3630     PRINT CHR$(128)
3640     DISP "STANDBY"
3650     WAIT 5000
3660     IF (Error=8) OR (Error=9) THEN GOSUB Arrow
3670     DISP "Select remedy in order to correct it:"
3680     DISP "1 Restart;"
3690     DISP "2 Re-read normal liquid spectra;"
3700     DISP "3 Re-read superfluid spectra;"
3710     DISP "4 Execute Smoother;"
3720     DISP "5 Restart plot;"
3730     DISP "6 Execute Baseline;"
3740     DISP "7 Execute Integration;"
3750     DISP "8 Erase and subtract again;"
3760     DISP "9 Continue this or start another subtraction;"
3770     DISP "10 Ignore error;"
3780     DISP "11 Stop program."
3790     DISP "Make your selection by number."
3800     INPUT Choice
3810     IF Choice=10 THEN Errign=1 ! Sets flag=1 for print-out
3820     IF Choice=11 THEN GOTO 1940
3830     IF Choice=10 THEN GOTO 3940
3840     IF Choice=9 THEN GOTO 980
3850     IF Choice=8 THEN GOTO 1300
3860     IF Choice=1 THEN GOTO 170
3870     IF Choice=2 THEN GOTO 420
3880     IF Choice=3 THEN GOTO 470
3890     Int=1
3900     IF Choice=4 THEN GOTO 730
3910     IF Choice=5 THEN GOTO 760
3920     IF Choice=6 THEN GOTO 880
3930     IF Choice=7 THEN GOTO 890
3940     IF Error=1 THEN Errs="R2#0"
3950     IF Error=2 THEN Errs="frac<.9"
3960     IF Error=3 THEN Errs="frac>1"
3970     IF Error=4 THEN Errs="imag shift"
3980     IF Error=5 THEN Errs="X>63.4"
3990     IF Error=6 THEN Errs="tilted"
4000     IF Error=7 THEN Errs="X/Xn>1"

```

```

4010     IF Error=8 THEN Err$="oversub"
4020     IF Error=9 THEN Err$="undersub"
4030     RETURN
4040 Arrow: !
4050     GRAPHICS
4060     WAIT 1500
4070     Pen=1
4080     PEN Pen
4090     X=Xo+Addneu-.5*Fwhm
4100     Y=Ypos+R2(X)-100
4110     MOVE X,Y
4120     DRAW X,Y-100
4130     MOVE X,Y
4140     DRAW X+8,Y-35
4150     MOVE X,Y
4160     DRAW X-8,Y-35
4170     MOVE X,Y-400
4180     LOG 5
4190     CSIZE 3
4200     IF Error=8 THEN LABEL USING "K";"OVERSUBTRACTION"
4210     IF Error=9 THEN LABEL USING "K";"SIGNAL"
4220     MOVE X,Y-500
4230     LABEL USING "K";"HERE"
4240     Pen=-1*Pen
4250     IF Pen=-1 THEN WAIT 5000
4260     IF Pen=1 THEN GOTO 4260
4270     GOTO 4080
4280     WAIT 1500
4290     EXIT GRAPHICS
4300     RETURN

```

```

10  ! ****Program: SPATEX ****
20  ! Last check or revision: 17 Sept 1984
30  ! This program computes the N-texture in space for the cylindrical
40  ! flow cell geometry.
50  DIM Files(10)
60  DIM Angle(20),R(20),Labels(30)
70  PRINTER IS 0
80  INPUT "Enter file name, peak # and # of intervals.",File#,P,I
90  PRINT TAB(3);Files;TAB(20);"Peak #";P
100 INPUT "Give description.",Name$
110 Name$="X"&Name$
120 OUTPUT 0 USING "+,K";CHR$(27)&"&n100c302q44r30s20t60u110v206W"!Chi replaces
    0.
130 OUTPUT 0 USING "+,K";CHR$(27)&"&n47c140p100t1u100v100W"!Sub i replaces /.
140 OUTPUT 0 USING "+,K";CHR$(27)&"&n77c70p50q70r1s"!Super o replaces ?.
150 PRINT Name$
160 PRINT TAB(2);"Interval#";TAB(15);"r'(mm)";TAB(27);"0";TAB(35);"sin(0)";TAB(
45);"Fraction"
170 REDIM Angle(1),R(1)
180 R=1.00 ! Radius= 1 millimeter.
190 S=1.00 ! Interval #
200 DEG
210 DISP "Start from the center of the cylinder and work toward the wall."
220 INPUT "Enter angle and fraction.",Ang,F
230 Sine=SIN(Ang)
240 IF S<1.00 THEN GOTO 270
250 R1=0
260 GOTO 280
270 R1=R1 ! Sets r(i-1)=r(i) of previous interval.
280 R1=(F*R+2*R1^2)^.5
290 DEG
300 Angle=ASN(Sine)
310 Angle(S)=Angle
320 R(S)=R1
330 PRINT USING "5X,DD,8X,Z.DDD,4X,2D.DDD,1A,5X,Z.DDD,6X,Z.DDD";S,R1,Angle,"?",
    Sine,F
340 S=S+1.00
350 BEEP
360 Choose$="CONT"
370 INPUT "To continue press CONT, new file type N, to plot type P, to stop typ
    e E.",Choose$
380 IF Choose$="CONT" THEN GOTO 220
390 IF Choose$="N" THEN GOTO 50
400 IF Choose$="P" THEN GOSUB Plot
410 IF Choose$="E" THEN GOTO 480
420 GOSUB Plot
430 GOTO 360
440 Yes=0
450 INPUT "Do you want to do the angular integration? (yes=1).",Yes
460 IF Yes=0 THEN GOTO 100
470 GOSUB Integration
480 OUTPUT 0 USING "+,K";CHR$(27)&"E"
490 PRINTER IS 16
500 END

```

```

510 Plot: 1
520 IF More$="N" THEN RETURN
530 PLOTTER IS "9672A"
540 LIMIT 5,210,5,275
550 LOCATE 16,61,13,119
560 PEN 1.00
570 OUTPUT 705;"VS10"
580 SCALE 0,1.00,0,100
590 INPUT "Label axes this time? Y/N",Q$
600 IF Q$="N" THEN GOTO 840
610 FRAME
620 AXES .1,10,0,0,1.00,1.00,3
630 FOR K=0 TO 1.00 STEP .2
640 CSIZE 3
650 LOG 6
660 MOVE K,-2
670 LABEL USING "Z.D";K
680 NEXT K
690 MOVE .1,-8
700 LOG 2
710 CSIZE 3
720 LDIR 0
730 LABEL USING "K";"Distance from axis (mm)"
740 LOG 5
750 CSIZE 3
760 FOR J=0 TO 100 STEP 10
770 MOVE -.1,J
780 LABEL USING "3D";J
790 NEXT J
800 LOG 2
810 LDIR 90
820 MOVE -.2,20
830 LABEL USING "K";"Angle between N and H (degrees)"
840 INPUT "Select y position on plotting area for this peak.",Y
850 MOVE 0,Y
860 INPUT "Which pen?",Pen
870 PEN Pen
880 Jmin=1.00
890 Jmax=1
900 CSIZE 3
910 LOG 5
920 FOR J=Jmin TO Jmax
930 MOVE R(J),Angle(J)+Y
940 LABEL USING "A";"e"
950 NEXT J
960 Lab$="Y"
970 INPUT "Any labels? Y/N",Lab$
980 IF Lab$="N" THEN GOTO 1080
990 INPUT "Give label position, (x,y).",Xo,Yo
1000 LDIR 0
1010 CSIZE 3
1020 LOG 2
1030 INPUT "Which pen?",C
1040 PEN C
1050 MOVE Xo,Yo
1060 INPUT "Give the label:",Label$
1070 LABEL USING "K";Label$
1080 INPUT "More? Y/N",More$
1090 IF More$="N" THEN GOTO 1110
1100 GOTO 990
1110 PEN 0
1120 RETURN
1130 Integration: This performs an integral of the texture angle over
1140 ! the channel (multiplied by r*r).
1150 PRINTER IS 0
1160 R(0)=0
1170 Jmax=1-1.00
1180 Num=Den=0
1190 FOR J=1.00 TO Jmax
1200 Ri=R(J)

```

```

1210      Rii=R(J+1.00)
1220      Raug=(Ri+Rii)/2
1230      Dr=Rii-Ri      ! Interval
1240      Angaug=(Angle(J)+Angle(J+1.00))/2
1250      Dang=Angle(J+1.00)-Angle(J)
1260      R3=Raug^3
1270      Num=Num+Raug*ABS(Dang)^2*Dr
1280      Dem=Dem+Angaug^2*Raug*Dr
1290      PRINT "Num=";Num,"Dem=";Dem
1300      NEXT J
1310      Integ=Num/Dem      ! Integral
1320      OUTPUT 0 USING "+,K";CHR$(27)&"&n45c30p30q44r20s40t41u30v04W"!Xsireplac
es %
1330      OUTPUT 0 USING "+,K";CHR$(27)&"&n52c60p110q20r41s170T"!Super 2 replaces
*
1340      OUTPUT 0 USING "+,K";CHR$(27)&"&n44c74R"!Super - replaces $.
1350      INPUT "Enter the pressure, Tc and long. shift squared (10~10 Hz^2).",Pr
ess,Tc,Lfss
1360      Rt=Lfss/(.53*Press+2.24)      ! Reduced temperature, (1-T/Tc).
1370      F=1.00-Rt      ! T/Tc
1380      Rt2=Rt^2
1390      T=F*Tc
1400      FIXED 3
1410      PRINT USING "K,3X,D";File$,P
1420      PRINT USING "3X,K,2D.DDDD,4X,K,.DDD,4X,K,.DDD,4X,K,Z.DDD,K,4X,K,.DDDD";
"<f>+>=",Integ,"(1-T/Tc)=",Rt,"T/Tc=",F,"T=",T,"mk","(1-T/Tc)*=",Rt2
1430      PRINT LIN(2)
1440      OUTPUT 0 USING "+,K";CHR$(27)&"E"
1450      RETURN

```

```

10  ! ****Program: MINII ****
20  ! Last check or revision: 18 Sept 1984
30  ! This program searches for a minimum of the bulk bending energy integrand
40  ! as a function of alpha, the angle which gives rise to an azimuthal
50  ! component in the texture.
60  PRINTER IS 16
70  OPTION BASE 1
80  SHORT Ri(100),Xi(100),Ri(100),Rneu(100),Xneu(100),Fract(100),Bend(2),Field(
2),Diffb(2),Diffh(2)
90  INPUT "Give today's date.",Date$
100 INPUT "Give file.",File$
110 INPUT "(A)Up sweeps average, (B)down, or (C)single peak?",B$
120 IF B$<"C" THEN GOTO 140
130 INPUT "Which peak?",Peak
140 INPUT "Is this an alpha determination? Y/N (Or just error calc)",O$
150 IF O$="N" THEN GOTO 1510
160 DISP " "
170 DISP "*****"
180 DISP "*** In order to correctly calculate the bulk-field term you must ***"
190 DISP "*** extrapolate the (r,X) data points to (0,0). ***"
200 DISP "*****"
210 DISP " "
220 INPUT "How many data points are there?",Dim
230 Newdim=Dim
240 REDIM Ri(Dim),Xi(Dim),Ri(Dim)
250 DISP "Input points starting from cylinder wall & moving toward the"
260 DISP "cylinder axis, in the form (r,X). "
270 MAT Ri=ZER
280 MAT Xi=ZER
290 Extra$="N" ! Extrapolate command
300 FOR K=1 TO Dim
310 IF Extra$="N" THEN GOTO 390
320 PRINT "Extrapolating...."
330 Slope=(Xi(K-2)-Xi(K-1))/(Ri(K-2)-Ri(K-1))
340 Ri(K)=Ri(K-1)-Xi(K-1)/Slope
350 Xi(K)=0
360 PRINT Ri(K),Xi(K)
370 Extra$="N"
380 GOTO 420
390 PRINT #";K
400 INPUT Ri(K),Xi(K)
410 INPUT "Extrapolate from this point? Y/N",Extra$
420 NEXT K
430 INPUT "Do you want to average the points near the wall? Y/N",Raverage$
440 IF Raverage$="N" THEN GOTO 780
450 INPUT "How many of the first points should be averaged?",Num
460 Newdim=Dim-Num+1
470 MAT Rneu=ZER
480 MAT Xneu=ZER
490 REDIM Rneu(Newdim),Xneu(Newdim),Fract(Newdim)
500 FOR J1=Dim TO Num+1 STEP -1

```

```

510      Rnew(J1-Num+1)=Ri(J1)
520      Xnew(J1-Num+1)=Xi(J1)
530      NEXT J1
540      Sum=0
550      FOR J2=1 TO Num
560          DISP "Enter the fraction of spins for the point ";J2
570          INPUT Fract(J2)
580          Sum=Sum+Fract(J2)
590      NEXT J2
600      Wghrad=Wghang=0      ! Weighted radius and weighted angle
610      FOR J3=1 TO Num
620          Wghrad=Wghrad+Ri(J3)*Fract(J3)/Sum
630          Wghang=Wghang+Xi(J3)*Fract(J3)/Sum
640      NEXT J3
650      PRINT "WEIGHTED AVERAGES: <Ri>=";Wghrad;"    <Xi>=";Wghang
660      INPUT "Are these adequate? Y/N",Q$
670      IF Q$="Y" THEN GOTO 690
680      INPUT "Give the preferred values for these averages:  Ri,Xi.",Wghrad,Wghang
690      Rnew(1)=Wghrad
700      Xnew(1)=Wghang
710      MAT Ri=ZER
720      MAT Xi=ZER
730      REDIM Ri(Newdim),Xi(Newdim),Ai(Newdim)
740      FOR J4=1 TO Newdim
750          Ri(J4)=Rnew(J4)
760          Xi(J4)=Xnew(J4)
770      NEXT J4
780      FOR J5=1 TO Newdim
790          DISP "Ri(";J5;")=";Ri(J5);"    Xi(";J5;")=";Xi(J5)
800      NEXT J5
810      INPUT "Do you wish to change any of these points? Y/N",Q$
820      IF Q$="N" THEN GOTO 850
830      DISP "To change the Jth point, execute Ri(J)=____,Xi(J)=____, for all point
s to
be changed. Pausing...."
840      PAUSE
850      INPUT "Has there flow during this point? Y/N",Flow$
860      BEEP
870      DISP "BEGIN INTEGRATION ROUTINE...."
880      Ibb=Ibh=0
890      Ibv=Ihv=0
900      Lmin=1
910      IF Xi(1)>63.4 THEN Lmax=Newdim-1
920      IF Xi(1)<63.4 THEN Lmax=Newdim
930      Xi=63.4*PI/180      ! X=63.4 degrees at the wall.
940      Ri=1      ! Millimeters.
950      Ai=60*PI/180      ! Alpha=60 degrees at the wall.
960      FOR L=Lmin TO Lmax
970          Min=1E99
980          IF Xi(L)<63.4 THEN GOTO 1020
990          X2=(Xi(L)+Xi(L+1))/2*PI/180      ! IF X>63.4 this averages with next X.
1000         R2=(Ri(L)+Ri(L+1))/2
1010         GOTO 1040
1020         X2=Xi(L)*PI/180
1030         R2=Ri(L)
1040         X=(X1+X2)/2      ! Average of X in this interval.
1050         R=(R1+R2)/2
1060         DxdR=(X1-X2)/(R1-R2)      ! First derivative of X.
1070         DxdR2=DxdR^2
1080         Dr=R1-R2
1090         Imin=0
1100         Imax=360
1110         Step=10
1120         FOR I=Imin TO Imax STEP Step
1130             IF I>360 THEN I=I-360
1140             A2=I*PI/180      ! Projected Alpha in radians.
1150             A=(R1+A2)/2      ! Average Alpha in this interval.
1160             Dadr=(R1-R2)/Dr      ! First derivative of Alpha.
1170             Dadr2=Dadr^2
1180             RAD
1190             C1=(3*SIN(X)^2+2)*COS(A)^2+11+2*SQR(15)*COS(X)*SIN(A)*COS(A)
1200             C2=(14*SIN(A)^2-3)*SIN(X)*COS(X)+SQR(15)*SIN(X)*SIN(A)*COS(A)*(COS(X)^2
+1)

```

```

1210 C3=2*SIN(X)+COS(X)+SIN(A)+COS(A)-SQR(15)*SIN(X)+((COS(X)+COS(A))^2-SIN(
A^2)
1220 C4=(5*SIN(X)^2+14)*SIN(X)^2+SIN(A)+COS(A)+SQR(15)*SIN(X)^2+COS(X)*(COS(
A)^2-SIN(A)^2)
1230 C5=(5*SIN(X)^2+11)*SIN(X)^2+COS(A)^2+13*(SIN(X)*SIN(A))^2-2*SQR(15)*SIN
(X)^2+COS(X)*SIN(A)+COS(A)
1240 C6=5*SIN(X)^4+SIN(A)^2+SIN(X)^2+(2*COS(A)^2+11)+2*SQR(15)*SIN(X)^2+COS(
X)*SIN(A)+COS(A)
1250 Intgnd=C1*Dxdr+2+C2*Dxdr/R-2*Dxdr+Dadr*C3+2*(C4+Dadr/R+C5+Dadr+2+C6/R-2
1260 IF Intgnd<Min THEN GOTO 1280
1270 GOTO 1300
1280 Min=Intgnd ! Stores the new minimum value.
1290 Address=I ! # of degrees which gives the minimum.
1300 NEXT I
1310 IF Step<=.1 THEN GOTO 1370
1320 Step=Step/10 ! Reduce Alpha search steps by 10.
1330 IF Address=360 THEN Address=0
1340 Imin=Address-10*Step ! Decrease region of search.
1350 Imax=Address+10*Step
1360 GOTO 1120
1370 A1(L)=Address ! New Alpha in degrees.
1380 Ibb=Ibb+R*D+Min ! Bulk bending integral.
1390 Ibh=Ibh+R*D+COS(X)^2 ! Bulk field integral.
1400 IF Flow$="N" THEN GOTO 1430
1410 Ibv=Ibh ! Bulk flow integral equals bulk field.
1420 Ihu=Ihu+R*D*(COS(X)^4-.4+COS(X)^2+.04) ! Field flow integral
1430 PRINT "Alpha found in interval 0;L; Alpha=";A1(L)
1440 BEEP
1450 X1=X2 ! Updates the chi value before moving to next interval.
1460 R1=R2 ! Updates the r value.
1470 A1=Address+PI/180 ! Updates the alpha value.
1480 NEXT L
1490 BEEP
1500 GOTO 1570
1510 BEEP
1520 INPUT "Do you have to input the radii and angles? Y/N",Q$
1530 IF Q$="N" THEN GOTO 1570
1540 INPUT "Is this a direct entry (for plot only)? Y/N",Direct$
1550 GOSUB Enter
1560 IF Direct$="Y" THEN GOTO 1860
1570 GOSUB Error
1580 OUTPUT 0 USING "+,K";CHR$(27)&"&n100c302q44r30s20t60u110v206W"!Chi-->0
1590 OUTPUT 0 USING "+,K";CHR$(27)&"&n45c66r90t90u66V"! Alpha --> 0
1600 OUTPUT 0 USING "+,K";CHR$(27)&"&n77c70p50q70r1S"! Super o replaces ?
1610 OUTPUT 0 USING "+,K";CHR$(27)&"&n136c161q160t110u160v110W"!Sub b for ^
1620 OUTPUT 0 USING "+,K";CHR$(27)&"&n44c120p120t121u160v120W"!Sub h for $
1630 OUTPUT 0 USING "+,K";CHR$(27)&"&n46c36q40r40s34t42u42v34W"!LC delta for &
1640 OUTPUT 0 USING "+,K";CHR$(27)&"&n47c21q104v50W"!sub v for '
1650 PRINTER IS 0
1660 IF Averages$="Y" THEN GOTO 1690
1670 PRINT USING "5X,K,5X,K,6X,K,9X,K,10X,K";File$, "r (mm)", "0", "%", Date$
1680 GOTO 1700
1690 PRINT USING "5X,K,5X,K,6X,K,9X,K,5X,K,10X,K";File$, "r (mm)", "0", "%", "(Fin
st data points averaged)", Date$
1700 IF D$="A" THEN PRINT " Upsweeps"
1710 IF D$="B" THEN PRINT " Downsweeps"
1720 IF D$="C" THEN PRINT " Peak#;Peak
1730 OUTPUT 0 USING "+,K";CHR$(27)&"&n43c4p12q12r13s12t152u104v72W"!Script I
1740 FOR J=1 TO Newdim
1750 IF A1(J)=0 THEN GOTO 1780
1760 PRINT USING "16X,Z.DDD,6X,DZ,D,K,4X,DDZ,D,K";R1(J),X1(J), "?", A1(J), "?"
1770 GOTO 1790
1780 PRINT USING "16X,Z.DDD,6X,DZ,D,K,4X,K";R1(J),X1(J), "?", " ---"
1790 NEXT J
1800 PRINT " @^=";Ibb;TAB(30); "@s=";Ibh
1810 PRINT " @^+&=";Bend(1);TAB(30); "@s+&=";Field(1)
1820 PRINT " @^+&=";Bend(2);TAB(30); "@s+&=";Field(2)
1830 IF Flow$="N" THEN GOTO 1850
1840 PRINT " @^=";Ibv;TAB(30); "@s=";Ihu
1850 OUTPUT 0 USING "+,K";CHR$(27)&"&n47c21q104v50W"!sub v for '
1860 PRINTER IS 16
1870 INPUT "Do you want a plot of this? Y/N",Plot$
1880 IF Plot$="N" THEN GOTO 1900
1890 GOSUB Plotter
1900 INPUT "Is there more data to be analyzed? Y/N",Q$

```



```

1910 IF Q$="Y" THEN GOTO 100
1920 END
1930 Enter:1
1940 DISP "***** SUB Enter *****"
1950 DISP "This subroutine allows for the manual entry of previously"
1960 DISP "calculated radii and angles in order to do the error estimate."
1970 INPUT "How many data points are there?",Dim
1980 REDIM Ri(Dim),Xi(Dim),Ri(Dim)
1990 Newdim=Dim
2000 INPUT "Is the wall point an average? Y/N",Averagef
2010 DISP "Starting from the wall (r=1mm) and moving toward the cylinder"
2020 DISP "axis, enter the data in the form:"
2030 DISP "  r (mm), X (deg), alpha (deg)."
```

FOR M=1 TO Dim

```

2040     DISP "R(;"M;")  X(;"M;")  A(;"M;")"
2050     INPUT Ri(M),Xi(M),Ri(M)
2060 NEXT M
2070
2080 INPUT "Enter the 2 integrals.  Ibb,Ibh",Ibb,Ibh
2090 IF Directs="N" THEN GOTO 2120
2100 INPUT "Enter the bending error max and min.",Bend(1),Bend(2)
2110 INPUT "Enter the field error max and min.",Field(1),Field(2)
2120 RETURN
2130 Error:1 This calculates the variation of the radial integrals using the
2140         assumed noise levels.
2150 DISP "***** SUB Error *****"
2160 PRINTER IS 16
2170 DISP "This subroutine allows for estimation of the 'correlated' error"
2180 DISP "in the integrals (ie assuming all errors contribute in the same"
2190 DISP "direction at once)."
```

PRINT LIN(2)

```

2200
2210 DISP "The assumed noise level us .0004.  If this is to be used, then"
2220 DISP "press CONTINUE.  Otherwise, EXECUTE Delf=____, then CONTINUE."
2230 Delf=.0004
2240 RAD ! Sets radian mode for the calculation
2250 PAUSE
2260 A=R=X=0
2270 Rused=Drused=0
2280 C1=C2=C3=C4=C5=C6=0
2290 Lmin=1
2300 Lmax=Newdim
2310 X1=63.4*PI/180
2320 R1=1 ! Millimeters
2330 A1=60*PI/180
2340 Delr1=0 ! Set uncertainty at wall (R=1mm) =0
2350 MAT Bend=ZER
2360 MAT Field=ZER
2370 DISP "CORRELATED ERROR CALCULATION PROCEEDING...."
2380 BEEP
2390 FOR L1=Lmin TO Lmax
2400     X2=X1(L1)*PI/180
2410     R2=R1(L1)
2420     A2=A1(L1)*PI/180
2430     X=(X1+X2)/2
2440     R=(R1+R2)/2
2450     Dr=R1-R2
2460     A=(A1+A2)/2
2470     IF R1(L1)=0 THEN GOTO 2500
2480     Delr2=Delf*(Lmax-L1+1)/(2*R2) ! Error estimate of radial position
2490     GOTO 2510
2500     Delr2=0 ! Sets uncertainty at axis (R=0mm) =0
2510     D1=SQR((Delr1^2+Delr2^2)/4) ! Uncertainty for averaging
2520     D2=SQR(Delr1^2+Delr2^2) ! Uncertainty for delta r
2530     FOR K=1 TO 2
2540         ! This method assumes that all the errors are in the
2550         ! same direction, either positive or negative, thus
2560         ! they are correlated to this extent.
2570         IF K=1 THEN S=-1
2580         IF K=2 THEN S=1
2590         Rused=R+S*D1 ! Value used, first time gives Rmin
2600         Drused=Dr+S*D2 ! First time gives (Dr)min

```

```

2610      C1=(3*SIN(X)^2+2)*COS(A)^2+11+2*SQR(15)*COS(X)*SIN(A)+COS(A)
2620      C2=(14*SIN(A)^2-3)*SIN(X)*COS(X)+SQR(15)*SIN(X)*SIN(A)+COS(A)+/
COS(X)^2+1)
2630      C3=2*SIN(X)*COS(X)*SIN(A)+COS(A)-SQR(15)*SIN(X)*((COS(X)*COS(A)
)^2-SIN(A)^2)
2640      C4=(5*SIN(X)^2+14)*SIN(X)^2*SIN(A)+COS(A)+SQR(15)*SIN(X)^2+COS(
X)*COS(A)^2-SIN(A)^2)
2650      C5=(5*SIN(X)^2+11)*SIN(X)^2+COS(A)^2+13*(SIN(X)*SIN(A))^2-2*SQR
(15)*SIN(X)^2+COS(X)*SIN(A)+COS(A)
2660      C6=5*SIN(X)^4+SIN(A)^2*SIN(X)^2*(2*COS(A)^2+11)+2*SQR(15)*SIN(X
)^2+COS(X)*SIN(A)+COS(A)
2670      Dxdn=(X1-X2)/Drused
2680      Dxdr2=Dxdn^2
2690      Dadr=(A1-A2)/Drused
2700      Dadr2=Dadr^2
2710      Intgnd=C1*Dxdr2+2*C2*Dxdn/Rused-2*Dxdn*Dadr*C3+2*C4*Dadr/Rused+
C5*Dadr2+C6/Rused^2
2720      Bend(K)=Bend(K)+Rused*Drused*Intgnd ! K=1 is max, K=2 is min
2730      Field(K)=Field(K)+Rused*Drused+COS(X)^2
2740      NEXT K
2750      X1=X2 ! Updates all the variables
2760      R1=R2
2770      A1=A2
2780      Delr1=Delr2
2790      NEXT L1
2800      ! Ibb=Ibb+Bend(1), Ibb=Bend(2)
2810      ! Ibh=Ibh+Field(1), Ibh=Field(2)
2820      Warnings="N"
2830      FOR K1=1 TO 2
2840          Diffb(K1)=ABS(Ibb-Bend(K1))
2850          Diffh(K1)=ABS(Ibh-Field(K1))
2860          IF Diffb(K1)>Ibb THEN Warnings="Y"
2870          IF Diffh(K1)>Ibh THEN Warnings="Y"
2880      NEXT K1
2890      IF Warnings="N" THEN GOTO 2940
2900      BEEP
2910      WAIT 250
2920      PRINT LIN(2)
2930      PRINT CHR$(129);TAB(15);"***** RELATIVE ERROR BLOW-UP *****"
";CHR$(126)
2940      BEEP
2950      PRINT LIN(2)
2960      PRINT TAB(15);"Ibb=";Ibb;" +dIbb=";Bend(1);" -dIbb=";Bend(2)
2970      PRINT TAB(15);"Ibh=";Ibh;" +dIbh=";Field(1);" -dIbh=";Field(2)
2980      PRINT LIN(2)
2990      DISP "Change the improper result as needed. Pausing...."
3000      PAUSE
3010      RETURN
3020 Plotter: ! This plots the radial integrals as they are determined.
3030      DISP "This plots the radial integrals as they are determined, on the"
3040      DISP "same page (using different scales), on the HP9872A."
3050      PLOTTER IS "9872A"
3060      OUTPUT 705;"VS5"
3070      INPUT "Do the axes need to be plotted? Y/N",Axes$
3080      LIMIT 0,215,0,279 ! 8.5" by 11"
3090      LOCATE 15,85,25,95
3100      SETUU
3110      SCALE 0,.15,0,500 ! 0-200 is for Ibb scale
3120      IF Axes$="N" THEN GOTO 3400
3130      PEN 1
3140      FRAME
3150 ! LABEL X AXIS
3160      AXES .05,100,0,0,1,1,3
3170      CSIZE 3
3180      DEG
3190      LDIR 0
3200      LOG 5
3210      FOR I=0 TO .15 STEP .1
3220          MOVE I,-20
3230          IF I=0 THEN LABEL USING "D";I
3240          IF I>0 THEN LABEL USING "2.D";I
3250      NEXT I
3260      MOVE .075,-50
3270      LABEL USING "K";"1-T/Tc"
3280 ! LABEL Ibb AXIS

```

```

3290 INPUT "Which pen?",Pen
3300 PEN Pen
3310 FOR I1=0 TO 500 STEP 100
3320 MOVE -.0075,I1
3330 LABEL USING "DD2";I1
3340 NEXT I1
3350 MOVE -.019,250
3360 LDIR 90.0
3370 LABEL USING "K";"Bulk-bending Integral"
3380 !
3390 !
3400 ! PLOT Ibb POINTS
3410 LDIR 0
3420 LOG 5
3430 CSIZE 3
3440 INPUT "Which pen?",Pen
3450 PEN Pen
3460 INPUT "What is (1-T/Tc)?",T
3470 MOVE T,Ibb
3480 OUTPUT 705;"SI;PU;PR6,8,-50,-50;PD;PR100,0,0,100,-100,0,0,-100;PU"
3490 IF Directs="N" THEN GOTO 3540
3500 FOR K3=1 TO 2
3510 Diffb(K3)=ABS(Ibb-Bend(K3))
3520 Diffh(K3)=ABS(Ibb-Field(K3))
3530 NEXT K3
3540 Bsize=(Diffb(1)+Diffb(2))*95/500 ! Switches from UDU to GDU
3550 IF Bsize<=2 THEN GOTO 3710 ! Skips bars if they're too small
3560 INPUT "Bar offset? Y/N,Offset="
3570 IF Offset="Y" THEN GOTO 3600
3580 IF Offset="N" THEN Offset=0
3590 GOTO 3620
3600 Offset=1
3610 INPUT "+ or - how much?",Delt
3620 FOR L2=1 TO 2 ! Draws the error bars
3630 MOVE T+Offset*Delt,Ibb
3640 DRAW T+Offset*Delt,Bend(L2)
3650 IF (Bend(L2)<0) OR (Bend(L2)>500) THEN GOTO 3670
3660 LABEL USING "K";"-"
3670 IF Offset="N" THEN GOTO 3700
3680 MOVE T,Ibb
3690 DRAW T+Offset*Delt,Ibb
3700 NEXT L2
3710 !
3720 !
3730 SETUU
3740 SCALE 0,.15,0,.5
3750 IF Axes="N" THEN GOTO 3940
3760 ! LABELS Ibh AXIS
3770 INPUT "Which pen?",Pen
3780 PEN 1
3790 CSIZE 3
3800 LOG 5
3810 LDIR 0
3820 AXES .05,.1,.15,.5,1,1,3
3830 PEN Pen
3840 FOR I3=0 TO .5 STEP .1
3850 MOVE .155,I3
3860 IF I3=0 THEN LABEL USING "D";I3
3870 IF I3>0 THEN LABEL USING ".D";I3
3880 NEXT I3
3890 LDIR -90.0
3900 MOVE .165,.25
3910 LABEL USING "K";"Bulk-field Integral"
3920 !
3930 !
3940 LDIR 0
3950 CSIZE 3
3960 LOG 5
3970 INPUT "Which pen?",Pen
3980 PEN Pen

```

```

3990 MOVE T,Ibh
4000 OUTPUT 705;"S1;PU;PR6,0,-75,-53;PD;PR150,0,-75,106,-75,-106;PU"
4010 Hsize=(Difch(1)+Difch(2))*95/.5 ! Switches from UDU to GDU
4020 IF Hsize<2 THEN GOTO 4180 ! Skips bars if they're too small
4030 INPUT "Bar offset? Y/N",Offset$
4040 IF Offset$="Y" THEN GOTO 4070
4050 IF Offset$="N" THEN Offset=0
4060 GOTO 4090
4070 Offset=1
4080 INPUT "+ or - how much?",Delt
4090 FOR I4=1 TO 2 ! Draws error bars
4100 MOVE T+Offset*Delt,Ibh
4110 DRAW T+Offset*Delt,Field(I4)
4120 IF (Field(I4)<0) OR (Field(I4)>.5) THEN GOTO 4140
4130 LABEL USING "K";"--"
4140 IF Offset$="N" THEN GOTO 4170
4150 MOVE T,Ibh
4160 DRAW T+Offset*Delt,Ibh
4170 NEXT I4
4180 !
4190 !
4200 INPUT "Any labels? Y/N",O$
4210 IF O$="N" THEN GOTO 4340
4220 INPUT "LORG, CSIZE, LDIR",Lorg,Csize,Ldir
4230 LORG Lorg
4240 CSIZE Csize
4250 LDIR Ldir
4260 INPUT "Pen",Pen
4270 PEN Pen
4280 INPUT "Where? X,Y",Xo,Yo
4290 MOVE Xo,Yo
4300 INPUT "Give label.",Label$
4310 LABEL USING "K";Label$
4320 INPUT "More? Y/N",O$
4330 IF O$="Y" THEN GOTO 4220
4340 PEN 0
4350 MOVE 215,279 ! Moves out of the way
4360 RETURN

```

```

10  ! ****Program: TIMER5 **** !
20  ! This program takes the data shown in line 80 at regular intervals
30  ! determined by the commands sent to the HP clock (lines 170,180) and
40  ! stores the data on tape as well as providing a plot. It does not take
50  ! the beat measurement, those lines have been blocked (!). Otherwise
60  ! identical to TIMER4.
70  OPTION BASE 0
80  COM Ccom$[50],SHORT Mano,Pump,Temp,Time,Sound,Amp,T2,Bf,Db,Mult,Int
90  INTEGER Nic(2000),Start,End
100 INPUT "Do you wish to take NMR data during this file? Y/N",Nmrs
110 IF Nmrs="N" THEN GOTO 170
120 INPUT "Give Start & End points for integration, Nic timebase & attenuation.
    ",Start,End,Mult,Db
130 INPUT "What ratio of flow & temp data to NMR data? 1:1=1,2:1=2,3:1=3",Mod
140 NmrCnt=Bf=0 ! Initialize counter to alternate FID & beat traces
150 OUTPUT 709;"OPN0" ! Arm NMR pulse switch
160 OUTPUT 709;"OPN1" ! Puts BNC switch in unpowered position-sound on,beat on
170 INPUT "Give the clock command string and position of the unit ID (2 numbers
    ),",Ccom$,C1,C2
180 INPUT "Give string position of the clock period.",C3,C4
190 INPUT "What is your thermometer? PLM(PLM) or resistance bridge(R)",Therm$
200 Period=VAL(Ccom$[C3,C4])
210 OUTPUT 9;Ccom$
220 Units=Ccom$[C1,C2]&"G"
230 OUTPUT 9;Units ! Tells defined unit to Go
240 GOTO 300 ! Skips clock period for initial set-up
250 ON INT #9,15 GOTO 510 ! Interrupt set-up
260 CONTROL MASK 9;120
270 CARD ENABLE 9
280 Wait: GOTO 280 ! Waits for interrupt here
290 RETURN
300 INPUT "Do you want the program to automatically set-up files? Y/N",Autos
310 IF Autos="N" THEN GOTO 380
320 INPUT "Give the data file base name (without file # attached).",Name$
330 INPUT "Set the file #.",FilCnt
340 IF FilCnt<10 THEN Name$=Name$&"0"
350 IF FilCnt>=10 THEN Name$=Name$
360 File$=Name$&VAL$(FilCnt)
370 GOTO 390
380 INPUT "Give the entire name for this data run.",File$
390 IF Nmrs="N" THEN CREATE File$&"T14",240,20 ! 240 records-8 hours at 1 da
    tum/2 minutes
400 IF Nmrs="Y" THEN CREATE File$&"T14",240,36
410 ASSIGN #1 TO File$&"T14"
420 PLOTTER IS 13,"GRAPHICS"
430 FRAME
440 SCALE 0,240,-.5,.5
450 AXES 10,.1,0,-.5
460 AXES 10,.1,240,.5
470 GRAPHICS
480 Tcount=0
490 Record=1
500 IF (Autos="Y") AND (FilCnt>1) THEN GOTO 250 ! Reset interrupt on auto

```

```

510 OUTPUT 9;"T" ! Outputs trigger on interrupt
520 Source=FEADIN(9)
530 IF NOT IIT(Source,0) THEN GOSUB Wait ! Verifies source of trigger,
540 ! proceeds with program if correct.
550 GOSUB Takedata
560 IF (Nmr$="Y") AND ((Record-1) MOD Mod=0) THEN GOTO 580
570 GOTO 630
580 GOSUB Takenmr
590 ! IF NmrCnt MOD 2=0 THEN GOSUB Integrate
600 ! IF NmrCnt MOD 2=1 THEN GOSUB Zeros
610 GOSUB Integrate
620 NmrCnt=NmrCnt+1
630 GOSUB Storedata
640 GOSUB Graphics
650 Tcount=Tcount+1
660 Record=Record+1
670 IF Record>240 THEN GOTO 690
680 GOTO 250 ! Reset interrupt conditions
690 PRINTER IS 0
700 DUMP GRAPHICS
710 PRINT "Mano=" Pump=" Temp=" Sound=" FID=" Beats$="
720 PRINTER IS 16
730 IF Auto$="N" THEN GOTO 760
740 FilCnt=FilCnt+1 ! Increment file counter
750 GOTO 340
760 END
770 !
780 !
790 !
800 !
810 Takedata: !
820 Sum=0
830 FOR I=1 TO 10
840 OUTPUT 709;"DCV2" ! Reads manometer bridge
850 ENTER 709;Mano
860 Sum=Sum+Mano
870 WAIT 300
880 NEXT I
890 Avg=Sum/10
900 Mano=Avg
910 !
920 OUTPUT 709;"DCV3" ! Reads pump bridge
930 ENTER 709;Pump
940 !
950 OUTPUT 709;"DCV4" ! Reads resistance bridge or PLM D/R for thermometry
960 ENTER 709;Temp
970 !
980 OUTPUT 709;"DCV5" ! Reads He-3 sound attenuation from boxcar
990 ENTER 709;Sound
1000 !
1010 Time=Tcount*Period/60 ! Time in minutes
1020 RETURN
1030 Storedata: !
1040 PRINTER IS 0
1050 IF Record>1 THEN GOTO 1080
1060 PRINT LIN(1)
1070 PRINT TAB(10);"***** ";File$;" *****"
*****
1080 IF Therm$="R" THEN PRINT Record;" Time=";Time;"min Mano=";Mano;" Pump=";Pump;" R4=";Temp;" Sound=";Sound
1090 IF Therm$="PLM" THEN PRINT Record;" Time=";Time;"min Mano=";Mano;" Pump=";Pump;" PLM=";Temp;" Sound=";Sound
1100 IF Nmr$="N" THEN GOTO 1170
1110 IF (Record-1) MOD Mod<>0 THEN GOTO 1170
1120 IF Fail$="Y" THEN GOTO 1150
1130 PRINT TAB(5);"Int=";Int;" Beat freq=";Bf;" Amp=";Amp;" T2=";T2;"usec Att'n=";Db;"dB"
1140 GOTO 1160
1150 PRINT TAB(5);"Int=";Int;" Beat not found";" Amp=";Amp;" T2=";T2;"usec Att'n=";Db;"dB"
1160 PRINT TAB(5);"Start=";Start*Mult*1E6;"usec End=";End*Mult*1E6;"usec"
1170 PRINTER IS 16
1180 IF Nmr$="N" THEN PRINT #1,Record;Time;Mano;Pump;Temp;Sound
1190 IF Nmr$="Y" THEN PRINT #1,Record;Time;Mano;Pump;Temp;Sound;Int;Bf;Amp;T2
1200 RETURN

```

```

1210 Graphics1!
1220 CSIZE 2,5
1230 Ymano=Mano*10 ! Expand mano trace to be able to see relaxation.
1240 IF (Ymano>=.5) AND (Ymano<=.5) THEN GOTO 1260
1250 IF Ymano<-.5 THEN Ymano=Ymano+1
1260 IF Ymano>.5 THEN Ymano=Ymano-1
1270 GOTO 1240
1280 MOVE Tcount,Ymano
1290 LABEL USING "A";"$"
1300 Ypump=Pump
1310 IF (Ypump>=.5) AND (Ypump<=.5) THEN GOTO 1350
1320 IF Ypump<-.5 THEN Ypump=Ypump+1
1330 IF Ypump>.5 THEN Ypump=Ypump-1
1340 GOTO 1310
1350 IF ABS(Ymano)>.05 THEN MOVE Tcount,Ypump
1360 IF ABS(Ymano)<=.05 THEN MOVE Tcount,Ypump-.3 ! Offset pump to see mano
1370 LABEL USING "A";"$"
1380 Ytemp=Temp
1390 IF (Ytemp>=.5) AND (Ytemp<=.5) THEN GOTO 1430
1400 IF Ytemp<-.5 THEN Ytemp=Ytemp+1
1410 IF Ytemp>.5 THEN Ytemp=Ytemp-1
1420 GOTO 1390
1430 MOVE Tcount,Ytemp
1440 LABEL USING "A";"$"
1450 Ysound=Sound/10 ! Expand sound trace to be able to see changes.
1460 IF (Ysound>=.5) AND (Ysound<=.5) THEN GOTO 1500
1470 IF Ysound<-.5 THEN Ysound=Ysound+1
1480 IF Ysound>.5 THEN Ysound=Ysound-1
1490 GOTO 1460
1500 MOVE Tcount,Ysound
1510 LABEL USING "A";"$"
1520 IF Nmr="N" THEN GOTO 1670 ! Don't plot Int or Beat if no NMR is taken
1530 Yfid=Int/1E5
1540 IF (Yfid>=.5) AND (Yfid<=.5) THEN GOTO 1580
1550 IF Yfid<-.5 THEN Yfid=Yfid+1
1560 IF Yfid>.5 THEN Yfid=Yfid-1
1570 GOTO 1540
1580 MOVE Tcount,Yfid
1590 LABEL USING "A";"o"
1600 Ybeat=Bf/1000
1610 IF (Ybeat>=.5) AND (Ybeat<=.5) THEN GOTO 1650
1620 IF Ybeat<-.5 THEN Ybeat=Ybeat+1
1630 IF Ybeat>.5 THEN Ybeat=Ybeat-1
1640 GOTO 1610
1650 MOVE Tcount,Ybeat
1660 ! LABEL USING "A";"$"
1670 RETURN
1680 Takenmr:GOTO Fid
1690 IF Nmrct MOD 2=0 THEN Fid
1700 IF Nmrct MOD 2=1 THEN Beat
1710 Fid: OUTPUT 709;"CLS1" ! Turns sound off & switches to FID on NMR
1720 WAIT 1000
1730 GOTO Fire
1740 Beat: OUTPUT 709;"OPN1" ! Makes certain that switch is in beat position
1750 WAIT 1000
1760 GOTO Fire
1770 Fire:CONTROL MASK 11;1
1780 CARD ENABLE 11
1790 OUTPUT 11 USING "#,B";0
1800 CONVERT 11;"I," " TO ","
1810 CONTROL MASK 11;1
1820 CARD ENABLE 11
1830 OUTPUT 11 USING "#,B";52
1840 CONTROL MASK 11;0
1850 CARD ENABLE 11
1860 OUTPUT 709;"CLS0" ! Fire the NMR pulse
1870 ENTER 11;Nrc(*)
1880 OUTPUT 709;"OPN1" ! Turn sound back on, now in beat position
1890 OUTPUT 709;"OPN0" ! Reset for next NMR pulse
1900 FOR I=1 TO 3 ! 3X3-point smooth

```

```

1910     FOR J=1 TO 1500
1920     Nic(J)=(Nic(J-1)+Nic(J)+Nic(J+1))/3
1930     NEXT J
1940     NEXT I
1950     Sum=0
1960     FOR K=1500 TO 2000
1970     Sum=Sum+Nic(K)
1980     NEXT K
1990     Base=Sum/501
2000     FOR L=1 TO 1500
2010     Nic(L)=Nic(L)-Base
2020     NEXT L
2030     Fail$="Y"
2040     RETURN
2050     Integrate:
2060     Amp=Nic(Start)
2070     Int=0
2080     FOR I=Start TO End
2090     Int=Int+Nic(I)
2100     IF (Nic(I))>Amp/EXP(1) AND (Nic(I+1)<=Amp/EXP(1)) THEN T2=I*Mult+1E6
2110     NEXT I
2120     RETURN
2130     Zeros:
2140     Fail$="N"
2150     Xzero1=Xzero2=0
2160     Bmax=Bmin=0
2170     Imax=Imin=0
2180     FOR I=Start TO End
2190     IF Nic(I)>Bmax THEN Setmax=I
2200     IF Nic(I)<Bmin THEN Setmin=I
2210     GOTO Nexti
2220     Setmax: Bmax=Nic(I)
2230     Imax=I
2240     GOTO Nexti
2250     Setmin: Bmin=Nic(I)
2260     Imin=I
2270     Nexti:NEXT I
2280     Begin=MIN(Imin,Imax)
2290     Finish=Begin+3*ABS(Imin-Imax)
2300     FOR K=1 TO 2
2310     FOR L=Begin TO Finish
2320     IF K=1 THEN Neg ! Search for neg-going crossing 1st
2330     IF K=2 THEN Pos ! Search for pos-going crossing 2nd
2340     Neg: IF (Nic(L-1))>0 AND (Nic(L)<=0) THEN Set01
2350     GOTO Nextl
2360     Pos: IF (Nic(L-1)<=0) AND (Nic(L))>0 THEN Set02
2370     GOTO Nextl
2380     Set01: IF ABS(Nic(L-1))=MIN(ABS(Nic(L-1)),ABS(Nic(L))) THEN Xzero1=L-1
2390     IF ABS(Nic(L))=MIN(ABS(Nic(L-1)),ABS(Nic(L))) THEN Xzero1=L
2400     GOTO Nextk
2410     Set02: IF ABS(Nic(L-1))=MIN(ABS(Nic(L-1)),ABS(Nic(L))) THEN Xzero2=L-1
2420     IF ABS(Nic(L))=MIN(ABS(Nic(L-1)),ABS(Nic(L))) THEN Xzero2=L
2430     GOTO Nextk
2440     Nextl:NEXT L
2450     Nextk:NEXT K
2460     IF ABS(Xzero1-Xzero2)<=10 THEN GOTO 2500 ! Prevents prog failure if beats
2470     ! found incorrectly.
2480     Bf=1/(2*ABS(Xzero1-Xzero2)*Mult) ! Beat frequency in Hertz
2490     GOTO 2510
2500     Fail$="Y"
2510     RETURN

```


APPENDIX C

MANUFACTURER'S LIST

American Magnetics, Inc., P.O. Box 2509, Oak Ridge, TN 37831, 615-482-1056.

Analog Modules Inc., 126 Baywood Ave., Longwood, FL 32750, 305-339-4356.

Buehler Ltd., 41 Waukegan Road, Lake Bluff, IL 60044, 312-295-6500.

Corning Glass Works, Science Products, 63 North Street, Medfield, MA 02052, 800-225-3232.

E.I. du Pont de Nemours and Co., Polymer Products Dept., Chestnut Run, Wilmington, DE 19898.

Emerson and Cuming, Inc., Canton, MA 02021, 617-828-3300.

Essex Group, Magnet Wire and Insulation Division, Fort Wayne, IN.

General Radio, West Concord, MA 01781, 617-369-4400.

Hewlett-Packard, P.O. Box 13910, 6177 Lake Ellenor Drive, Orlando, FL 32809, 305-859-2900.

Instruments for Technology Ltd., Mannerheimintie 87 A 21, 00270 Helsinki 27, Finland.

Kepco Inc., 131-38 Sanford Ave., Flushing, NY 11352, 212-461-7000.

Lake Shore Cryotronics, 64 E. Walnut Street, Westerville, OH 43081, 614-891-2243.

Leico Industries, Inc., 250 West 57th Street, New York, NY 10107, 212-765-5290.

Lindberg, 304 Hart Street, Watertown, WI 53094, 414-261-7000.

Linear Research, Inc., 5231 Cushman Place, Suite 21, San Diego, CA 92110, 619-299-0719.

Matec, Inc., 60 Montebello Road, Warwick, RI 02886, 401-739-9030.

Materials Research Corp., Orangeburg, NY 10962, 914-359-4200.

Merrimac Research and Development Inc., 41 Fairfield Place, West Caldwell, NJ 07006, 201-228-3890.

Micro-Surface Finishing Products, Box 456, Wilton, IO 52778.

Millipore Corp., 80 Ashby Road, Bedford, MA 01730, 800-225-1380.

Mini-Circuits, P.O. Box 166, Brooklyn, NY 11235, 718-934-4500.

MKS Instruments Inc., 34 Third Avenue, Burlington, MA 01803, 617-272-9255.

Nicolet Instrument Corp., 5225 Verona Road, Madison, WI 53711, 608-271-3333.

Princeton Applied Research Corp., P.O. Box 2565, Princeton, NJ 08540,
609-452-2111.

Programmed Test Sources, Inc., 9 Beaverbrook Road, P.O. Box 617, Littleton,
MA 01460, 617-486-3008.

Ralmike's Tool-A-Rama, South Plainfield, NJ 07080.

Supercon, Inc., 9 Erie Drive, Natick, MA 01760.

Vacuum Metallurgical Co., Ltd., No. 14-10, 1-Chome, Ginza, Chuo-Ku, Tokyo,
Japan.

REFERENCES

- M.I. Aalto, H.K. Collan, R.G. Gylling, and K.O. Nores, *Rev. Sci. Instrum.* 44, 1075 (1973).
- W.R. Abel, A.C. Anderson, and J.C. Wheatley, *Phys. Rev. Lett.* 7, 299 (1961).
- A. Abragam, Principles of Nuclear Magnetism, Oxford University Press, Oxford (1961).
- A.A. Abrikosov and I.M. Khalatnikov, *Rep. Prog. Phys.* 22, 329 (1959).
- A.I. Ahonen, T.A. Alvesalo, M.T. Haikala, M. Krusius, and M.A. Paalanen, *J. Phys. C* 8, L269 (1975).
- A.I. Ahonen, M. Krusius, and M.A. Paalanen, *J. Low Temp. Phys.* 25, 421 (1976).
- T.A. Alvesalo, H.K. Collan, M.T. Lojonen, O.V. Lounasmaa, and M.C. Veuro, *J. Low Temp. Phys.* 19, 1 (1975).
- A.C. Anderson, W. Reese, and J.C. Wheatley, *Phys. Rev.* 127, 671 (1962).
- P.W. Anderson, in The Physics of Liquid and Solid Helium, Vol. II, K.H. Bennemann and J.B. Ketterson, editors, chapter 3, Wiley-Interscience, New York (1978).
- P.W. Anderson and P. Morel, *Physica* 26, 671 (1960a).
- P.W. Anderson and P. Morel, *Phys. Rev. Lett.* 5, (E) 136, 282 (1960b).
- P.W. Anderson and P. Morel, *Phys. Rev.* 123, 1911 (1961).
- E.R. Andrew, Nuclear Magnetic Resonance, Cambridge University Press, Cambridge (1958).
- O. Avenel and E. Varoquaux, *Phys. Rev. Lett.* 55, 2704 (1985).
- R. Balian and N.R. Werthamer, *Phys. Rev.* 131, 1553 (1963).
- J. Bardeen, L.N. Cooper, and J.R. Schrieffer, *Phys. Rev.* 108, 1175 (1957).
- G. Barton and M.A. Moore, *J. Low Temp. Phys.* 21, 489 (1975).

- G. Baym and C. Petick, in The Physics of Liquid and Solid Helium, Vol. II, K.H. Bennemann and J.B. Ketterson, editors, chapter 1, Wiley-Interscience, New York (1978).
- M.T. Béal-Monod and S. Doniach, J. Low Temp. Phys. 28, 175 (1977).
- R.F. Berg, PhD. Dissertation, University of Florida (1983).
- D.S. Betts, B.E. Keen, and J. Wilks, Proc. Roy. Soc. A 289, 34 (1965).
- H.M. Bozler, D.M. Bates, and A.L. Thomson, Phys. Rev. B 27, 6992 (1983).
- D.F. Brewer, in The Physics of Liquid and Solid Helium, Vol. II, K.H. Bennemann and J.B. Ketterson, editors, chapter 6, Wiley-Interscience, New York (1978).
- W.F. Brinkman and M.C. Cross, in Progress in Low Temperature Physics, Vol. 7A, D.F. Brewer, editor, chapter 2, North-Holland Publishing, New York (1978).
- W.F. Brinkman, H. Smith, D.D. Osheroff, and E.I. Blount, Phys. Rev. Lett. 33, 624 (1974).
- R.S. Brodkey, The Phenomena of Fluid Motions, Addison-Wesley, Reading, Pennsylvania (1967).
- K.A. Brueckner, T. Soda, P.W. Anderson, and P. Morel, Phys. Rev. 118, 1442 (1960).
- S. Brunauer, P.H. Emmett, and E. Teller, J. Am. Chem. Soc. 60, 309 (1938).
- L.J. Buchholtz, in Proceedings of the 17th International Conference on Low Temperature Physics, V. Eckern, A. Schmid, W. Weber, and H. Wühl, editors, p. 987, North-Holland, Amsterdam (1984).
- L.J. Buchholtz, Phys. Rev. B 33, 1579 (1986).
- L.N. Cooper, Phys. Rev. 104, 1189 (1956).
- L.N. Cooper, R.L. Mills, and A.M. Sessler, Phys. Rev. 114, 1377 (1959).
- H. Darcy, Les Fontaines Publiques de la Ville de Dijon, Dalmont, Paris (1856).
- J.G. Dash and M. Schick, in The Physics of Liquid and Solid Helium, Vol. II, K.H. Bennemann and J.B. Ketterson, editors, chapter 5, Wiley-Interscience, New York (1978).
- J.G. Daunt and E. Lerner, Monolayer and Submonolayer Helium Films, Plenum Press, New York (1973).
- P.G. de Gennes, Phys. Lett. A 44, 271 (1973).
- J.M. Delrieu, M. Roger, and J.H. Hetherington, J. Low Temp. Phys. 40, 71 (1980).

- G.J. Ehnholm, J.P. Ekström, M.T. Lopenon, and J.K. Soini, *Cryogenics* 19, 673 (1979).
- V.J. Emery and A.M. Sessler, *Phys. Rev.* 119, 43 (1960).
- B.N. Engel, R.F. Berg, and G.G. Ihas, *Phys. Rev. Lett.* 54, 1331 (1985).
- B.N. Engel, G.G. Ihas, E.D. Adams, and C. Fombarlet, *Rev. Sci. Instrum.* 55, 1489 (1984).
- S. Engelsberg, W.F. Brinkman, and P.W. Anderson, *Phys. Rev. A* 9, 2592 (1974).
- W.M. Fairbank and G.K. Walters, *Nuovo Cim.* 9, Supp. 1, 297 (1958).
- A.L. Fetter, *J. Low Temp. Phys.* 23, 245 (1976).
- E.B. Flint, R.M. Mueller, and E.D. Adams, *J. Low Temp. Phys.* 33, 43 (1978).
- L.J. Friedman, A.K.M. Wennberg, S.N. Ytterboe, and H.M. Bosler, *Rev. Sci. Instrum.* 57, 410 (1986).
- R.A. Guyer, *Phys. Rev. Lett.* 39, 1091 (1977).
- P.J. Hakonen and G.E. Volovik, *J. Phys. C* 15, L1277 (1982).
- J. Harris, *Rheology and Non-Newtonian Flow*, Longman Group, New York (1977).
- J.O. Hirschfelder, C.F. Curtiss, and R.B. Bird, *Molecular Theory of Gases and Liquids*, J. Wiley and Sons, New York (1954).
- J. Hutchins, D.F. Brewer, and D. Kruppa, *Phys. Rev. Lett.* 55, 1410 (1985).
- G.G. Ihas and F. Pobell, *Phys. Rev. A* 9, 1278 (1974).
- G.G. Ihas and G.F. Spencer, in *Quantum Fluids and Solids, 1983 Sanibel Symposium*, E.D. Adams and G.G. Ihas, editors, A.I.P. Conference Proceedings No. 103, p.355, New York (1983).
- O.T. Ikkala, G.E. Volovik, P.J. Hakonen, Y. M. Bunkov, S.T. Islander, and G.A. Kharadze, *Zh. Eksp. Teor. Fiz. Pis'ma Red.* 35, 338 (1982).
- J.E. Jaffe, *J. Low Temp. Phys.* 37, 567 (1979).
- H.H. Jensen, H. Smith, P. Wölflé, K. Nagai, and T.M. Bisgaard, *J. Low Temp. Phys.* 41, 473 (1980).
- H. Jichu and Y. Kuroda, *Prog. Theor. Phys.* 67, 715 (1982).
- T. Kasuya, *Prog. Theor. Phys.* 16, 45 (1956).
- M. Knudsen, *Ann. Phys.* 28, 75 (1909).

- M. Knudsen, Kinetic Theory of Gases, J. Wiley and Sons, New York (1950).
- L.D. Landau, Sov. Phys. JETP 3, 920 (1956).
- L.D. Landau and E.M. Lifshitz, Fluid Mechanics, Pergamon Press, Oxford (1978).
- D.M. Lee and R.C. Richardson, in The Physics of Liquid and Solid Helium, Vol. II, K.H. Bennemann and J.B. Ketterson, editors, chapter 4, Wiley-Interscience, New York (1978).
- A.J. Leggett, Phys. Rev. A 140, 1869 (1965).
- A.J. Leggett, Phys. Rev. Lett. 29, 1227 (1972).
- A.J. Leggett, Phys. Rev. Lett. 31, 352 (1973).
- A.J. Leggett, Ann. Phys. (New York) 85, 11 (1974).
- A.J. Leggett, Rev. Mod. Phys. 47, 331 (1975).
- F. London, Superfluids, Vol. II, John Wiley and Sons, New York (1954).
- O.V. Lounasmaa, Contemp. Phys. 15, 353 (1974a).
- O.V. Lounasmaa, Experimental Principles and Methods Below 1 K, Academic Press, New York (1974b).
- K. Maki and M. Nakahara, Phys. Rev. B 27, 4181 (1983).
- K. Mendelssohn, Quest for Absolute Zero, McGraw-Hill, New York (1966).
- K.A. Muething, PhD. Dissertation, Ohio State University (1979).
- Y. Okuda, A.J. Ikushima, and H. Kojima, Phys. Rev. Lett. 54, 130 (1985).
- D.D. Osheroff, Phys. Rev. Lett. 33, 1009 (1974).
- D.D. Osheroff and W.F. Brinkman, Phys. Rev. Lett. 32, 584 (1974).
- D.D. Osheroff, S. Engelsberg, W.F. Brinkman, and L.R. Corruccini, Phys. Rev. Lett. 34, 190 (1975).
- D.D. Osheroff, W.J. Gully, R.C. Richardson, and D.M. Lee, Phys. Rev. Lett. 29, 920 (1972a).
- D.D. Osheroff, R.C. Richardson, and D.M. Lee, Phys. Rev. Lett. 28, 885 (1972b).
- W. Ostwald, Z. Physik. Chem. 111A, 62 (1924).
- D. Pines and P. Nozières, The Theory of Quantum Liquids, W.A. Benjamin, Inc., New York (1966).

A.C. Pipkin, Lectures on Viscoelasticity Theory, Springer-Verlag, New York (1972).

I. Pomeranchuk, Zh. Eksp. Teor. Fiz. 20, 919 (1950).

J.D. Reppy, in Proceedings of the Hakone International Symposium, T. Sugawara, S. Nakajima, T. Ohtsuki, and T. Usui, editors, Physical Society of Japan, Tokyo (1978).

P.M. Richards and M.B. Salamon, Phys. Rev. B 9, 32 (1974).

P.R. Roach, J.B. Ketterson, and M. Kuchnir, Rev. Sci. Instrum. 43, 898 (1972).

A.C. Rose-Innes, Low Temperature Techniques, English Universities Press, London (1964).

M.A. Ruderman and C. Kittel, Phys. Rev. 96, 99 (1954).

A.E. Scheidegger, The Physics of Flow Through Porous Media, University of Toronto, Toronto (1960).

H. Smith, W.F. Brinkman, and S. Engelsberg, Phys. Rev. B 15, 199 (1977).

G.F. Spencer and G.G. Ihas, Phys. Rev. Lett. 48, 1118 (1982).

G.F. Spencer and G.G. Ihas, in Proceedings of the 17th International Conference on Low Temperature Physics, Vol. I, V. Eckern, A. Schmid, W. Weber, and H. Wühl, editors, p. 415, North-Holland, Amsterdam (1984).

G.F. Spencer and G.G. Ihas, Rev. Sci. Instrum. 56, 1838 (1985).

G.F. Spencer and G.G. Ihas, submitted (1986).

G.F. Spencer, P.W. Alexander, and G.G. Ihas, Cryogenics 22, 167 (1982).

G.F. Spencer, G.G. Ihas, and P.W. Alexander, Physica 107B, 289 (1981).

Z. Tesanovic and O.T. Valls, in Proceedings of the 17th International Conference on Low Temperature Physics, Vol. II, V. Eckern, A. Schmid, W. Weber, and H. Wühl, editors, p. 985, North-Holland, Amsterdam (1984).

Z. Tesanovic and O.T. Valls, Phys. Rev. B 33, 3139 (1986).

W.C. Thomlinson, G.G. Ihas, and F. Pobell, Phys. Rev. B 11, 4292 (1975).

A.L. Thomson, H. Meyer, and E.D. Adams, Phys. Rev. 128, 509 (1962).

R.A. Webb, R.E. Sager, and J.C. Wheatley, Phys. Rev. Lett. 35, 615 (1975).

R.A. Webb, R.E. Sager, and J.C. Wheatley, J. Low Temp. Phys. 26, 439 (1977).

J.C. Wheatley, Rev. Mod. Phys. 47, 415 (1975).

P. Wölflle, Rep. Prog. Phys. 42, 269 (1979).

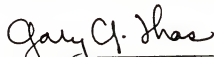
K. Yosida, Phys. Rev. 106, 893 (1957).

K. Yosida, Phys. Rev. 110, 769 (1958).

BIOGRAPHICAL SKETCH

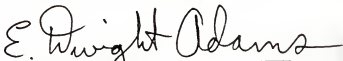
Gregory F. Spencer was born on September 20, 1953, in the low rolling hills of Dade City, Florida. Having graduated from Pasco High School he attended the University of South Florida in Tampa and took a Bachelor of Science degree with honors in physics. After acquiring a Master of Science degree in physics from the University of Illinois at Urbana-Champaign, he returned to Florida to pursue a Ph.D. at the University of Florida. On a bright sunny day on the 20th of June, 1986, he and Sheila Ann Fenelon were married. Upon successful completion of his dissertation, he and Sheila will travel to Lancaster, England, where he will take a post-doctoral position at the University of Lancaster.

I certify that I have read this study and that in my opinion it conforms to acceptable standards of scholarly presentation and is fully adequate, in scope and quality, as a dissertation for the degree of Doctor of Philosophy.



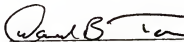
Gary C. Inas, Chairman
Professor of Physics

I certify that I have read this study and that in my opinion it conforms to acceptable standards of scholarly presentation and is fully adequate, in scope and quality, as a dissertation for the degree of Doctor of Philosophy.



E. Dwight Adams
Professor of Physics

I certify that I have read this study and that in my opinion it conforms to acceptable standards of scholarly presentation and is fully adequate, in scope and quality, as a dissertation for the degree of Doctor of Philosophy.



David B. Tanner
Professor of Physics

I certify that I have read this study and that in my opinion it conforms to acceptable standards of scholarly presentation and is fully adequate, in scope and quality, as a dissertation for the degree of Doctor of Philosophy.



Paul H. Holloway
Professor of Materials Science
and Engineering

This dissertation was submitted to the Graduate Faculty of the Department of Physics in the College of Liberal Arts and Sciences and to the Graduate School, and was accepted as partial fulfillment of the requirements for the degree of Doctor of Philosophy.

August 1986

Dean, Graduate School